1977

The effects of cryoforming and aging on the structure and mechanical properties of an austenitic stainless steel alloy

Justin Opoku
Iowa State University

INFORMATION TO USERS

This material was produced from a microfilm copy of the original document. While the most advanced technological means to photograph and reproduce this document have been used, the quality is heavily dependent upon the quality of the original submitted.

The following explanation of techniques is provided to help you understand markings or patterns which may appear on this reproduction.

1. The sign or "target" for pages apparently lacking from the document photographed is "Missing Page(s)". If it was possible to obtain the missing page(s) or section, they are spliced into the film along with adjacent pages. This may have necessitated cutting thru an image and duplicating adjacent pages to insure you complete continuity.

2. When an image on the film is obliterated with a large round black mark, it is an indication that the photographer suspected that the copy may have moved during exposure and thus cause a blurred image. You will find a good image of the page in the adjacent frame.

3. When a map, drawing or chart, etc., was part of the material being photographed the photographer followed a definite method in "sectioning" the material. It is customary to begin photoing at the upper left hand corner of a large sheet and to continue photoing from left to right in equal sections with a small overlap. If necessary, sectioning is continued again — beginning below the first row and continuing on until complete.

4. The majority of users indicate that the textual content is of greatest value, however, a somewhat higher quality reproduction could be made from "photographs" if essential to the understanding of the dissertation. Silver prints of "photographs" may be ordered at additional charge by writing the Order Department, giving the catalog number, title, author and specific pages you wish reproduced.

5. PLEASE NOTE: Some pages may have indistinct print. Filmed as received.

University Microfilms International
300 North Zeeb Road
Ann Arbor, Michigan 48106 USA
St. John's Road, Tyler's Green
High Wycombe, Bucks, England HP10 8HR

The effects of cryoforming and aging on the structure and mechanical properties of an austenitic stainless steel alloy

by

Justin Opoku

A Dissertation Submitted to the
Graduate Faculty in Partial Fulfillment of
The Requirements for the Degree of
DOCTOR OF PHILOSOPHY

Major: Mechanical Engineering

Approved:

Signature was redacted for privacy.

In Charge of Major Work

Signature was redacted for privacy.

For the Major Department

Signature was redacted for privacy.

For the Graduate College

Iowa State University
Ames, Iowa

1977

TABLE OF CONTENTS

	Page
LIST OF SYMBOLS	v
I. INTRODUCTION	1
A. Literature Review	1
1. Factors influencing the effectiveness of cryoforming	2
a. Alloy composition	2
b. Austenitizing temperature	3
c. Deformation temperature	5
d. Amount of deformation	5
e. Type of deformation	7
f. Rate of deformation	7
2. Effect of post-deformation aging temperature and time	8
3. Strengthening mechanisms	9
4. The martensite transformation in austenitic steels	11
B. Relevance and Scope of This Study	13
II. EXPERIMENTAL PROCEDURE	15
A. Cryoforming and Testing Equipment	15
B. Material Selection	19
C. Properties of the Annealed Material	20
1. Optical microscopy	20
2. X-ray diffraction	22
3. Mechanical properties	22
4. Lattice parameter of austenite	23
5. Density of pure austenite	23
D. Thermomechanical Processing and Cryogenic Testing	24
E. Metallography	25
1. Determination of the nature of transformation products	25
2. Determination of the amounts of transformation products	25

		Page
	a. Density measurements	25
	b. Magnetic measurements	27
	3. Morphology of the product and parent phases	30
III.	RESULTS AND DISCUSSION	31
	A. Structure and Properties of the Annealed Material	31
	1. Structure and physical properties	31
	2. Mechanical properties	35
	B. Effects of Processing Parameters on Structure and Mechanical Properties	39
	1. Effects of temperature and level of deformation on structure and mechanical properties	41
	2. Effects of aging temperature on structure and mechanical properties	45
	a. Specimens cryoformed and tested at -196°C	45
	b. Specimens cryoformed at -73°C and tested at -196°C	55
	c. Specimens deformed at room temperature (25°C) and tested at -196°C	68
	C. Effects of Processing Parameters on Martensite Stability	71
	D. Morphology of the Transformation Products	73
	E. Optimum Effects of Cryoforming and Aging on Cryogenic Mechanical Properties	83
	F. Correlations Between Structure and Mechanical Properties	90
	1. Naturally aged specimens	91
	2. Artificially aged specimens	94
IV.	CONCLUSIONS AND RECOMMENDATIONS	97
	A. Conclusions	97
	B. Recommendations	99

			Page
V.	REFERENCES		101
VI.	ACKNOWLEDGMENTS		109
VII.	APPENDIX A.	MARTENSITE VOLUME FRACTION DETERMINATION	110
VIII.	APPENDIX B.	LATTICE PARAMETERS OF AUSTENITE AND MARTENSITE	116
IX.	APPENDIX C.	CARBIDE PARTICLE SIZE ATTAINABLE BY DIFFUSION CONTROLLED GROWTH DURING AGING	120
X.	APPENDIX D.	ESTIMATE OF PARTICLE SIZE AND MEAN INTERPARTICLE SPACING FOR EFFECTIVE STRENGTHENING BY PRECIPITATES	123

LIST OF SYMBOLS

A_o	original cross sectional area of tensile specimen
Ar	area reduction
M_s	temperature at which spontaneous allotropic transformation would occur
M_d	highest temperature at which allotropic transformation can be induced by plastic deformation
N	number of data points
S_u	tensile strength
S_y	yield strength
ΔS_y	increase in yield strength
$V_{\alpha'}$	volume fraction of martensite
W_a	weight of specimen in air
W_w	weight of specimen in water
a_γ	lattice parameter of austenite
$a_{\alpha'}$	lattice parameter of martensite
d	mean interparticle spacing of precipitates
r	mean particle radius
ϵ	true strain
ϵ_u	true strain at maximum load
ρ	density of specimen
ρ_α	density of pure martensite
ρ_γ	density of pure austenite
σ	specific saturation magnetic moment of specimen
σ_s	specific saturation magnetic moment of pure martensite
μ	saturation magnetic moment of specimen

I. INTRODUCTION

A major concern of physical and process metallurgists is the development of new techniques for improving the properties of existing engineering materials. Thermomechanical treatment, the strengthening of materials by combining plastic deformation and phase transformation, is one of them.

Several definitions of thermomechanical processing have been offered (1-3). Duckworth (1) offers the most precise definition of thermomechanical processing as: "the use of deformation prior to or during an allotropic change so as to obtain an improvement in mechanical properties."

Cryoforming involves strengthening by transformation during plastic deformation. Since the process involves deformation at temperatures below ambient, its benefits can be attained mostly in materials with M_s and M_d temperatures below room temperature. M_s is the temperature at which spontaneous allotropic transformation would occur, while M_d is the highest temperature at which allotropic transformation can be induced by plastic deformation.

A. Literature Review

Binder (4), Krivobok and Talbot (5), McDowell and Mihalisin (6) and several other authors (7-31) have studied the improvement of the mechanical properties of various materials produced by cryoforming. Prominent among the materials known

to be favorably affected by cryoforming are the austenitic stainless steels. Deformation at cryogenic temperatures induces martensitic transformation leading to improved strength.

1. Factors influencing the effectiveness of cryoforming

The effectiveness of the process is dependent on the following variables:

a. Alloy composition

b. Austenitizing temperature

c. Deformation temperature

d. Amount of deformation

e. Type of deformation

f. Rate of deformation.

a. Alloy composition Post and Eberly (32) have defined a stability factor for austenitic stainless steels based on the equivalent nickel content of the alloy. Their relationship predicts a destabilizing effect of manganese and carbon, and contradicts the expected effects of these elements on austenite stability (33). Eichelman and Hull (34), on the other hand, have defined a stability factor, S, which is consistent with the expected effects of the alloying elements on the stability of austenite:

$$S = (Ni) + 0.68\,(Cr) + 0.55\,(Mn) + 0.45\,(Si) + 27\,(C + N) \qquad (I\text{-}1)$$

The weight percent of each element is inserted in the corresponding parentheses. Higher S values indicate greater

stability. They have also derived the following equation for determining the M_s temperatures of 18-8 type stainless steels:

$$M_s(^{\circ}F) = 75\ (14.6\text{-Cr}) + 110\ (8.9\text{-Ni}) + 60\ (1.33\text{-Mn}) + 50\ (0.47\text{-Si}) + 3000\ [0.068 - (C+N)] \qquad (I\text{-}2)$$

Angel (35) has derived a similar relationship between composition and $M_{d_{30}}$, the temperature at which 30% strain would produce 50% martensite. This temperature was selected as an arbitrary measure of the stability of the alloys during plastic deformation, since actual M_d would be difficult to determine experimentally. Similar relationships have been derived for austenitic steels in both the annealed and hot worked condition by Gerberich et al. (36).

All the relationships cited above underscore the effect of composition on the stability of austenitic steels. Experimental results by Binder (4), Krivobok and Talbot (5), McDowell and Mihalisin (6) and Llewellyn and Murray (7) support the proposition that increasing alloy content stabilizes the austenite. Thus the lower alloy austenitic stainless steels, 301, 302, and 304, are less stable than the 310 and 316 grades. The mechanical properties of the lower alloy grades are therefore more significantly improved by cryoforming than those of the higher alloy grades.

b. Austenitizing temperature The austenitizing temperature affects the grain size of the material and the extent to which alloying elements are dissolved. A lower austenitiz-

ing temperature leads to smaller grain size which promotes higher strengthening by thermomechanical treatments. The "unit" size of the martensite formed during processing is proportional to the grain size of the austenite from which it was formed (37, 38). There is usually a range of grain sizes in the martensite formed. The first plates formed are limited to the austenite grain size since martensite plates do not cross the austenite grain boundaries, while the last plates are formed in an austenite region subdivided by the existing martensite. Thus smaller austenitic grains lead to smaller average martensite "unit" sizes. Refinement of the martensite leads to increased strength and ductility. Smaller "grains" have shorter distances between dislocation sources and grain boundary barriers. For a given applied stress, dislocation sources can generate fewer dislocations before becoming inoperative leading to improved strength (39, 40). In addition, the number of dislocations piled up at a grain boundary decreases as the "units" become smaller. This reduces the likelihood of crack initiation and increases the ductility. The austenitizing temperature also affects the solution of carbon and other alloying elements which influence hardenability or may subsequently combine to form precipitates. For precipitation hardenable steels, the higher the austenitizing temperature, the more alloying elements go into solution and the better is the response to post-deformation aging (41).

c. Deformation temperature Angel (35) observed a strong influence of deformation temperature on the course of the martensitic transformation in austenite stainless steels. The higher the deformation temperature, the larger is the amount of deformation required to produce a specified volume fraction of martensite. As temperature decreases, the free energy difference between martensite and austenite decreases (42). Thus, the energy required for transformation decreases and the amount of martensite produced by a specified amount of deformation increases. Experimental results obtained by McDowell and Mihalisin (6) and Fiedler et al. (8) corroborate those of Angel.

Chukleb and Martynov (10) have observed that deformation of an austenitic steel at -183°C produced 25 to 30 times as much martensite as the same amount of conventional cold work would produce. Thus deformation at the lower temperature enhanced the mechanical properties more than conventional cold work. Decreasing deformation temperature increases the strain hardening rates of both retained austenite and martensite. The increased dislocation density associated with increased strain hardening rate results in larger improvements in strength.

d. Amount of deformation For any deformation temperature, larger amounts of deformation produce more martensite and therefore larger improvements in strength. Angel (35) has observed that the martensite content of an 18-8 stainless steel is related to strain by the relationship:

$$\ln \frac{f}{1-f} = n \ln \epsilon + k \qquad \text{(I-3)}$$

where:

$f = \frac{V_{\alpha'}}{V_T}$

V_T = maximum volume fraction of martensite that can be produced by plastic deformation

$V_{\alpha'}$ = volume fraction of martensite

ϵ = true strain

n,k = constants; n is dependent on temperature and alloy composition while k is dependent on composition only.

Gerberich et al. (36) have proposed that the volume fraction of martensite, $V_{\alpha'}$, produced by cryoforming previously deformed TRIP steels is related to the strain ϵ by a parabolic equation:

$$V_{\alpha'} = m\epsilon^{\frac{1}{2}}$$

For a given set of test conditions, m is a constant referred to as the stability coefficient, high m values denote lower stability. The value of m is zero at the M_d temperature and increases as temperature decreases below M_d. As the deformation temperature decreases, the rate of transformation with strain increases and the amount of deformation required to produce a specified amount of martensite decreases.

Greater deformation and decreasing deformation temperature produce more martensite. The exact values of the parameters, n, k, and m, depend on material composition and processing conditions.

Maxwell et al. (11) have observed two types of martensite in deformed TRIP steels. The first, stress-induced, was formed at low stresses before plastic deformation had started. The second, strain-induced, was produced by plastic strain. They have noted that in the presence of stress-induced martensite exact functional relationships could not be derived between true strain, ϵ, and the martensite content, V_α,.

e. Type of deformation Patel and Cohen (42) have proposed a thermodynamic model for the effect of applied stress on the martensitic transformation. They observed that

1. Shear stresses always induce the martensite transformation while uniaxial stresses may either promote or inhibit it, depending on whether they are tensile or compressive.
2. The M_d temperature is raised by tensile and shear stresses and lowered by compressive stresses and hydrostatic pressure.

f. Rate of deformation Bressanelli and Moskowitz (43) have reported a lowering of the cryogenic tensile strength and degree of martensitic transformation in 301 stainless steel when the test speed was increased from 0.1 in./min to 0.5 in./min. No significant changes were observed in the tensile strength when the cross head speed was further increased up to 1000 in./min. They observed serrations in the load elongation curve of 301 stainless steel tested at a slow speed 0.5 in./min but none at high speed (20 in./min). The sudden

drops in load were attributed to localized necking and martensite transformation in the necked region. The recovery in the load was due to the strengthening effect of the martensite. After localized strengthening occurred in that region, the deformation proceeded in areas away from the original neck. Similar tests on the more stable 310 austenitic steel revealed no serrations. Herzog et al. (12) have reported that a change in strain rate from 0.05 min^{-1} to 1.5 min^{-1} had no effect on the mechanical properties of several cryoformed materials including some austenitic stainless steels. It is suggested that the effects of deformation rate would depend on the range of strain rates investigated as well as the stability of the austenite.

2. Effect of post-deformation aging temperature and time

Several investigators have reported further increases in the strength of cryoformed austenitic steels upon subsequent aging (5, 9, 10, 12-18). Chukleb and Martynov (10) observed that along with increased hardness, the magnetic susceptibility of a cryoformed 18-8 type stainless steel increased after aging between 225°C and 425°C. They established that the optimum aging temperature of the alloy was 400°C and that the time response of the aging process was significant only during the first hour at elevated temperatures. They have proposed that the strengthening was due to carbide precipitation and further martensitic transformation but failed to present quantitative

estimates of their respective contributions to strength.

Floreen and Mihalisin (19) have suggested that further strengthening can occur during aging only if there is some retained austenite in the cryoformed material. They attribute the strengthening to the thermally induced transformation of some retained austenite into martensite. Mangonon and Thomas (20, 21) suggest the same mechanism for the secondary strengthening of thermomechanically treated 304 stainless steel. They have observed carbide precipitates in the matrix but neglected their contribution to strengthening.

In a recent review of his own research on martensite, Kurdjumov (44) has observed that a redistribution of carbon atoms in freshly formed martensite occurs in heating from cryogenic temperatures to room temperature. This results in a decrease in the c/a ratio for martensites of "abnormally high" tetragonality and an increase in the c/a ratio for martensites of "abnormally low" tetragonality. Normal tetragonality was defined by:

$$c/a = 1 + 0.046\ (\%C)$$

Kurdjumov also reported that for carbon contents of up to 0.2 percent room temperature is the transition point from the tetragonal to a cubic lattice.

3. Strengthening mechanisms

The strength of cryoformed austenitic stainless steels has been attributed to the formation of stress- and strain-

induced martensite (4-31). Higher levels of deformation increase the amount of martensite produced, providing larger strengthening. Only Chukleb and Martynov (10) have attributed part of the secondary hardening after aging to the precipitation of carbides. They do not present any quantitative estimates of the strengthening due to precipitates. Mangonon and Thomas (20, 21) have derived a linear relationship between the yield strength and the martensite content of thermomechanically treated 304 stainless steel. Their formulation has neglected any contributions due to work hardening and carbide precipitation, even though the latter was observed in the aged specimens. Instead, they have attributed a significant amount of secondary hardening to a disproportionately small amount of thermally induced martensite.

Novikov and Gorodyskii (17) have reported linear relationships between both the cryogenic yield and tensile strengths and the volume fraction of martensite in cryoformed 310 stainless steel. They have not investigated the effects of testing temperatures, other than those at which cryoforming was carried out. It is expected that the occurrence of further martensitic transformation in partially transformed specimens would contribute to improved strength and ductility. The work hardening rate increases with increasing martensite content. Bressanelli and Moskowitz (43), Zackay et al. (45), and Rosen et al. (46) have observed that a martensitic transformation may be either beneficial or detrimental to ductility. While

too little martensite fails to prevent the progress of necking, too much causes premature failure in the brittle martensite. Since further martensitic transformation affects the ductility and tensile strength, only the yield strength is directly related to the martensite content after thermomechanical treatment.

The work hardening contribution of both the martensite and the retained austenite to yield strength has been neglected. For specimens deformed below the M_d temperature both martensitic transformation and extensive strain-hardening of the freshly formed martensite and retained austenite occur during the latter stages of deformation. Therefore, work hardening should contribute significantly to the yield strength of specimens cryoformed to high strain levels.

4. The martensite transformation in austenitic steels

The martensitic transformation can be induced in austenitic steels either spontaneously or as a result of plastic deformation (7, 10, 12-14, 22, 24, 47-63). An overwhelming majority of the investigators have reported that the sequence of the transformation is $\gamma \rightarrow \epsilon \rightarrow \alpha'$ (i.e., fcc → hcp → bcc) (20, 21, 47-50). On the other hand, a few researchers have failed to observe the hcp ϵ phase in partially transformed austenitic steels (51-53). Reed (54) has proposed that for ϵ to form, every $(111)_\gamma$ plane must fault and that if the faulting periodicity is random, stacking faults are formed

in place of ϵ. Otte (55) has observed that the ϵ phase is an ordered arrangement of stacking faults and that its formation is markedly promoted by chromium and manganese. In a study of the effects of cyclic loading on 301 and 304 steels, Henessy et al. (53) have noted that the α' phase can form either from γ or from ϵ. Breedis (56) and Lecroisey and Pineau (57) have observed that the morphology of the transformation products is dependent on composition. Composition, along with temperature determines the relative free energies of the three phases as well as the stacking fault energy of the austenite. The stacking fault energy determines the deformation behavior of austenite and influences the nucleation and morphology of the product phases. Since the stacking fault energy decreases with decreasing temperature, lower deformation temperatures favor stacking fault formation. These faults may form as an hcp ϵ phase.

Fahr (26) and Maxwell et al. (11, 27) have observed different morphologies for stress-induced and strain-induced martensites. The stress-induced martensite was plate-like, while the strain-induced type appeared along slip bands as "sheaves of fine parallel laths strung out on $(111)_\gamma$ planes" (26). Fahr observed that between the M_s and M_d temperatures the transformation could be either stress-induced or strain-induced.

The general consensus of most investigators is that in both the $\gamma \rightarrow \epsilon$ and $\gamma \rightarrow \alpha'$ transformations, the close packed

planes and directions are parallel in the parent and product phases (11, 20, 21, 26, 27, 49, 50, 52, 56, 60, 61), i.e.:

$$(111)_\gamma \parallel (0001)_\epsilon \quad , \quad [0\ \bar{1}\ 1]_\gamma \parallel [\bar{1}\ 2\ \bar{1}\ 0]_\epsilon$$

$$(111)_\gamma \parallel (110)_{\alpha'} \quad , \quad [\bar{1}\ 0\ 1]_\gamma \parallel [\bar{1}\ 1\ 1]_{\alpha'}$$

This is in agreement with the orientation relationship proposed by Kurdjumov and Sachs (58).

B. Relevance and Scope of This Study

Cryoforming is slowly becoming a part of modern industrial practices. Foster Wheeler Corporation (29) and Arde Inc. (64) have successfully applied cryogenic explosive forming and stretch forming respectively to the manufacture of 301 stainless steel pressure vessels.

A large proportion of previous investigations into the effects of cryoforming on austenitic stainless steels have involved property evaluation at room temperature. Since these materials also find widespread application at cryogenic temperatures, detailed studies of cryogenic properties would complement well the knowledge available. More information on the effects of test and cryoforming temperatures on mechanical properties would contribute to a better understanding of the process. The exact nature of the secondary strengthening phenomenon of cryoformed and aged austenitic stainless steels is yet to be established. It is felt that while thermally induced α' may partially contribute to the strengthening, the effects of carbides and the strain hardening characteristics

of the martensite and austenite play a more significant role than has been previously proposed (17, 20, 21).

It is the purpose of this study to investigate the effects of deformation temperature, level of deformation, and post-deformation aging on the cryogenic mechanical properties of a cryoformed and aged austenitic stainless steel.

Specimens were cryoformed and tested in tension at -196°C and -73°C. The effects of three levels of deformation, representing 50%, 75%, and 90% of the strain at maximum load for each deformation temperature, were investigated. Specimens aged at temperatures ranging from 25°C to 500°C were tested at -196°C to determine an optimum aging temperature. Testing at -73°C was carried out only on specimens subjected to optimum thermomechanical processing. Transmission electron microscopy, x-ray diffraction, precision density and magnetic susceptibility measurements were used to establish the microstructural changes accompanying the processing.

Qualitative and quantitative correlations between microstructure and mechanical properties were established. Mechanisms have been proposed to explain the improvement of the cryogenic mechanical properties due to thermomechanical treatment.

II. EXPERIMENTAL PROCEDURE

A. Cryoforming and Testing Equipment

Cryoforming and testing were carried out on a SATEC 20GBN universal testing machine modified for cryogenic testing as shown in Figure 1. A stainless steel dewar was fitted with pull rods and pin connectors to facilitate tensile loading. The size of the dewar and lengths of the pull rods were selected so that during testing the specimen was completely submerged in the cryogenic medium (Figure 2). This ensured that no temperature gradient existed along the length of the specimen and also reduced thermal fluctuations in the cross section to a minimum. The lower pull rod was permanently threaded to the dewar bottom and properly sealed. During deformation, the entire cryostat assembly moved with the lower crosshead. The movement was monitored with a SATEC model PD-3M deflectometer. Load elongation curves were plotted on a Leeds and Northrup model 660 chart recorder.

Flat, pin loaded, tensile specimens of the configuration shown in Figure 3 were used. After each sample had been loaded into the dewar, the cryostat was filled with the cryogenic medium and the system allowed to come to equilibrium before deformation was started. To avoid preloading, the lower pin holes were slightly elongated to allow room for the contraction of the specimen.

All cryostraining and testing were carried out in tension

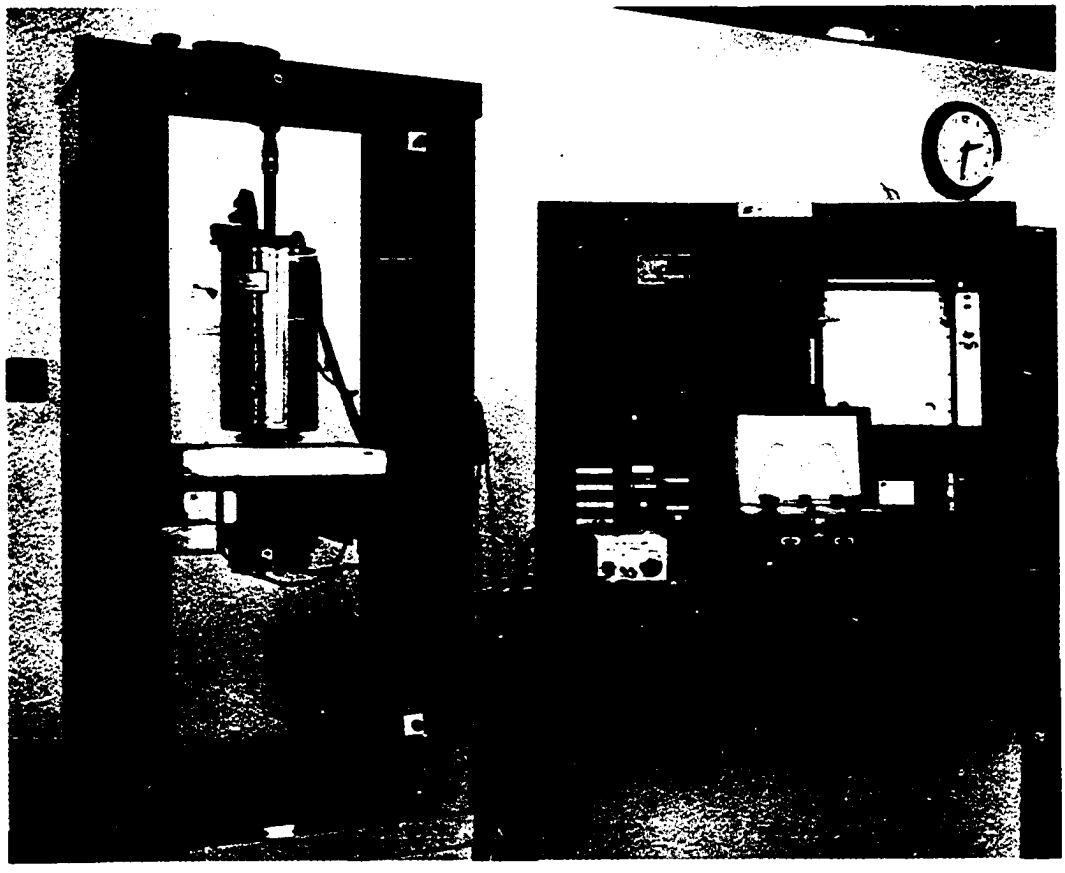

Figure 1. SATEC Model 20 GBN Universal Testing Machine modified for cryogenic testing.

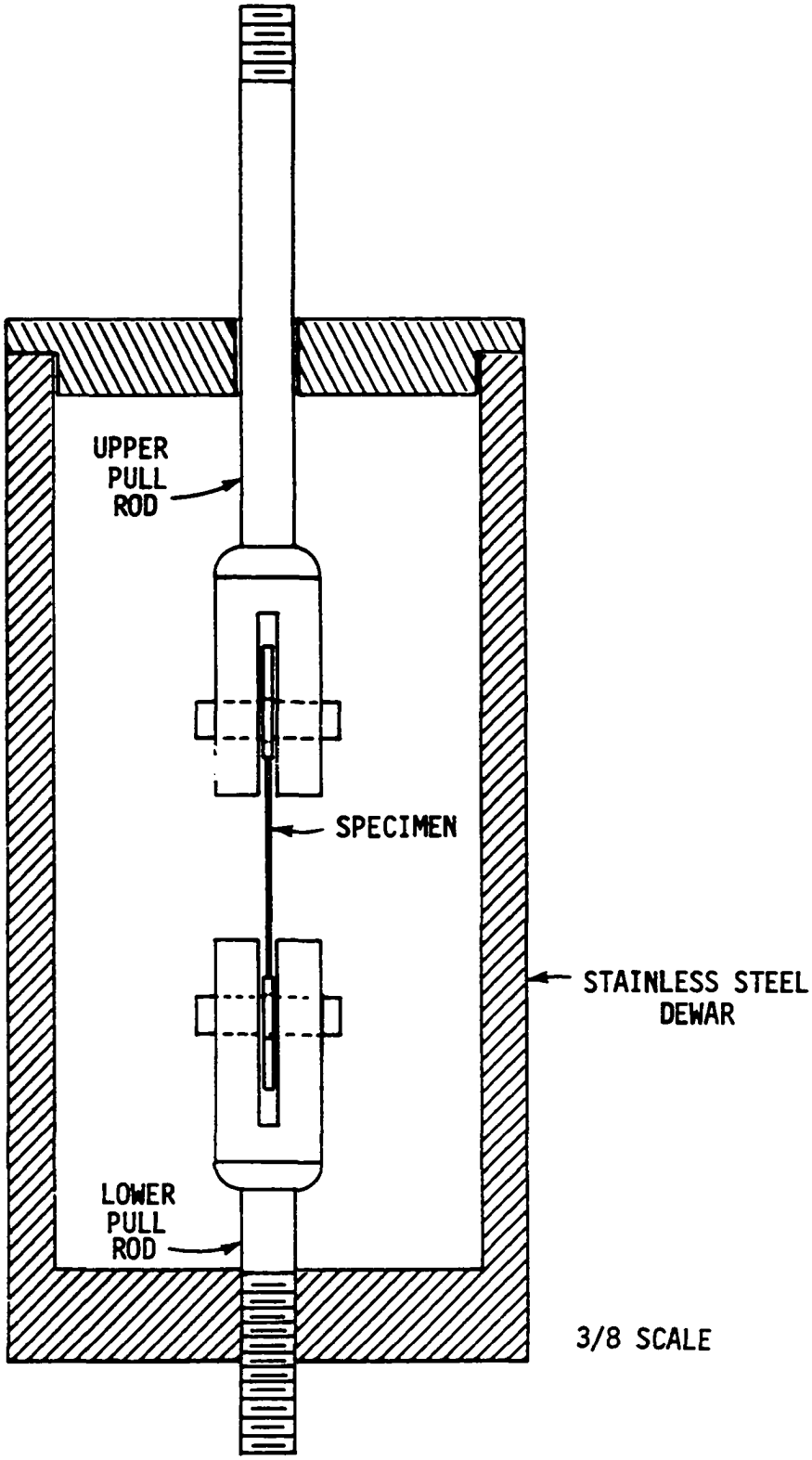

Figure 2. Section through cryostat showing the relative sizes of specimen and pull rods. (3/8 mm = 1 mm)

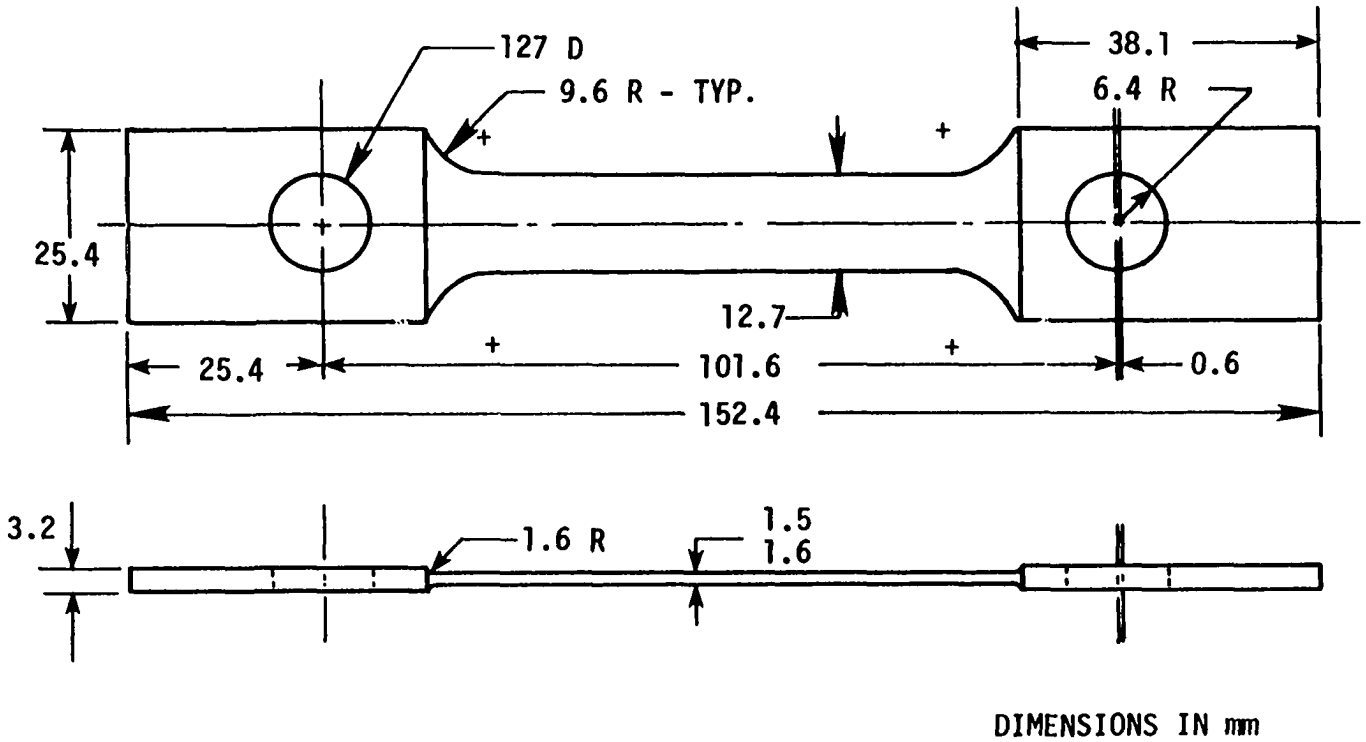

Figure 3. Configuration of cryostraining specimen.

at -196°C and -73°C. Some specimens were also deformed at room temperature to serve as a basis for evaluating the advantages of cryoforming. For cryostraining and testing at -196°C, liquid nitrogen was used as the cryogenic medium. For deformation and testing at -73°C, the cryostat was filled with isopropyl alcohol and liquid nitrogen was circulated through a copper coil placed in the dewar. The temperature of the alcohol was controlled by a solenoid valve regulated by a potentiometer and thermocouple. A second thermocouple was used to measure the temperature of the bath periodically. It was possible to control the bath temperature to within $\pm$ 5°C during a deformation process.

Initially, a crosshead speed of 0.1 in./min, corresponding to a strain rate of approximately 0.05 min^{-1}, was used for cryostraining and testing. The effects of a tenfold increase in strain rate were investigated for a few specimens which exhibited a "burst" phenomenon during testing.

B. Material Selection

It has been observed that the lower grade austenitic stainless steels are most favorably affected by cryoforming. Binder (4), Krivobok and Talbot (5), and Llewellyn and Murray (7) have all reported that the 301, 302 and 304 austenitic stainless steels are more responsive to cryoforming than the 310, 316 and 347 types. To complement the information already available on these materials, 302 stainless steel was selected

for this study.

The material was purchased in the annealed condition from a single heat in strips 0.3 cm thick by 2.5 cm wide. Chemical analysis from three different strips yielded the results shown in Table 1. It was noted that the chromium contents in two of the three specimens fell outside the standard specification for 302 steel. Since compositions listed in Table 1 fall within those of the low grade austenitic stainless steels, the material was considered suitable for this study. In spite of the high chromium content, the M_s temperature as estimated from Eichelman and Hull's relationship (34) is -205°C which is still lower than the two cryogenic temperatures. Therefore, a spontaneous martensitic transformation was not expected.

C. Properties of the Annealed Material

1. Optical microscopy

Samples of the as-received material were mounted, ground and electropolished in a 6% perchloric acid - methanol solution at -70°C. They were then etched in a solution consisting of 10 parts nitric acid, 10 parts acetic acid, and 15 parts hydrochloric acid and a few drops of glycerol. The approximate grain size of the material was determined by comparison with standard ASTM grain size charts. Optical micrographs were obtained from the prepared samples using a Bausch and Lomb bench metallograph.

Table 1. Composition of steel investigated[a]

C	Mn	P	S	Si	Ni	Cr	Mo	Cu	Ti	Al
0.07	1.89	0.023	0.018	0.50	8.71	18.50	0.34	0.025	<0.01	<0.01
0.07	1.89	0.030	0.018	0.50	8.50	19.33	0.30	0.025	<0.01	<0.01
0.07	1.89	0.030	0.018	0.52	8.60	19.33	0.30	0.025	<0.005	<0.005

[a]Analysis provided by Chicago Spectro Service Laboratory Inc.

2. X-ray diffraction

To ensure that the material was all austenitic, an x-ray diffraction pattern was obtained from the metallographic specimen using CuK_α radiation and a bent LiF monochromator. The range of 2θ values covering the strongest peaks of the γ, ε, and α' phases was scanned. The peaks of interest were $(111)_\gamma$, $(110)_{\alpha'}$, $(10.1)_\epsilon$, $(200)_\gamma$, and $(200)_\alpha$, (65).

3. Mechanical properties

Uniaxial tensile testing was carried out on the annealed material at -196°C, -73°C and room temperature (25°C). Tensile strength, yield strength and percent area reduction were determined.

Separate experiments were carried out at each temperature to determine ϵ_u, the strain at maximum load. Since the specimen was completely enclosed in the dewar, it was not possible to determine ϵ_u by monitoring the change in dimensions in the gage region during testing. A pair of light marks were made 5.0 centimeters apart in the gage region of a number of specimens. A minimum of two specimens were then deformed to maximum load at each of the three temperatures and unloaded. From the elongations in the original two-inch region ϵ_u values were obtained. The values of ϵ_u obtained at the three temperatures served as a basis for establishing the prestraining levels. Since the cryoforming was done in tension, the ϵ_u values were the maximum uniform strain levels to which the specimens could

be deformed. At each prestraining temperature, specimens were deformed to 50%, 75% and 90% of ϵ_u, respectively.

4. Lattice parameter of austenite

A rectangular sliver, about 0.03 cm^2 x 0.5 cm was carefully machined from the as-received austenitic stainless steel stock. It was electropolished to about half the original size. A Debye-Scherrer diffraction pattern was obtained from this wire using CrK_α radiation at 18 milliamps and 40 kV.

The lattice parameter for austenite was determined from the indexed pattern by a least squares extrapolation with the Nelson-Riley coefficient (66).

5. Density of pure austenite

The weight-in-air, weight-in-fluid technique described by Smakula (67) was used to determine the density of pure austenite. A piece of the material was electropolished to provide surfaces smooth enough to ensure good wetting during weighing in the fluid, and to eliminate surface martensite. The specimen was weighed in air, then in distilled water to which a drop of a wetting agent had been added. The density of austenite ρ_γ was obtained from the relationship:

$$\rho_\gamma = \frac{W_a}{W_a - W_w} \rho_w \qquad \text{(II-1)}$$

where

W_a = weight in air

W_w = weight in distilled water

ρ_w = density of distilled water.

The weighing was carried out on a Torbal microbalance capable of measuring to within 0.0001 g. The balance was placed in a constant temperature environment where air circulation was minimal. The pan on the balance was replaced by a small stainless steel wire bent into a hook at one end for holding the specimen. The temperature of the distilled water was maintained at 25°C ± 1°C. The density values were reproducible to within 0.01 g/cm^3.

D. Thermomechanical Processing and Cryogenic Testing

About 25 specimens were deformed to 50% and 90% of ϵu respectively at each of three temperatures: -196°C, -73°C and room temperature (25°C). They were subjected to aging treatments of up to 6 weeks at room temperature, and one hour at temperatures between 300°C and 500°C. A minimum of 3 specimens were subjected to each set of thermomechanical treatments, at least two of which were later tested at -196°C.

For each combination of prestraining parameters, the aging temperature producing the highest yield and tensile strengths along with acceptable ductility (Ar >10%) was selected as an optimum and used for further evaluation of the thermomechanical processing. Specimens were deformed 50% and 90% of ϵ_u respectively at each of the three temperatures. They were aged at the previously determined optimum aging temperatures and tested at -73°C.

To investigate the effects of an intermediate level of cryoforming, a number of specimens were deformed to 75% of ϵ_u at -196°C and -73°C. They were aged at an optimum temperature and tested at the two cryogenic temperatures.

E. Metallography

The nature and the amounts of the transformation products were determined by x-ray diffraction, density, and magnetic measurements. Optical microscopy and transmission electron microscopy were used to study the morphology.

1. Determination of the nature of transformation products

For each temperature and level of deformation, the gage region of a specimen was sectioned for x-ray diffraction studies. To determine the presence of the various phases, martensite (α' and ϵ), and austenite (γ), the range of 2θ values covering their strongest peaks was scanned. Since x-ray penetration was small, surface martensite had to be eliminated by electropolishing.

2. Determination of the amounts of transformation products

a. Density measurements From x-ray diffraction studies, it was observed that all the thermomechanically processed samples were either a mixture of martensite (α') and austenite (γ), or fully martensitic. The determination of the volume fraction of α' was based on a linear relationship between the density of the cryoformed specimen and the densi-

ties and volume fractions of the two phases (68). The density, ρ, of the partially transformed material is given by:

$$\rho = \rho_\gamma V_\gamma + \rho_{\alpha'} V_{\alpha'} \qquad \text{(II-2)}$$

where

ρ_γ, $\rho_{\alpha'}$ = densities of austenite and martensite respectively

V_γ, $V_{\alpha'}$ = volume fractions of austenite and martensite respectively

Noting that:

$$V_{\alpha'} + V_\gamma = 1 \qquad \text{(II-3)}$$

equation II-2 becomes

$$V_{\alpha'} = \frac{\rho_\gamma - \rho}{\rho_\gamma - \rho_{\alpha'}} \qquad \text{(II-4)}$$

Since a standard, 100% martensitic specimen was not available. the density of martensite was determined from a relationship between the density of austenite and the lattice parameters of austenite and martensite as follows:

$$\rho_{\alpha'} = \frac{a_\gamma^3}{2a_{\alpha'}^3}\,\rho_\gamma \qquad \text{(II-5)}$$

where

a_γ = lattice parameter for austenite

$a_{\alpha'}$ = lattice parameter for martensite.

A value of $a_\gamma = 3.5891$ Å was determined from the as-received material using the Debye-Scherrer method.

A specimen deformed to 90% of ϵ_u at -196°C was found by

x-ray diffraction to be fully martensitic. Using this specimen as a standard values of $a_{\alpha'}$ and $\rho_{\alpha'}$ were determined. An electropolished "wire" obtained from the standard specimen was used to measure a lattice parameter of $a_{\alpha'}$ = 2.8662 Å.

Error analysis on the relationships used showed that the technique is capable of determining percent martensite to within ± 5% (Appendix A.1); this variation was considered satisfactory.

Plastic deformation is known to introduce vacancies and other defects that reduce the material density. The effects of deformation on density have been considered negligible in this study. For example, for high purity iron, deformed 40% at -53°C, Rogers and Coffin (69) have reported reductions of the order of 0.005 g/cm^3. No such information is available on austenitic stainless steels. Due to the higher impurity content of the stainless steels, it is expected that larger reductions would be produced for identical amounts of deformation. The discrepancy between the calculated and measured densities of highly deformed specimens were of the same order of magnitude as the variation observed by Rogers et al. The effects of variations of this magnitude were shown to be insignificant (Appendix A.1).

b. Magnetic measurements A magnetometric method was used to double check the martensite volume fractions obtained by the density technique. Martensite is ferromagnetic while austenite is not. The volume fraction of α' was

determined from the relation:

$$V_{\alpha'} = \frac{\sigma}{\sigma_s} \qquad \text{(II-6)}$$

where

σ = saturation magnetic moment per unit mass for the thermomechanically processed specimen

σ_s = saturation magnetic moment per unit mass for pure martensite.

Similar relationships have been used by several investigators to determine the volume fraction of martensite in partially transformed austenitic steels (20, 21, 59). Magnetic saturation values were used since they depend on the structure only and are unaffected by any other changes caused by thermomechanical treatment (70).

An oscillating sample magnetometer schematically shown in Figure 4, was used to measure the saturation magnetic moments. The specimen was vibrated by a loudspeaker system. The oscillating magnetic field of the sample induced a voltage in a set of stationary coils placed close to the specimen. Magnetic moments were determined from this voltage by comparing the signals generated by the samples and a standard cylindrical nickel specimen. With the equipment available, only small samples ($\sim$0.03 cm^3) could be used for magnetic measurements. The samples were sectioned wet from the center of the gage length and electropolished before measurements were taken.

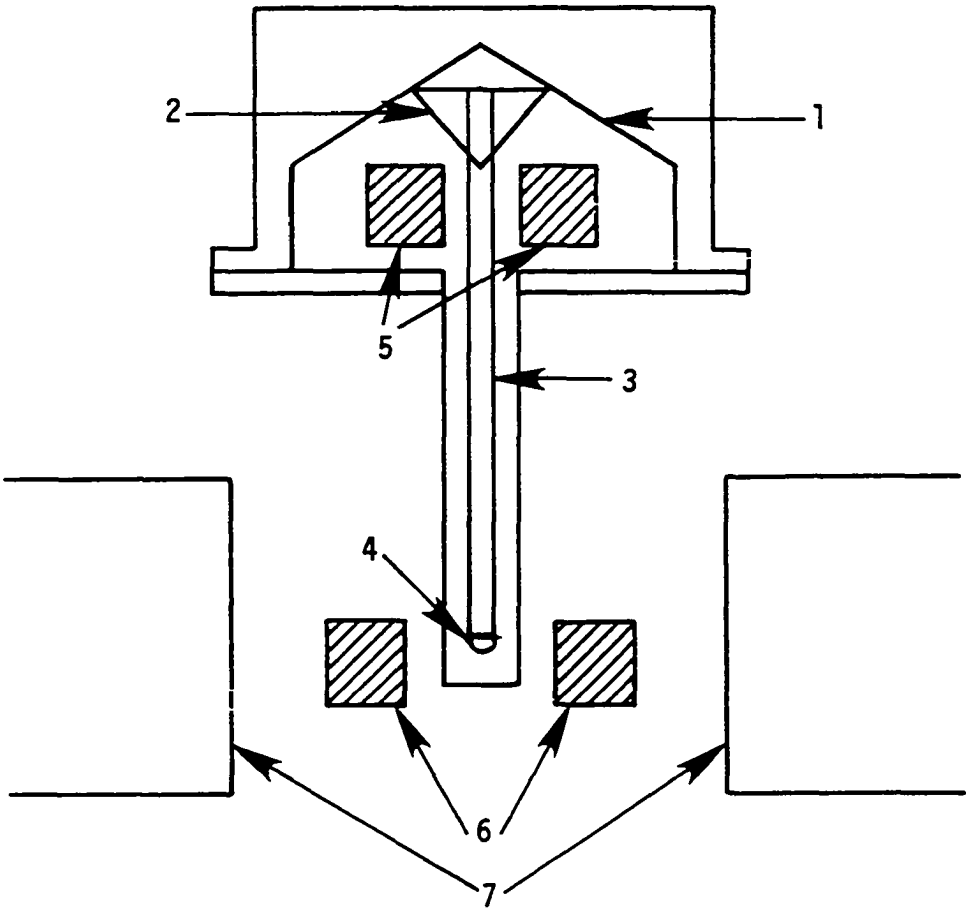

1. LOUDSPEAKER TRANSDUCER
2. CONICAL PAPER CUP SUPPORT
3. SPECIMEN HOLDER
4. SAMPLE
5. REFERENCE COILS
6. SAMPLE COILS
7. MAGNET POLES

Figure 4. Schematic drawing of vibrating sample magnetometer.

3. Morphology of the product and parent phases

Foils were prepared from samples taken from along the gage section of a select number of specimens. To avoid severe deformation in the foil, the specimens were first polished on a 320 grit emery paper to a thickness of about 0.02 cm and then on a 600 grit paper to about 0.01 cm. Discs, 0.3 cm in diameter, were punched out of the foils and electropolished in a 6% perchloric acid - methanol solution at 22 milliamps and 50 volts. The foils were examined in a Siemens Elmiskop-I transmission electron microscope operating at 100 kV and both the bright field and selected area diffraction micrographs were obtained. The remaining gage sections were used for optical metallography.

III. RESULTS AND DISCUSSION

A. Structure and Properties of the Annealed Material

1. Structure and physical properties

Optical micrographs of the as-received material are shown in Figure 5. The annealed ASTM grain size number is estimated to be between 6 and 7. This represents grain diameters ranging from 3.5×10^{-2} mm to 5×10^{-2} mm. The presence of several annealing twins and the absence of slip lines indicate that the as-received material was fully annealed.

The x-ray diffraction pattern of the annealed material revealed only the $(111)_\gamma$ and $(200)_\gamma$ peaks confirming that the annealed material was fully austenitic (Figure 6).

An indexed Debye-Scherrer powder diffraction pattern of the annealed material is shown in Figure 7. Using the Nelson-Riley correlation and a least squares curve fitting technique, a lattice parameter of $a_\gamma = 3.5891$ Å was obtained (Appendix B.1). This value compares favorably with those reported by Reed and Guntner and others (8, 48, 54, 55, 59, 71).

Results of the weight-in-air, weight-in-fluid technique for density measurement are shown in Table 2. The density of the pure austenite was determined to be 7.9584 ± 0.0029 g/cm^2 with a 95% confidence limit.

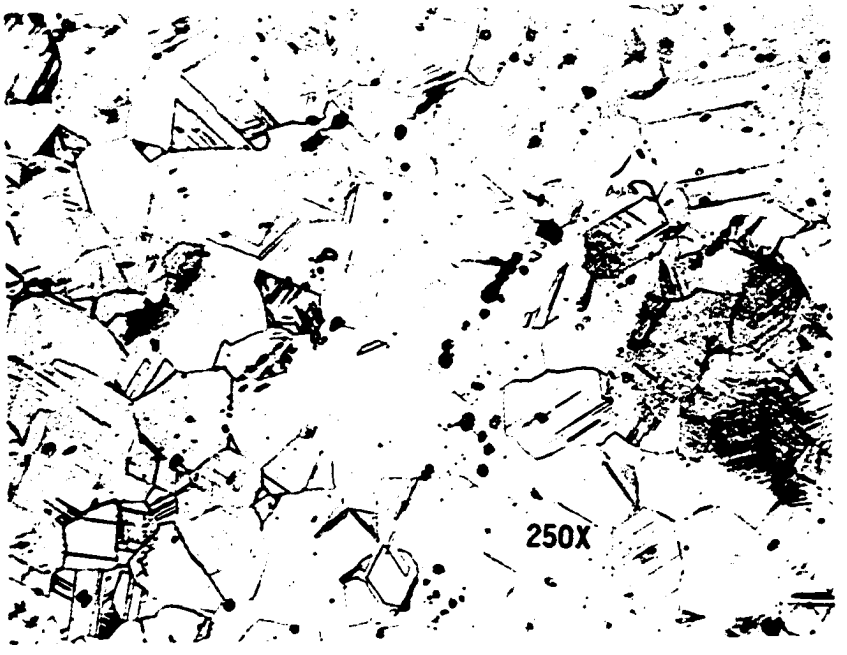

a.

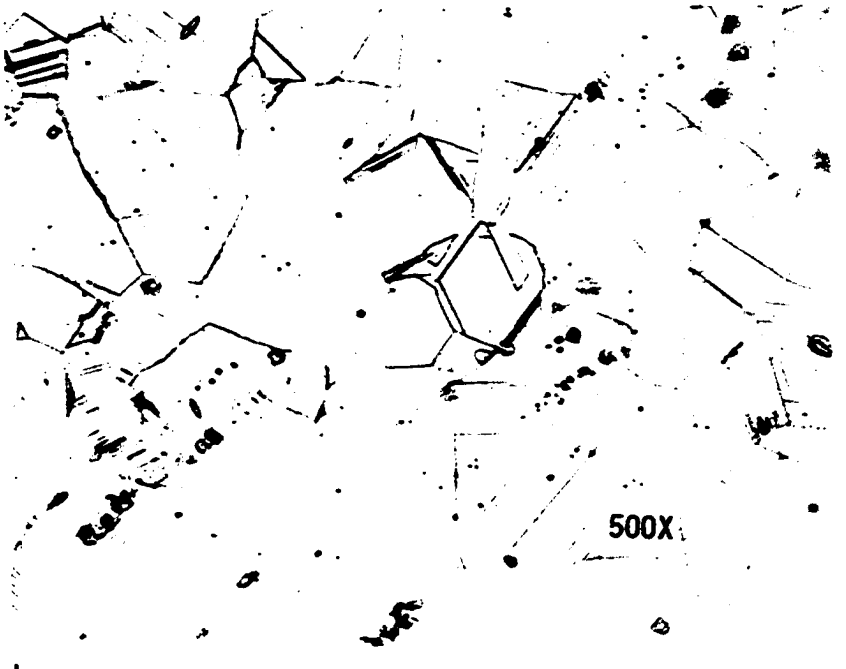

b.

Figure 5. Optical micrograph of the as-received austenitic stainless steel.

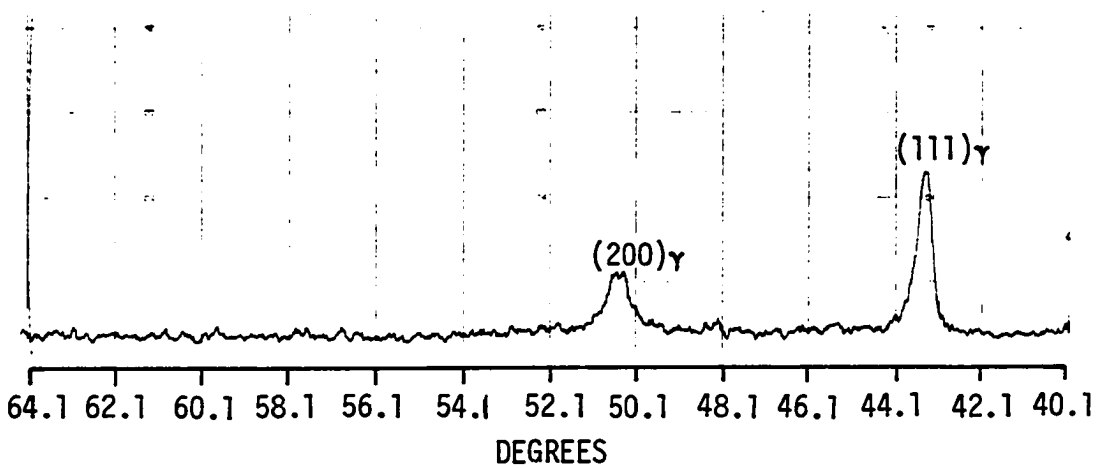

Figure 6. X-ray diffraction pattern obtained from as-received stock

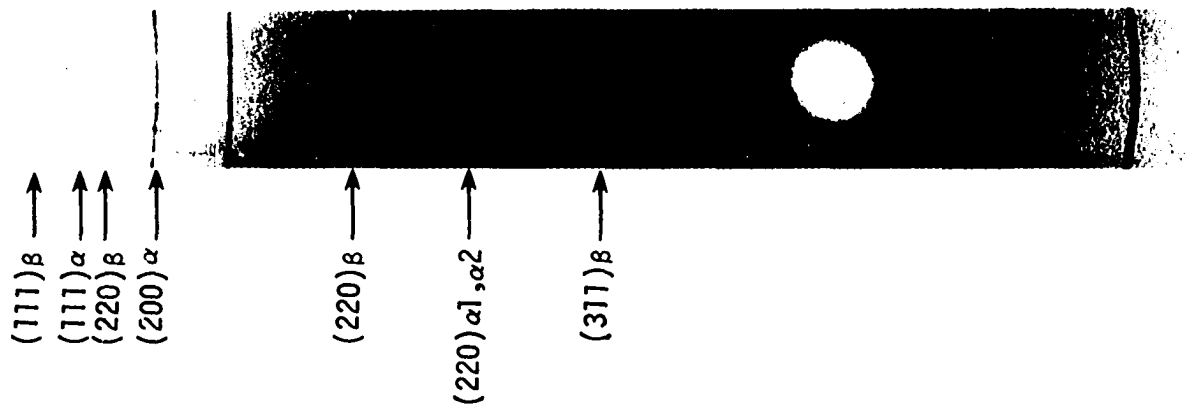

Figure 7. Debye-Scherrer diffraction pattern of the fully annealed material.

Table 2. Results of density measurement for austenite

Weight in air W_a g	Weight in water W_w g	Density ρ g/cm^2
2.8332	2.4772	7.9584
2.8332	2.4773	7.9606
2.8332	2.4772	7.9584
2.8332	2.4771	7.9562

2. Mechanical properties

The mechanical properties of the annealed material at -196°C, -73°C and 25°C are listed in Table 3. The tensile strength and the 0.2% offset yield strength increased while area reduction decreased with decreasing temperature. Only a minor reduction in strain at maximum load was observed between room temperature and -196°C. The high ϵ_u values obtained at -73°C and -196°C are attributed to the martensite transformation which tends to enhance ductility. The formation of strain induced martensite, after the initiation of necking, results in localized strengthening. Thus, further plastic deformation would occur only in austenite grains outside the transformed region.

The load-elongation curves obtained from the tests at the three temperatures are shown in Figure 8. Plateau regions, characteristic of rapid martensitic transformation, were ob-

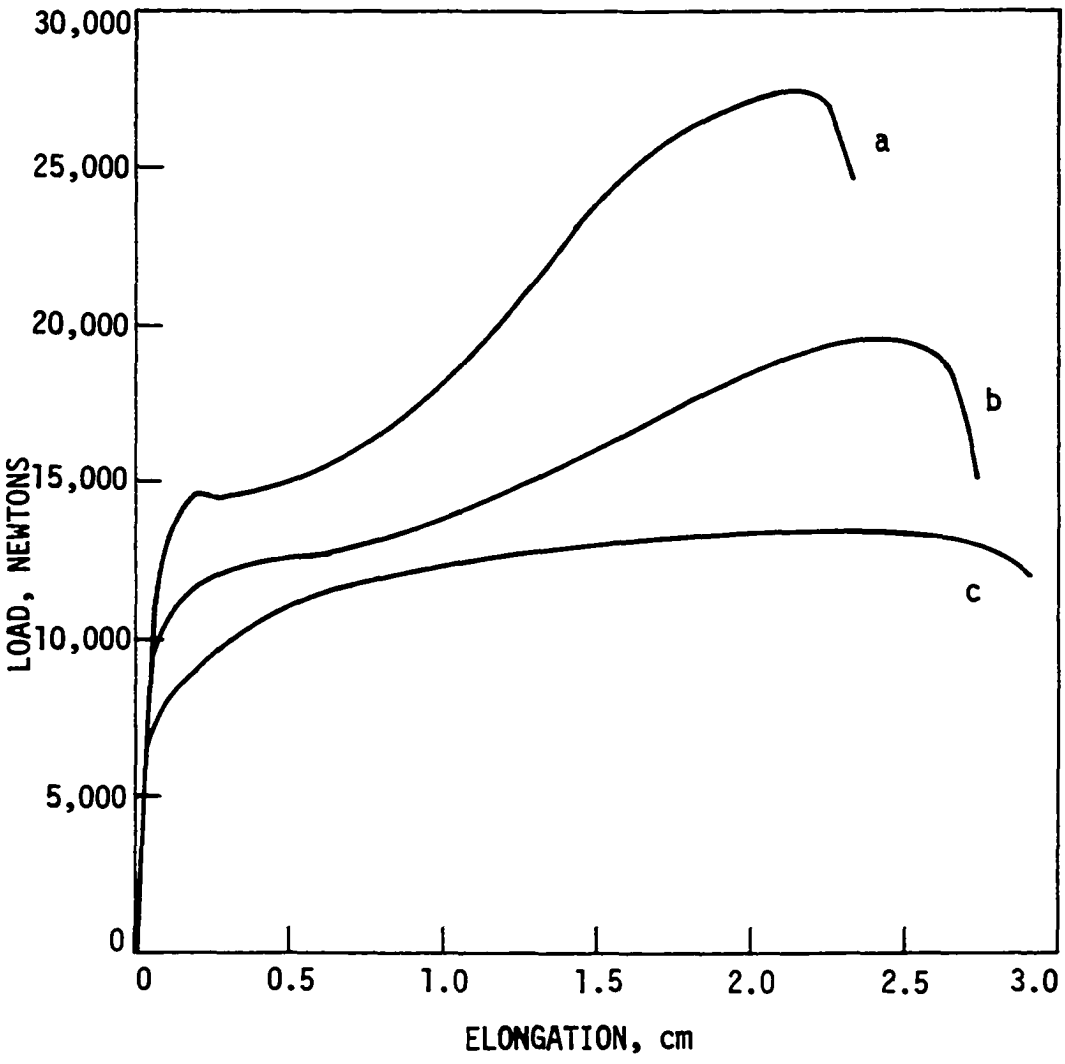

Figure 8. Load elongation curve of annealed austenitic stainless steel at: a. $-196^{o}C$, $A_o = 0.180\ cm^2$
b. $-73^{o}C$, $A_o = 0.176\ cm^2$
c. Room temperature, $A_o = 0.210\ cm^2$

Table 3. Mechanical properties of the annealed austenitic stainless steel alloy

Temperature T °C	Yield strength S_y MPa	Tensile strength S_u MPa	Strain at ultimate ϵ_u	Area reduction Ar %
-196	726	1549	0.33	34
	786	1579	0.32	30
-73	581	1104	0.36	42
	636	1097	0.36	42
25	413	656	0.36	48
25	439	645	0.36	46

served in the curves obtained by testing at -196°C and -73°C but not at room temperature. This was evidence that the M_d temperature of the alloy was higher than -73°C but lower than room temperature. The load-elongation curve of the material tested at room temperature showed only a strain hardening plastic region. On the other hand, those obtained by testing at the two cryogenic temperatures showed three different regions in the plastic range as shown in Figure 9. These regions have been identified as representing three distinct phenomena. The region a-b represents yielding and strain hardening of the parent austenite phase. The almost horizontal region b-c represents rapid martensitic transformation under applied stress. The region c-d represents work hardening of both retained austenite and freshly formed martensite, accompanied by further transformation of retained austenite to

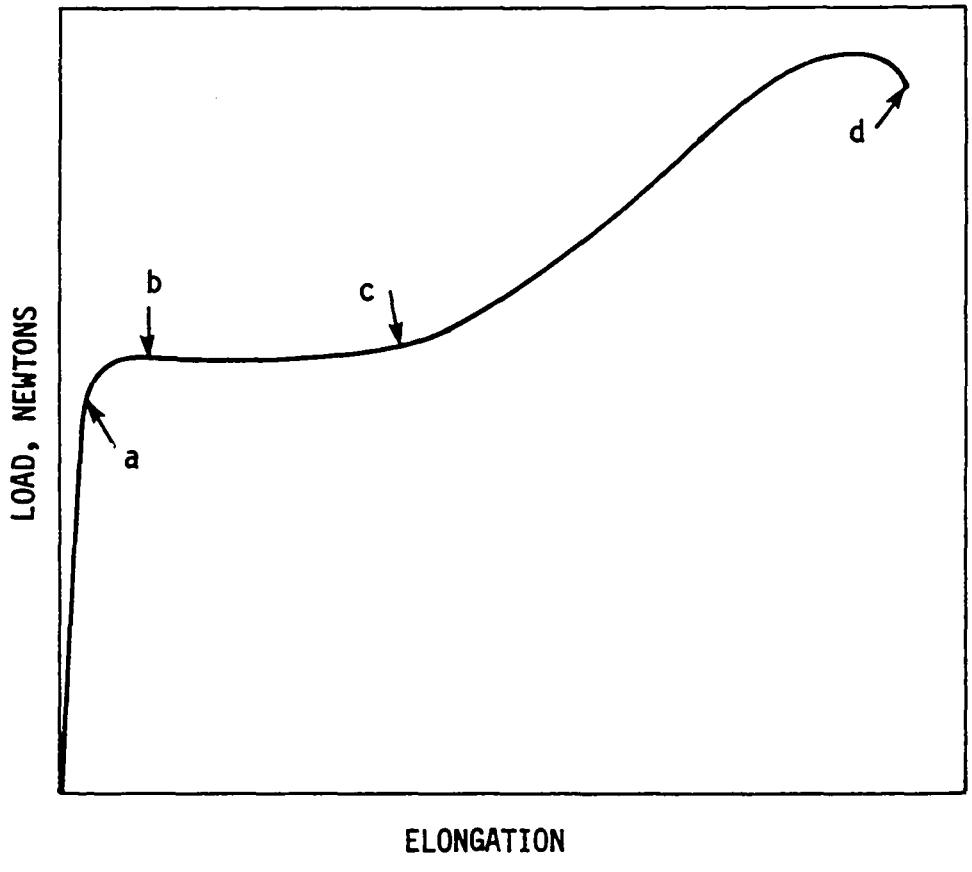

Figure 9. Schematic drawing of load-elongation curve for specimens deformed below M_d.

martensite. Similar results have been reported by Angel (35), Bressanelli and Moskowitz (43) and other investigators (11, 21, 26, 45, 46, 51).

A stimulating effect of applied stress on martensitic transformation is operative at the beginning of deformation, while a stabilizing effect exists during the latter stages. At the beginning of deformation, a threshold value of stress must be reached before transformation can start. This stress value is usually a function of chemical composition and increases with increasing alloy content and decreasing temperature of deformation. Once the transformation has started, it proceeds rather rapidly. This accounts for the flattening of the load elongation curve in region b-c. The decreasing reaction rate in the last stage of deformation is due to two effects both of which collaborate to reduce the rate of transformation. First, increased dislocation density in the austenite tends to inhibit the atomic movements required for martensitic transformation (26). Secondly, as the volume of retained austenite decreases with progressive deformation, the amount of austenite available for transformation decreases.

B. Effects of Processing Parameters on Structure and Mechanical Properties

The effects of processing parameters on mechanical properties have been evaluated by testing at -196°C. Testing at a second cryogenic temperature, -73°C, was only carried out

on specimens subjected to the combination of processing parameters producing optimum mechanical properties at -196°C. Specimens were deformed to both 50% and 90% of the strain at maximum load, ϵ_u, respectively. The effects of an intermediate deformation level, 75% of ϵ_u, were only evaluated on samples aged at an optimum aging temperature.

The levels of deformation and equivalent amounts of strain and percent elongation are shown in Table 4. The volume fraction of martensite, $V_{\alpha'}$, was determined by precision density and magnetic measurements. With the exception of a few naturally aged specimens, there was good agreement between the $V_{\alpha'}$ values obtained by the two techniques. Due to a restriction placed on the specimen size by the equipment available, the magnetic measurements were taken on small specimens which were susceptible to localized heating during sectioning. The localized heating caused some austenite reversion in a few of the naturally aged specimens, but had no effect on the artificially aged ones. The time at the slightly raised temperature was insufficient to cause any further transformations in the artificially aged specimens.

The density measurements have been obtained from large samples which were more representative of the bulk properties of the material. Thus in the specimens which showed significant discrepancies between the $V_{\alpha'}$ values obtained by the two techniques, the precision density values have been cited in the discussion.

Table 4. Prestraining levels

% ϵ_u	Deformation temperature °C	Elongation %	Average strain
50	-196	17-18	0.16
	-73	19-20	0.18
	25	19-20	0.18
75	-196	26-27	0.24
	-73	30-31	0.27
90	-196	32-33	0.29
	-73	36-38	0.32
	25	36-38	0.32

1. Effects of temperature and level of deformation on structure and mechanical properties

The yield strength and martensite content of specimens deformed at -73°C and -196°C increased with increasing amount of deformation (Figures 10 and 11). A linear relationship

$$V_{\alpha'} = A\epsilon + B \qquad \text{(III-1)}$$

where A and B are constants, fits the data. For a deformation temperature of -196°C, B = -0.02 and A = 3.85; for -73°C, B = -0.07 and A = 3.48. The constant A is identical to the transformation coefficient defined by Gerberich et al. (36). As the deformation temperature decreased below M_d, the stability of the austenite decreased and the rate of transformation with strain increased. The stacking fault energy (SFE) of the austenite is directly related to stability through its role in initiating the $\gamma \rightarrow \alpha'$ transformation. Since the SFE of Fe-Ni-Cr

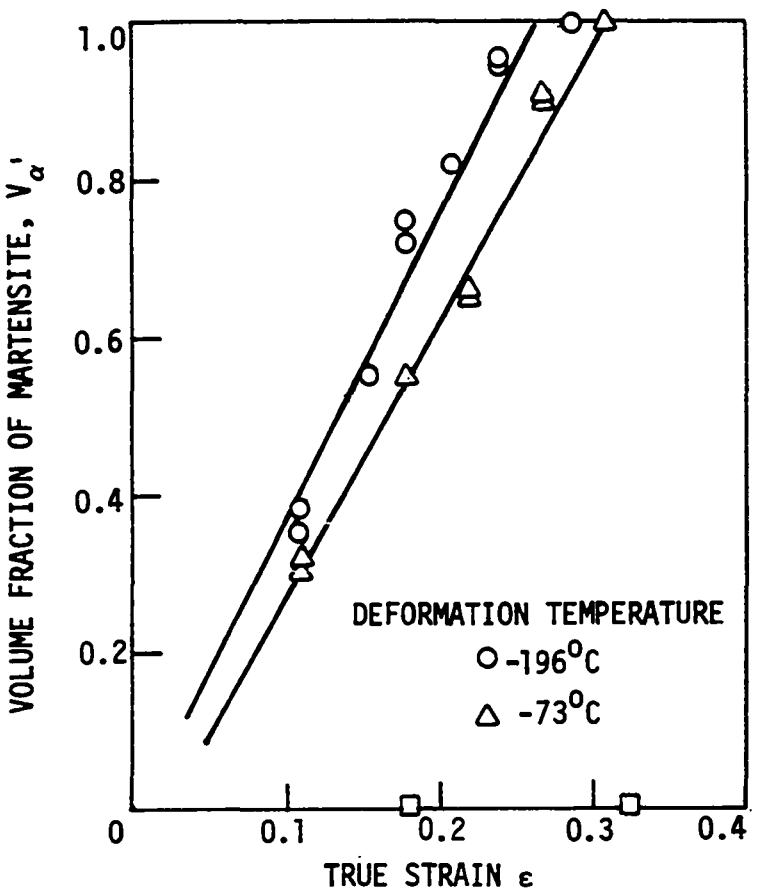

Figure 10. Effects of temperature and level of deformation on martensite content.

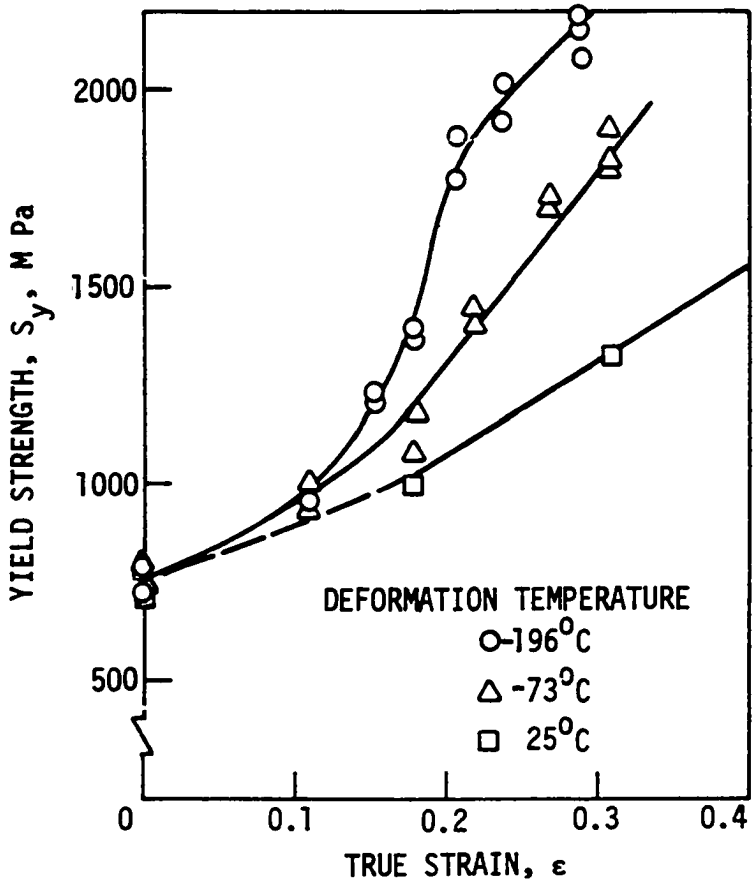

Figure 11. Effects of temperature and level of deformation on yield strength.

alloys increases linearly with increasing temperature, decreasing temperature reduces the austenite stability (51).

The volume fraction of α' and the yield strength were higher for specimens cryoformed at -196°C than those for specimens deformed at -73°C, for the same amount of strain. The difference in yield strengths of specimens cryoformed at the two temperatures became more pronounced as prestrain at each temperature increased. The stability of austenite is lower at -196°C than at -73°C. Thus, the amount of mechanical energy required to produce a unit volume of martensite was lower at -196°C than at -73°C. Both austenite and martensite have higher strain hardening exponents at -196°C. The increased strain hardening rate is associated with increased dislocation density. As specimens were prestrained to levels where considerable strain hardening of both α' and γ occurred, the difference between the yield strengths of specimens cryoformed at the two temperatures increased. The increased yield strength of specimens deformed at room temperature, with increasing prestrain was all due to the work hardening of austenite. As indicated by the plateaus in the load-elongation curves, martensite transformation and the propagation of Luders bands in the retained austenite were the major contributors to the plastic strain during deformation at the two cryogenic temperatures. Only deformation by slip occurred when the annealed material was deformed at room temperature.

2. Effects of aging temperature on structure and mechanical properties

a. Specimens cryoformed and tested at -196°C Specimens deformed 90% of ϵ_u at -196°C and aged at temperatures between 25°C and 450°C remained fully martensitic (Figure 12). As a result of the low ductility of martensite at -196°C, these specimens failed without substantial plastic deformation (Figure 13). Aging in the range of 300°C to 450°C increased the yield and tensile strengths by up to 200 MPa over natural aging (Figure 12). The increase in yield and tensile strength, in the absence of any further martensitic transformation suggested that carbide precipitation could be responsible for the secondary strengthening. Electron micrographs of a specimen aged at 400°C revealed the presence of alloy carbides in the martensite matrix (Figure 14). The electron diffraction spot showing up the carbides in a dark field electron micrograph was indexed to be either the (134) Fe_3C or the (248) $M_{23}C_6$ spot (72). The carbides have been identified as $(FeCr)_{23}C_6$. In accordance with the theory of carbide precipitation in stainless steels, the iron-chromium carbides were formed by the diffusion of chromium into existing iron carbide (33). The resultant carbide was complex and contained both iron and chromium. It was not surprising that the carbide indexed close to both Fe_3C and $M_{23}C_6$ spot.

Dislocations served as nucleation sites for the precipitates. Cahn (73) has shown that, for example, at a dislocation density level of 10^8 per square centimeter, the rate of heterogeneous nucleation is 10^{78} times as fast as the rate of

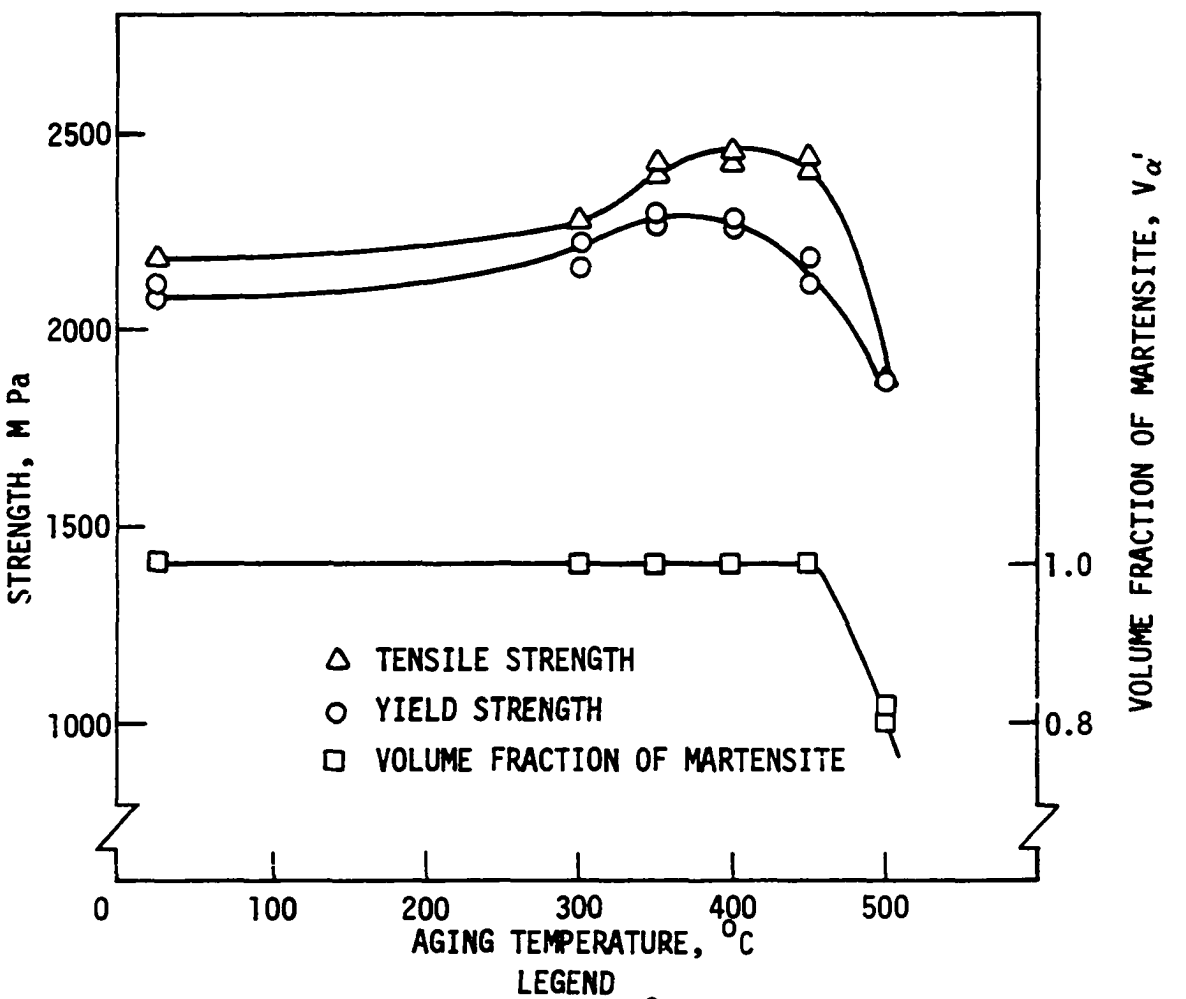

LEGEND

Cryoforming: 90% of ε_u at -196°C

Aging: Up to 3 days at room temperature, 1 hr. at temperatures between 300°C and 500°C

Testing: -196°C

Figure 12. Effects of aging temperature on yield strength, tensile strength, and martensite content.

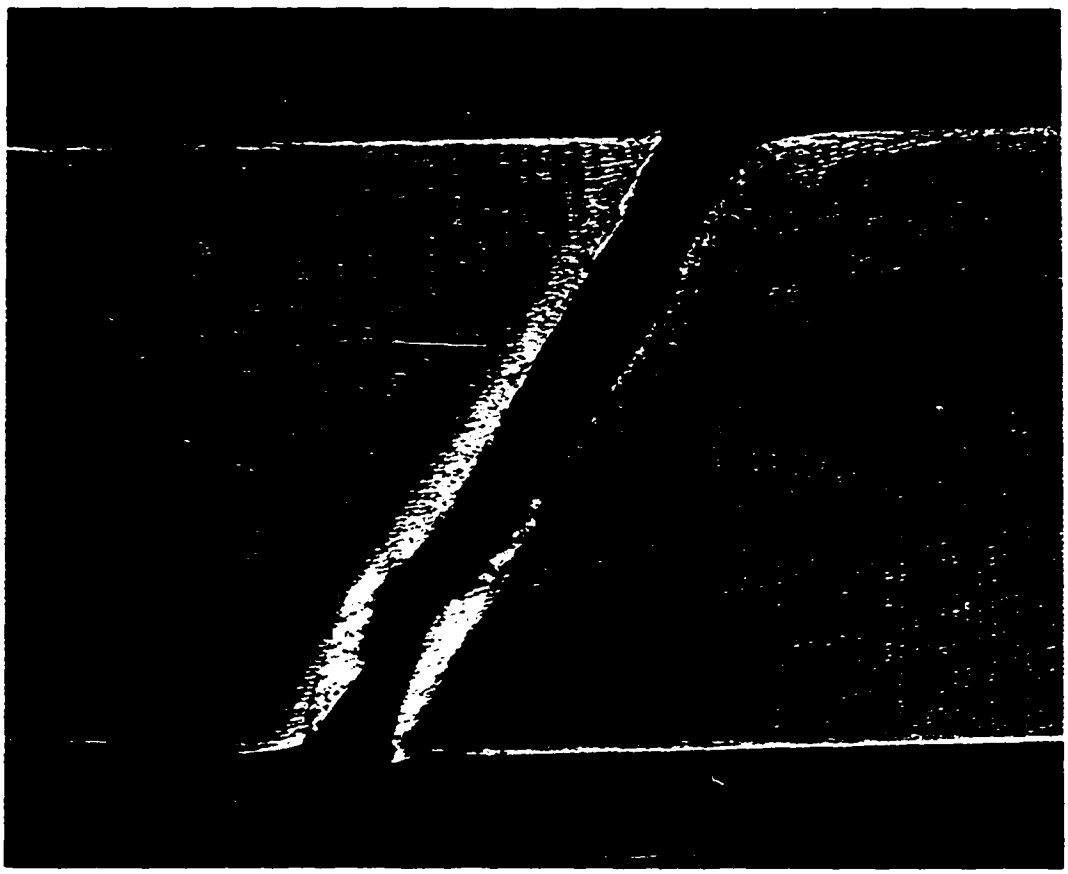

Figure 13. Typical fracture surface of specimen which failed without substantial plastic deformation.

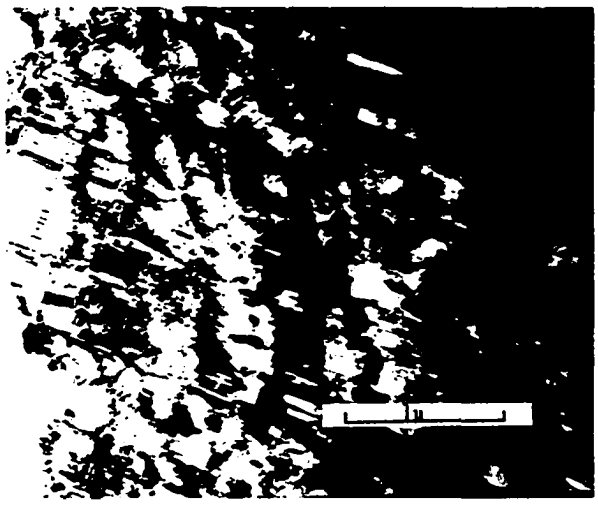

a. Bright field.

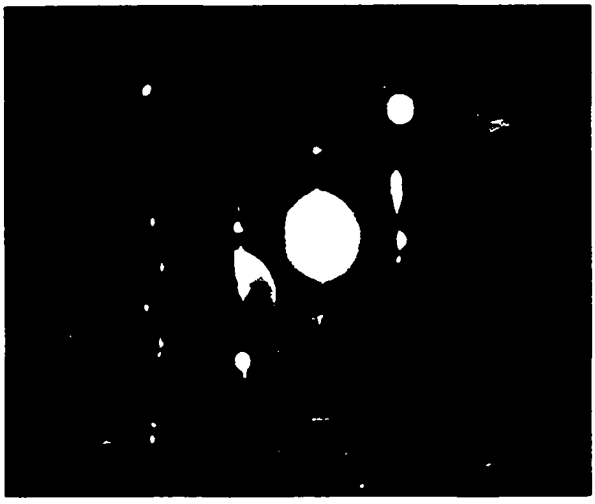

b. Selected area diffraction pattern showing $(FeCr)_{23}C_6$ spot used to obtain "c".

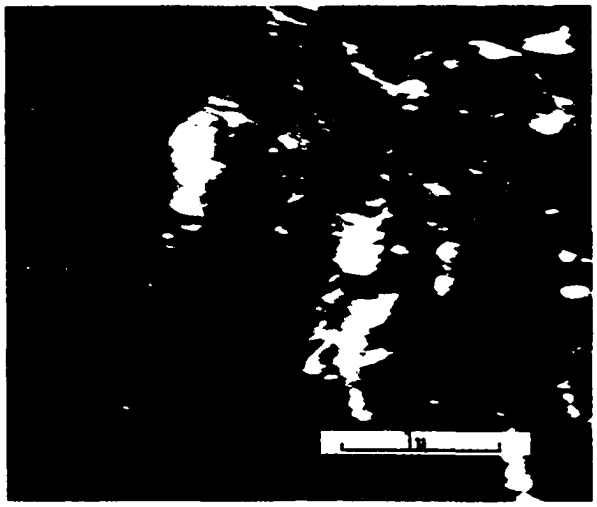

c. Dark field of "a".

Figure 14. Transmission electron micrograph of a specimen showing carbide aggregates in a martensite matrix.

homogeneous nucleation. The carbides in the thermomechanically processed material would, therefore, be more likely to form heterogeneously on dislocations. The random distribution of dislocations in strain-induced martensite was responsible for the uneven distribution of precipitates in the martensite matrix. Carbide precipitation, following thermomechanical treatment, has been observed in similar alloys by Chukleb and Martynov (10) and Mangonon and Thomas (20, 21).

After aging at 500°C significant reductions in yield strength, tensile strength and volume fraction of martensite were observed (Figure 12). The reduction in strength was due to the combined effects of austenite reversion, recovery, and growth and coalescence of carbides leading to increased interparticle spacing (74). The specimens cryoformed to 90% of ϵ_u at -196°C exhibited an upper yield point phenomenon when aged at room temperature before testing (Figure 15). This is attributed to the locking of dislocations by carbon atoms, as reported by Kurdjumov (44) and other workers (75, 76). The yield strength of specimens deformed 50% of ϵ_u at -196°C and aged up to 450°C increased slightly (Figure 16). Aging between 300°C and 500°C resulted in austenite reversion (Figure 17). The increase in yield strength was due to precipitation of carbides. Aging up to 450°C had no significant effect on the tensile strength. Both the yield and tensile strengths decreased after aging at 500°C. The tensile strength was dependent on the work hardening rate during final testing. As a result of further martensitic transformation, the work hardening rate increased. The two major factors contributing to the

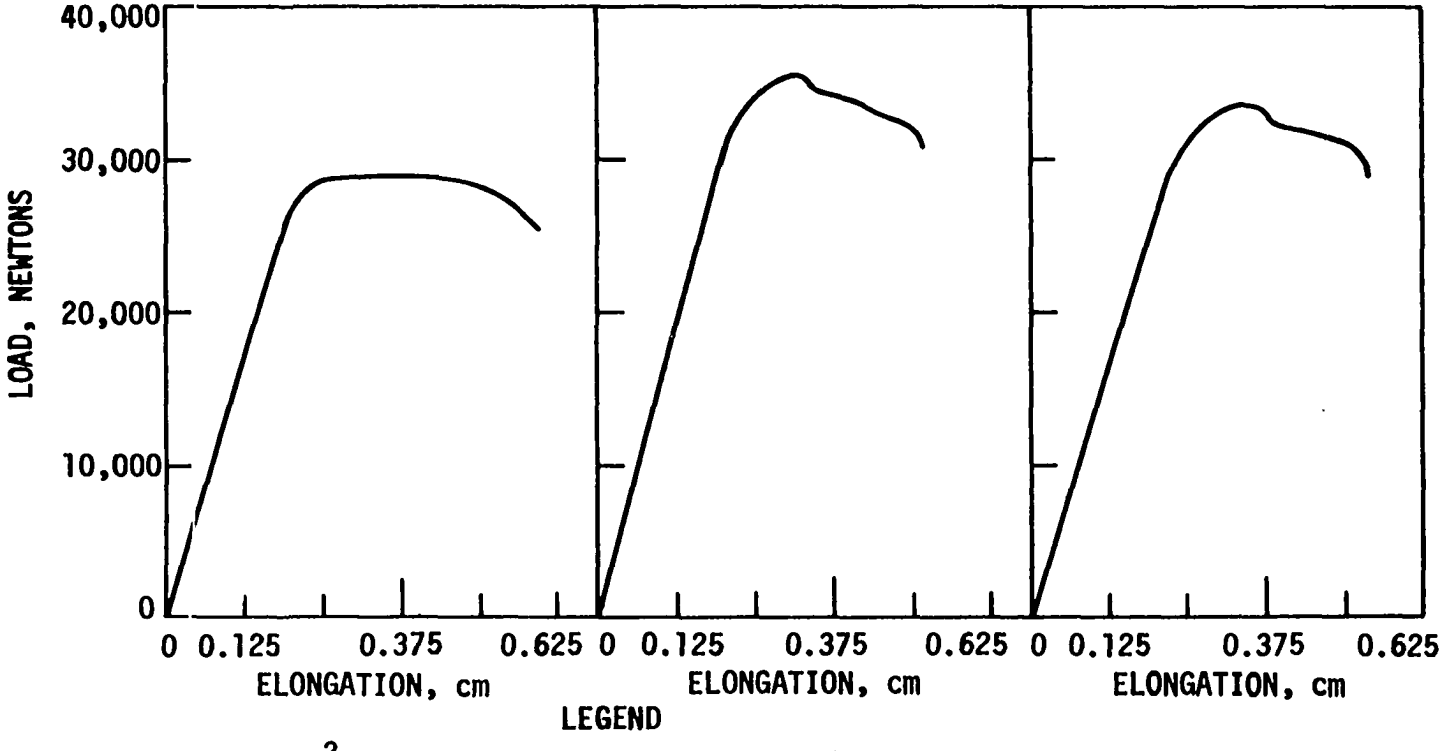

a. No aging; $A_o = 0.140\ cm^2$
$S_y = 2076$ MPa, $S_u = 2081$ MPa
$A_r = 5.0\%$

b. Room temperature, 1 day
$A_o = 0.163\ cm^2$, $S_y = 2173$ MPa
$S_u = 2197$ MPa, $A_r = 3.0\%$

c. Room temperature, 3 days
$A_o = 0.153\ cm^2$
$S_y = 2148$ MPa
$S_u = 2192$ MPa
$A_r = 3\%$

Figure 15. Load-elongation curves showing the upper yield point phenomenon in naturally aged specimens.

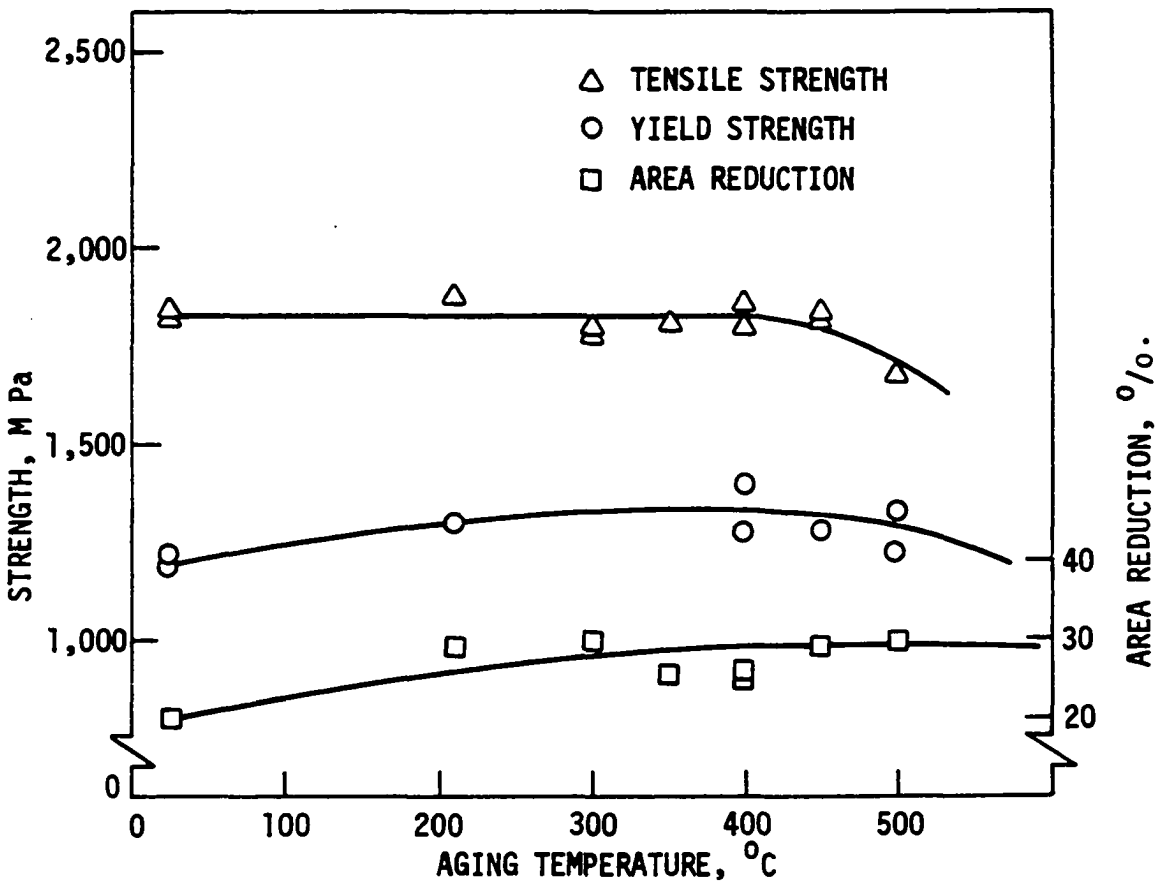

LEGEND

Cryoforming: 50% of ε_u at -196°C

Aging: Up to 3 days at room temperature, 1 hr. at temperatures between 210°C and 500°C.

Testing: -196°C.

Figure 16. Effects of aging temperature on mechanical properties.

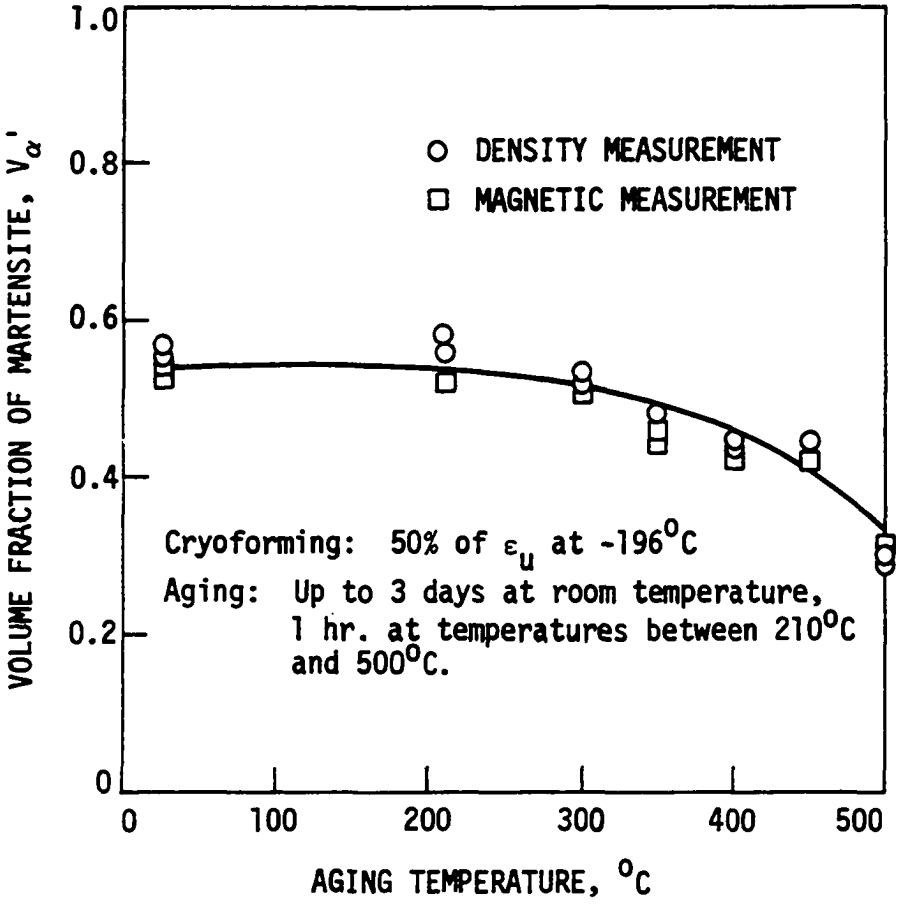

Figure 17. Effect of aging temperature on martensite content.

rate of increase were austenite stability and the amount, sizes and distribution of carbides in the matrix. These factors were not completely independent of each other. Precipitation reduced austenite stability by depleting the matrix of alloying elements. On the other hand, it also generated dislocations which would tend to stabilize the matrix. It was, therefore, impossible to determine the exact contribution of each factor to strengthening.

The load-elongation curves for the naturally aged specimens were significantly different from those of the artificially aged ones (Figure 18). The former indicated a strong influence of strain hardening. On the other hand, the artificially aged specimens showed two plateau regions indicative of rapid martensitic transformation. Each plateau was followed by a predominantly strain hardening region. The higher aging temperatures, in addition to causing austenite reversion, destabilized the retained austenite. Thus, austenite of two different stability levels was available for transformation during final testing. The reverted austenite, the less stable of the two, was formed from martensite which had undergone extensive depletion of alloying elements due to preferential precipitation, and was responsible for the first plateau. Rapid transformation of retained austenite was responsible for the second plateau. Area reduction increased slightly with artificial aging. This was due to the enhancement of ductility by martensite transformation.

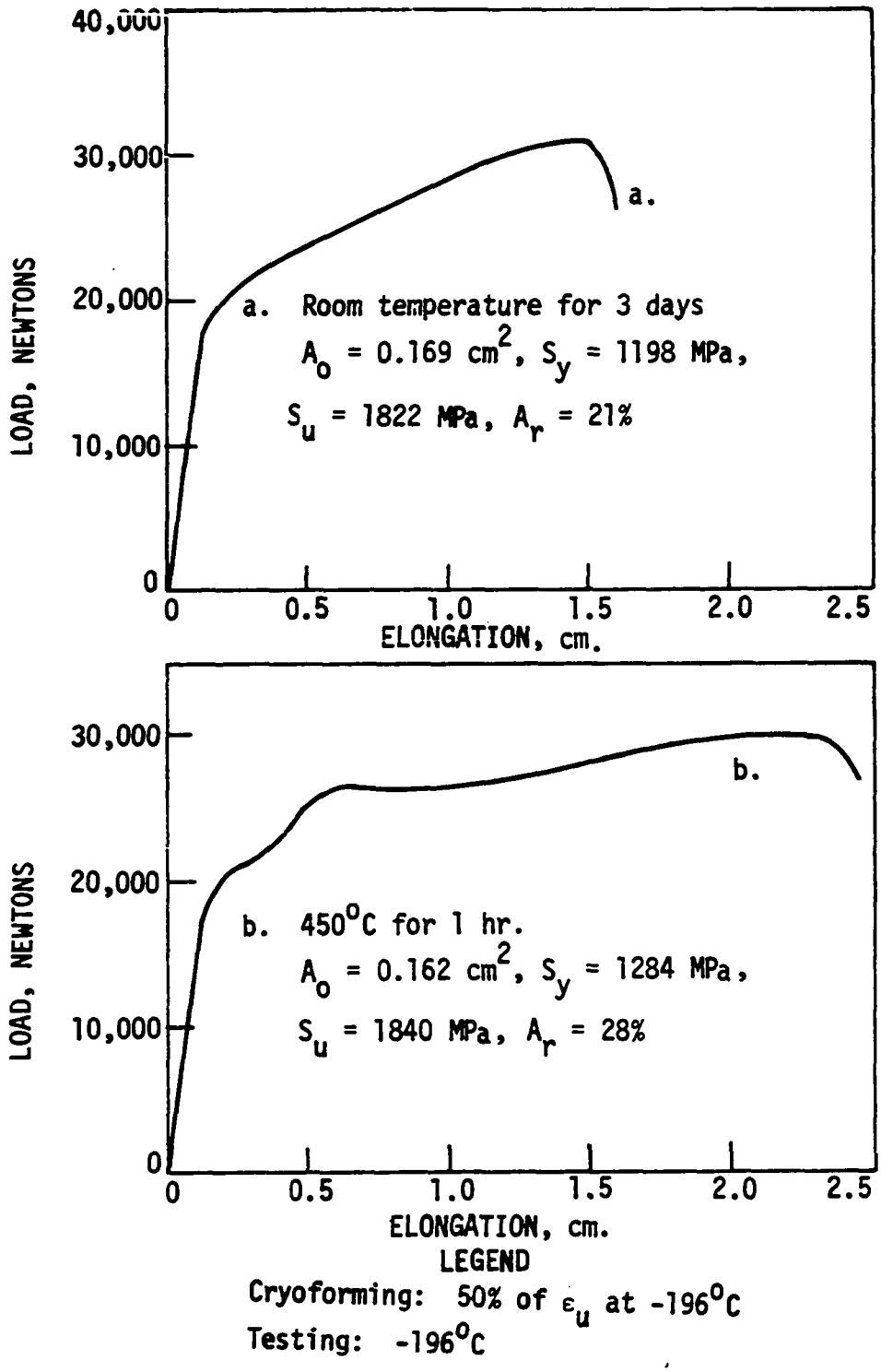

Figure 18. Load-elongation curves for naturally and artificially aged specimens

Experiments were conducted to investigate the effects of a lower aging temperature on the martensite content and mechanical properties of the cryoformed specimens. Specimens were aged for one and twelve hours respectively at 210°C. Slight increases in the volume fraction of martensite (~5%) and the yield strength (~70 MPa) were observed in the specimens aged for 12 hours. It was concluded that prolonged aging had no significant advantage over aging for shorter periods. This corroborates the observation made by Chukleb and Martynov (10).

Room temperature aging prior to testing did not produce the upper yield point phenomenon observed in the specimens strained 90% of ϵ_u at the same temperature (Figure 19). The lower dislocation density in the less deformed samples provided fewer sites for elastic interactions with carbon atoms. This reduced the effect of the dislocation locking process responsible for the yield point phenomenon. The interactions were, however, strong enough to produce a slight increase in the yield strength after prolonged exposure.

b. Specimens cryoformed at -73°C and tested at -196°C

The specimens deformed 90% of ϵ_u had fully transformed to martensite. Artificial aging resulted in austenite reversion. The discrepancy between the magnetic and density values of the martensite (Figure 20) was probably due to localized heating during sectioning of the small specimens used for the magnetic measurements.

The yield and tensile strengths increased by 150 MPa after

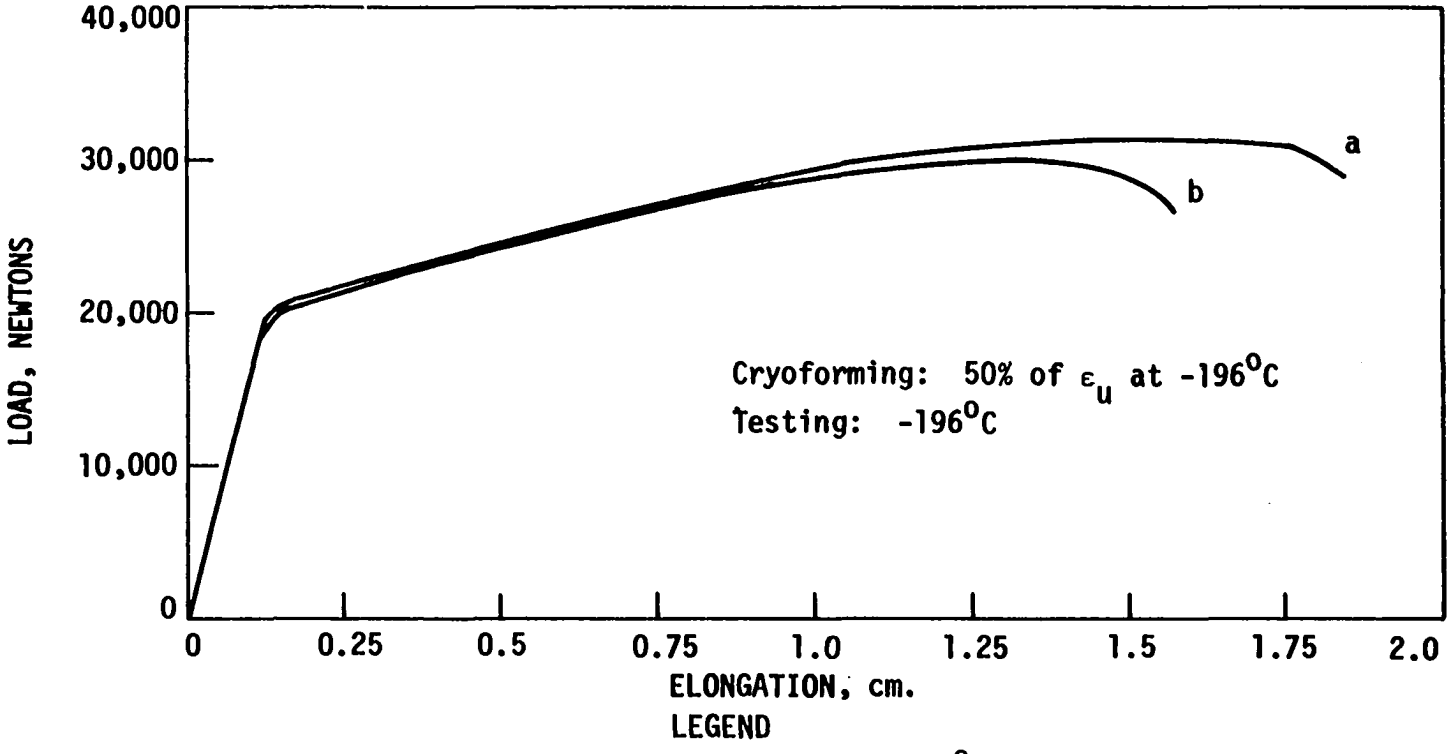

LEGEND

a. Retested immediately; $A_o = 0.175\ cm^2$, $S_y = 1189$ MPa, $S_u = 1811$ MPa, $A_r = 22\%$

b. Room temperature for 6 weeks. $A_o = 0.160\ cm^2$, $S_y = 1321$ MPa, $S_u = 1874$ MPa, $A_r = 18\%$

Figure 19. Load elongation curve showing the effect of low deformation level on the yield point phenomenon.

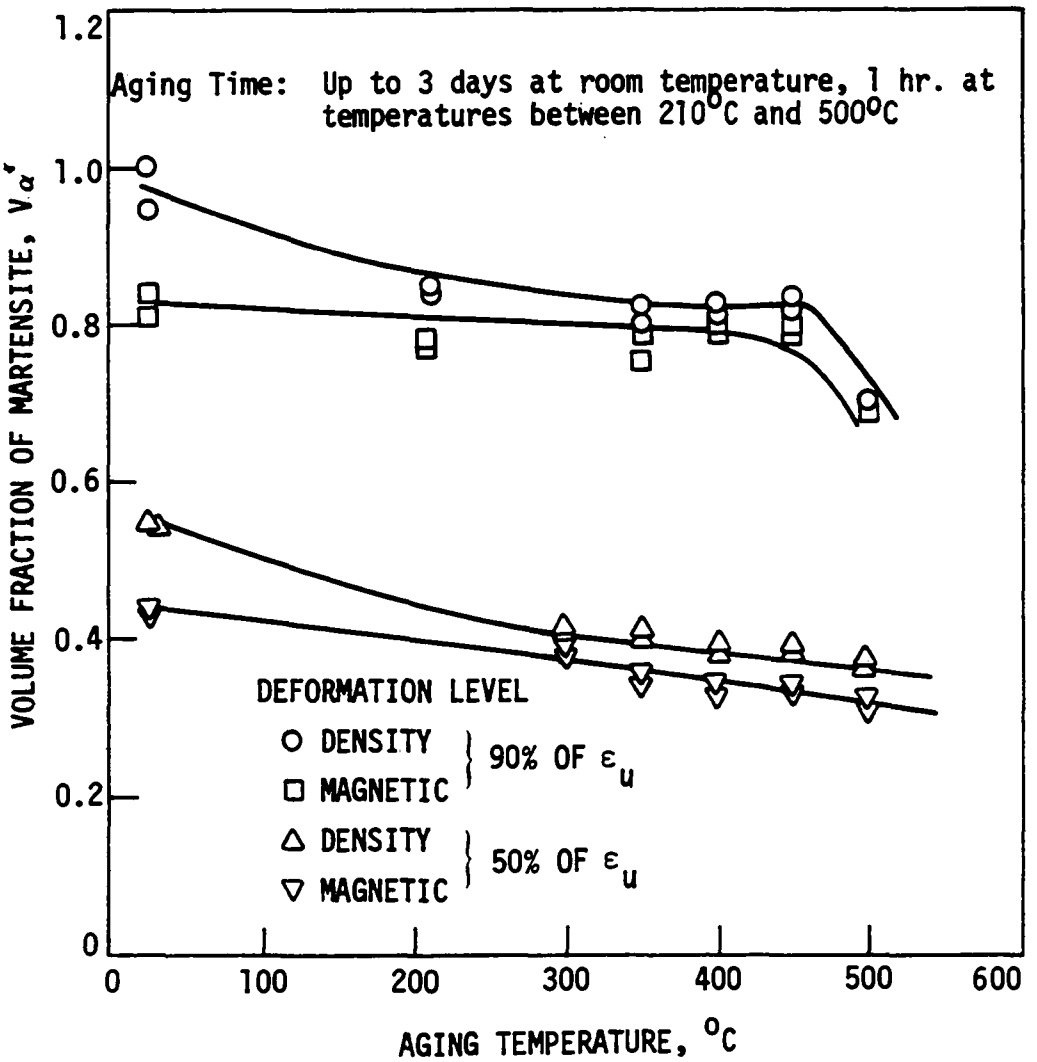

Figure 20. Effects of aging temperature on martensite content of specimen cryoformed at -73°C.

aging at temperatures up to 400°C and decreased with higher aging temperatures (Figure 21). The yield strength increase was due to carbide precipitation. The tensile strength was dependent on the presence of the carbides and the stability of the austenite available for transformation to martensite. Both factors controlled the work hardening rate of the material during testing. Transmission electron microscopy was used to establish the presence of carbides in the artificially aged specimens. An upper limit analysis indicated that the sizes of the carbides formed at 500°C would be within the resolution power of the transmission electron microscope (Appendix C). For easy observation, therefore, a specimen aged for 1 hour at 500°C was selected for metallographic examination. An electron micrograph of the specimen showing Widmanstatten carbides in a large martensite lath is shown in Figure 22. Exposure to room temperature for about 5 minutes after pre-straining produced an upper yield point phenomenon in the specimen. Exposure for up to 6 weeks, resulted in large plateaus in the load elongation curves with a 100 MPa decrease in yield strength (Figure 23) and a 10% reduction in volume fraction of martensite. The transformation of the reverted austenite back to martensite was responsible for the plateau region.

The specimens aged at temperatures between 210°C and 500°C also showed large plateaus in the load elongation curves (Figure 24). For specimens aged in the 300°C to 500°C

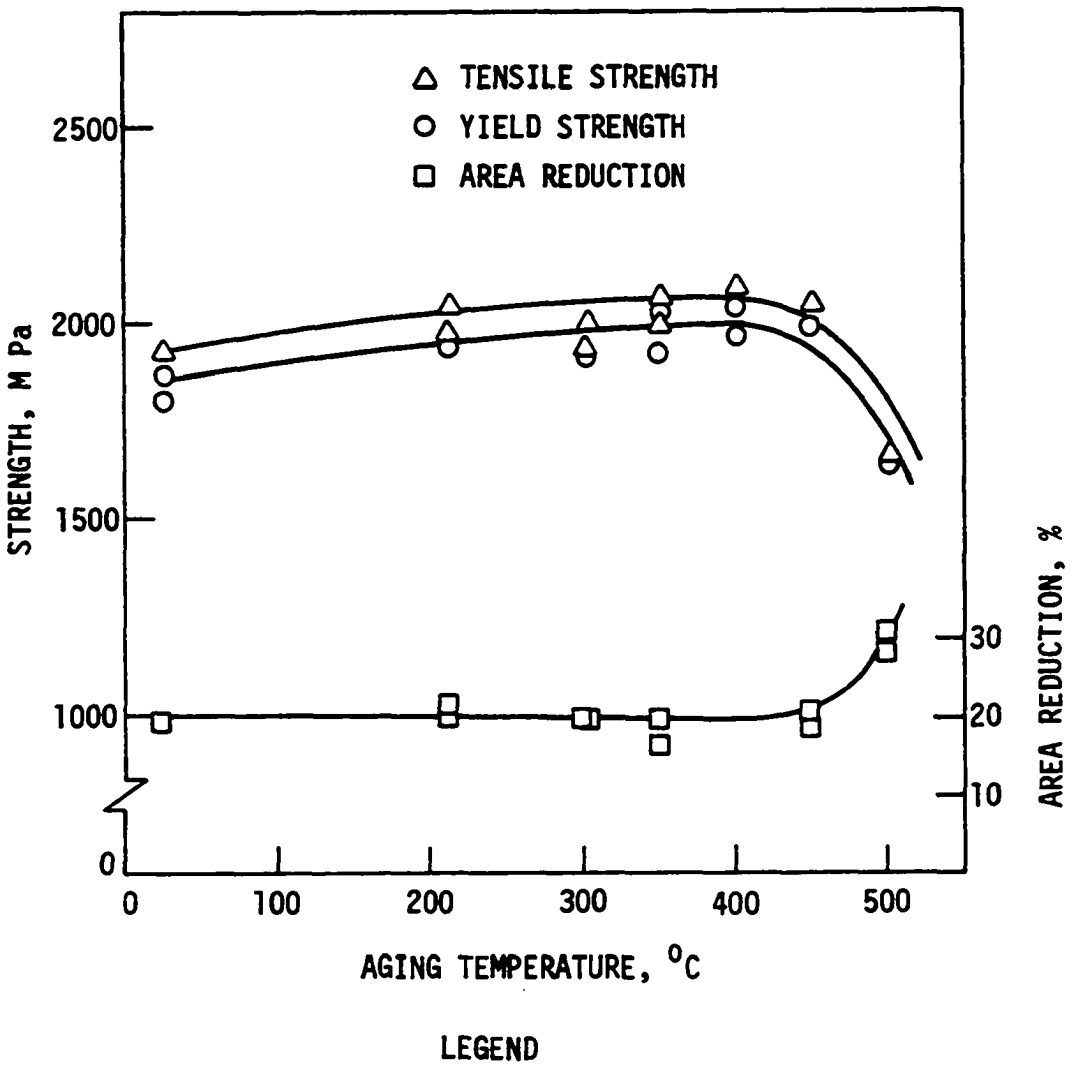

Figure 21. Effects of aging temperature on mechanical properties.

a. Bright field

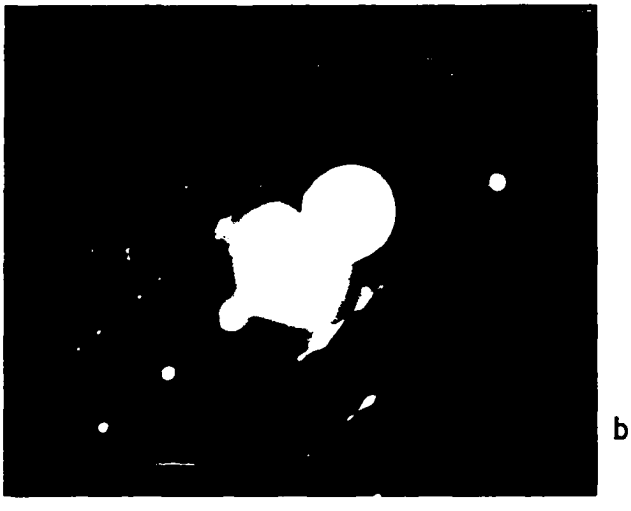

b. Selected area diffraction pattern showing $(FeCr)_{23}C_6$ spot used to obtain "c".

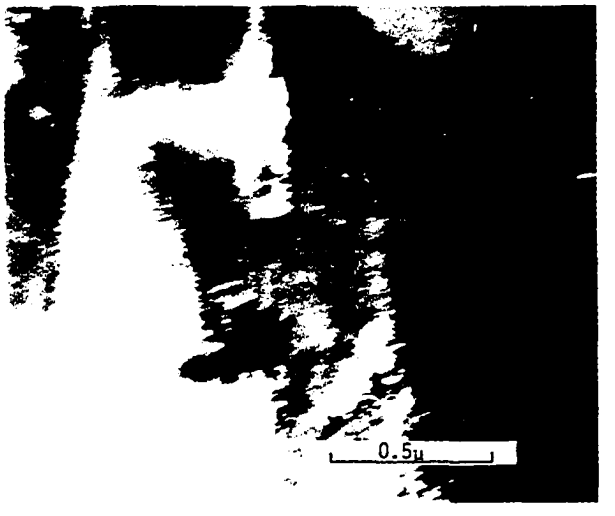

c. Dark field of "a".

Figure 22. Transmission electron micrograph of a specimen showing Widmanstätten carbides in a large martensite lath.

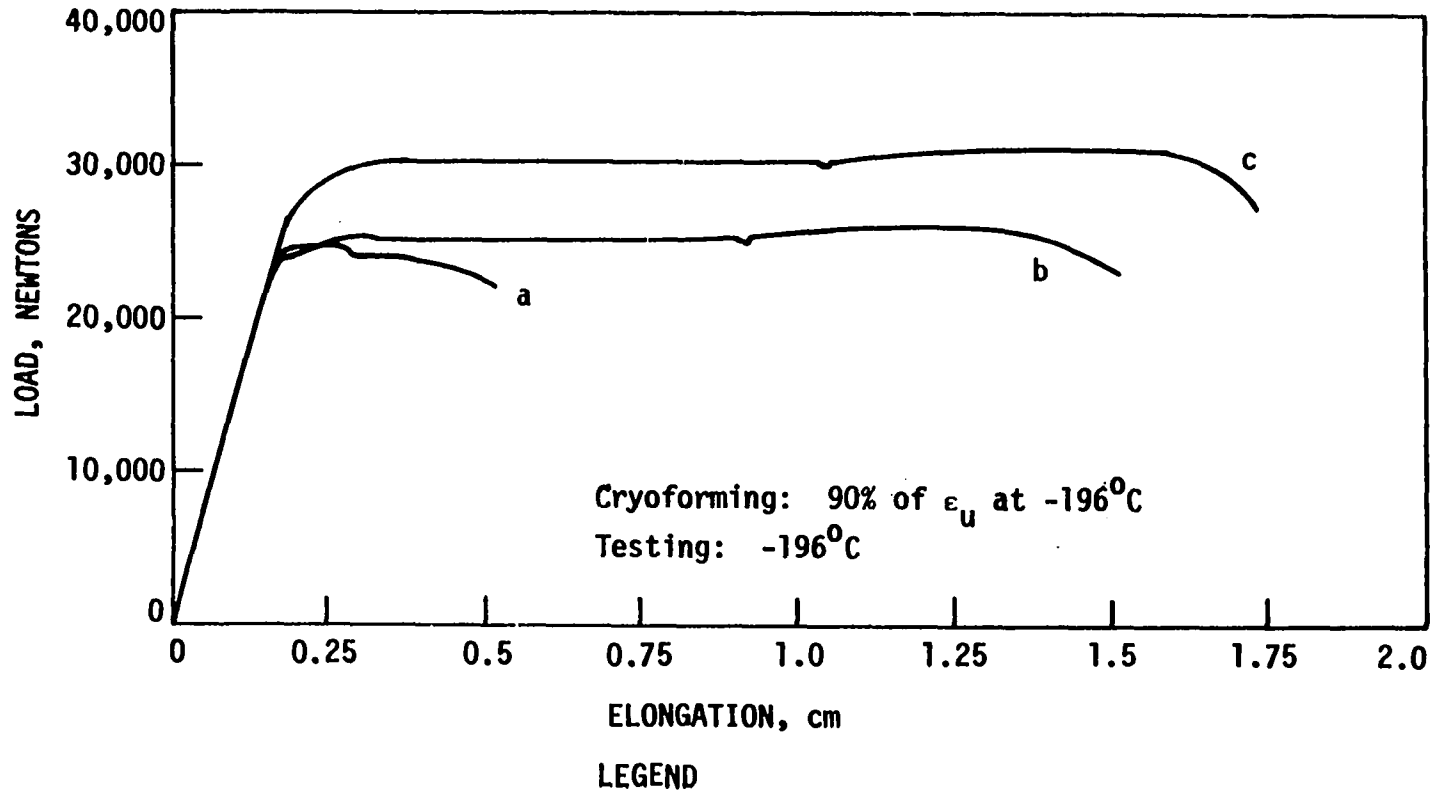

LEGEND

a. 5 mins at room temperature; $A_o = 0.130\ cm^2$, $S_y = 1899$ MPa, $S_u = 1923$ MPa, $A_r = 10\%$

b. 3 days at room temperature; $A_o = 0.135\ cm^2$, $S_y = 1822$ MPa, $S_u = 1926$ MPa, $A_r = 19\%$

c. 6 weeks at room temperature; $A_o = 0.162\ cm^2$, $S_y = 1810$ MPa, $S_u = 1922$ MPa, $A_r = 25\%$

Figure 23. Load-elongation curves showing the effects of natural aging on mechanical properties.

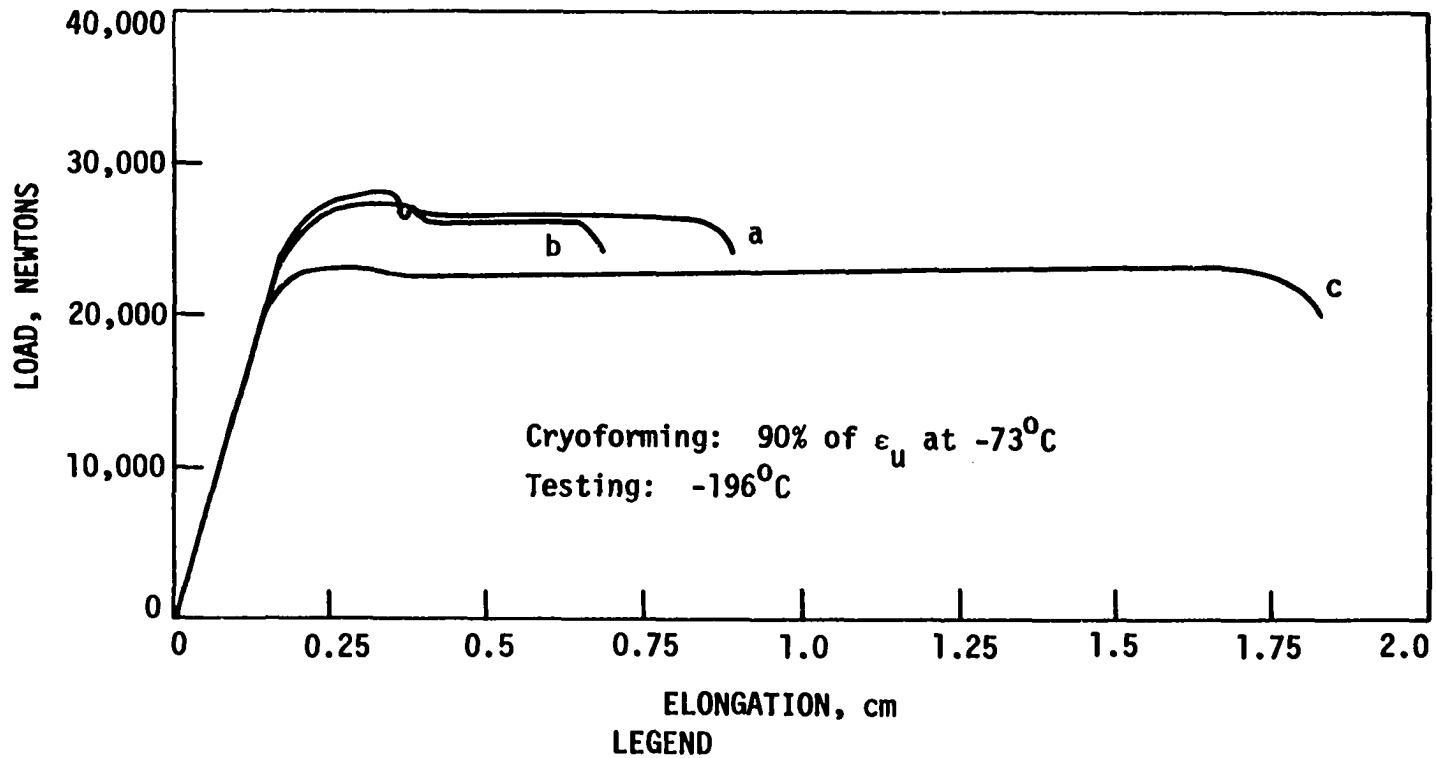

LEGEND

a. 1 hr. at 210°C A_o = 0.141 cm^2, S_y = 1917 MPa, S_u = 2000 MPa, A_r = 19%

b. 1 hr. at 350°C A_o = 0.139 cm^2, S_y = 1930 MPa, S_u = 2000 MPa, A_r = 16%

c. 1 hr. at 500°C A_o = 0.141 cm^2, S_y = 1623 MPa, S_u = 1650 MPa, A_r = 31%

Figure 24. Load-elongation curves showing the effects of aging temperature on the martensitic transformation during testing.

range, the size of the plateau increased with increasing aging temperature. However, the specimens aged at 210°C showed a larger plateau than that aged at 300°C. This was attributed to the difference in stability levels of the austenite formed by low and high temperature aging. The austenite available for transformation after low-temperature aging (25°C-210°C) was more stable than that present after high-temperature aging. Low-temperature aging produced migration of carbon atoms to dislocation stress fields resulting in a loss of tetragonality. High-temperature aging caused carbide precipitation and reduced the matrix stability (15, 44, 75-80). The higher austenite stability could be either beneficial or detrimental to ductility. The beneficial effect was obtained if the initiation of a neck caused enough martensitic transformation to inhibit the progress of necking. The results indicated that for the specimens deformed 90% of ϵ_u at -73°C, low aging temperatures were more favorable to ductility enhancement than aging temperatures between 300°C and 450°C.

Specimens deformed 50% of ϵ_u showed yield strength increases of up to 200 MPa and austenite reversion with artificial aging (Figures 20 and 25). The tensile strength remained the same after aging up to 450°C and decreased when the specimens were aged at 500°C. The increase in yield strength was due to carbide precipitation. The load-elongation curves for the naturally and artificially aged specimens were significantly different (Figure 26). The specimens aged at temperatures up to

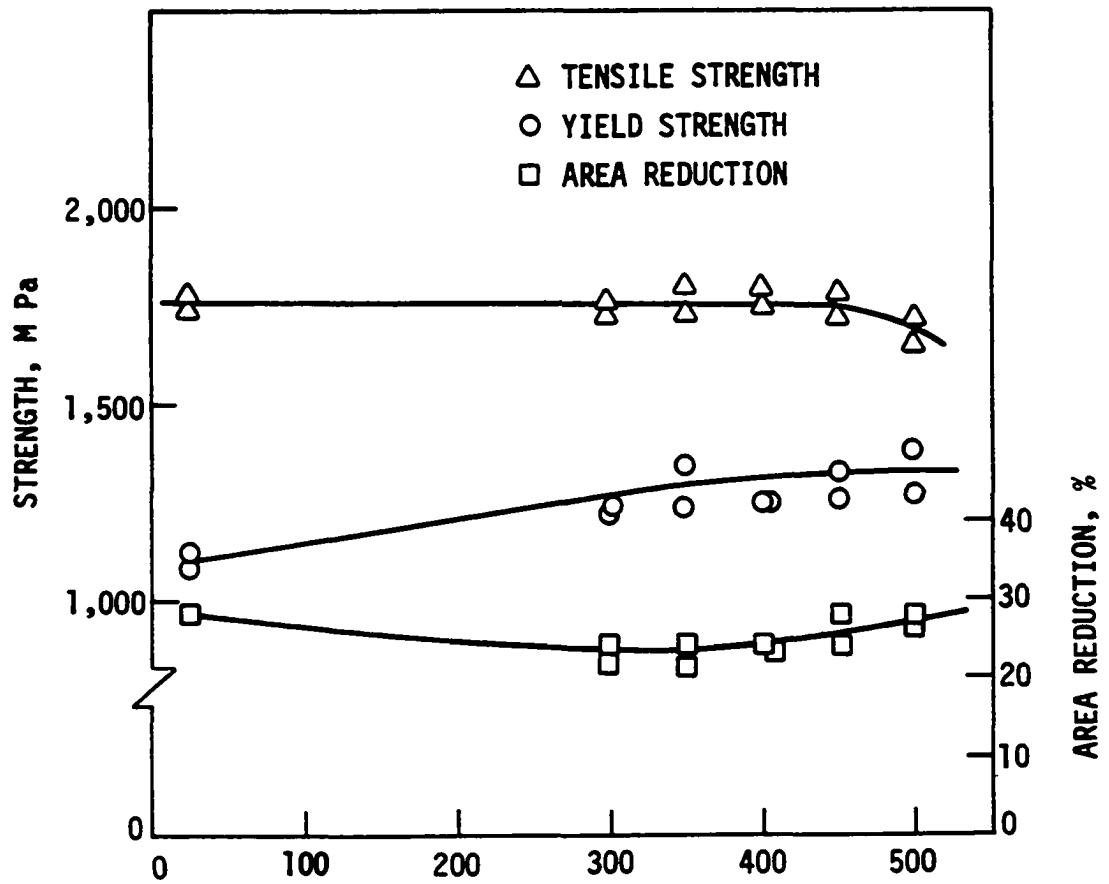

LEGEND

Cryoforming: 50% of ε_u at -73°C

Aging: Up to 6 weeks at room temperature, 1 hr. at temperatures between 210°C and 500°C

Testing: -196°C

Figure 25. Effects of aging temperature on mechanical properties.

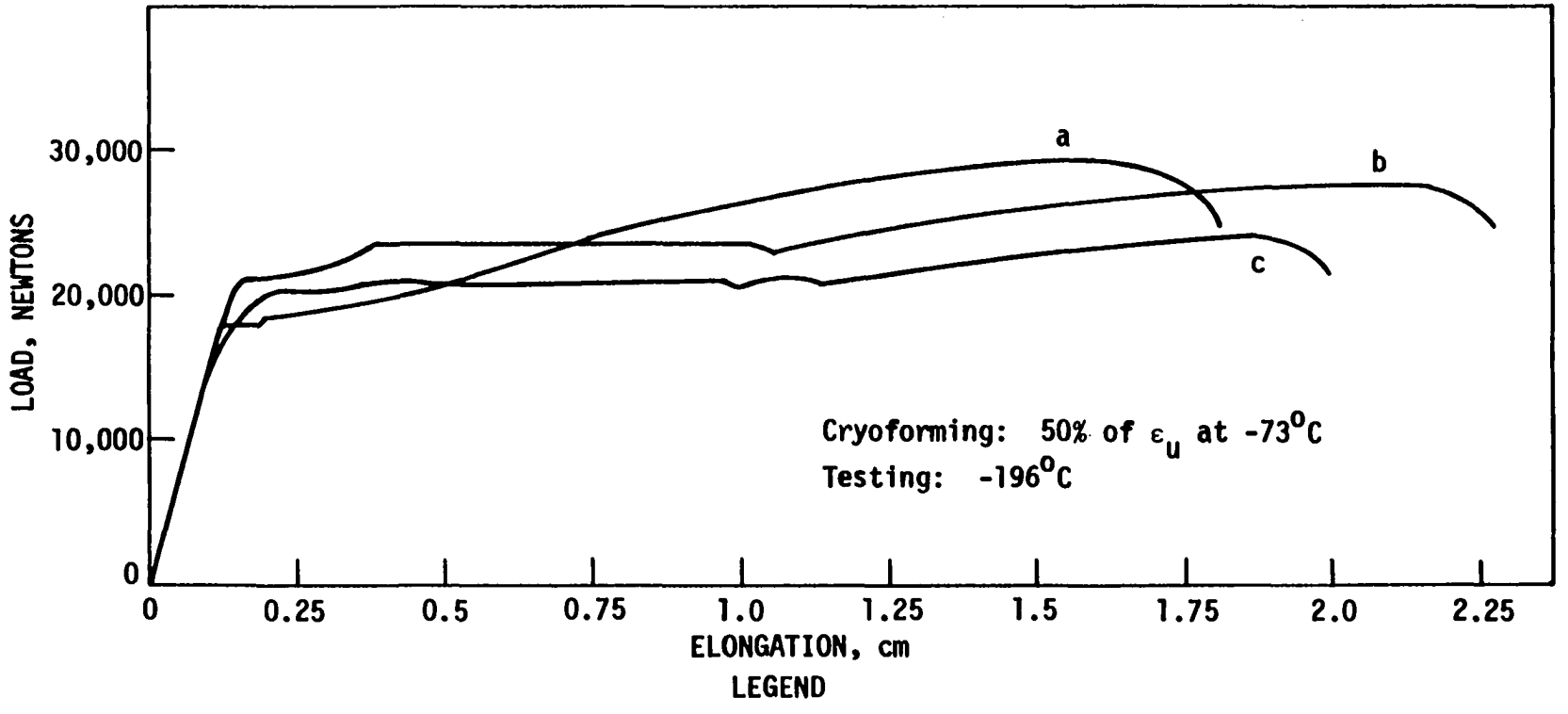

LEGEND

a. Room temperature for 3 days. A_o = 0.173 cm^2, S_y = 1075 MPa, S_u = 1698 MPa, A_r = 26%

b. 350°C for 1 hr. A_o = 0.160 cm^2, S_y = 1341 MPa, S_u = 1735 MPa, A_r = 28%

c. 500°C for 1 hr. A_o = 0.146 cm^2, S_y = 1384 MPa, S_u = 1649 MPa, A_r = 27%

Figure 26. Load-elongation curves showing the effects of artificial aging on the martensite transformation rate during testing.

450°C showed two plateaus each followed by a predominantly strain hardening region. The first plateau represented rapid transformation of the less stable reverted austenite. The second represented transformation of retained austenite. For the specimens aged between 300°C and 450°C, a distinct drop in load was observed at the end of the second plateau. Those aged at 500°C showed a large second plateau with several load drops. The drops in load were probably due to the occurrence of a burst transformation. As the retained austenite transformed locally, heavy faulting occurred in the neighboring grains. These stacking faults served as embryos and stimulated some martensitic transformation without requiring additional mechanical energy. Experiments were carried out to determine the amounts of reverted and retained austenite responsible for the two plateaus. Volume fractions of martensite were determined for specimens aged at 450°C and subjected to interrupted testing. The levels of interrupted testing are shown in Figure 27. A comparison of the V_α, values with that of the naturally aged specimen is shown in Table 5.

The first plateau represented transformation of 67% of the total amount of reverted austenite, and the second, about 50% of the retained austenite. The remainder transformed in the latter stages of testing simultaneously with strain hardening of the freshly formed martensite. The elongations in the plateaus were due to the martensitic transformation and to the propagation of Luders bands in the remaining austenite.

Experiments were carried out to investigate the effects

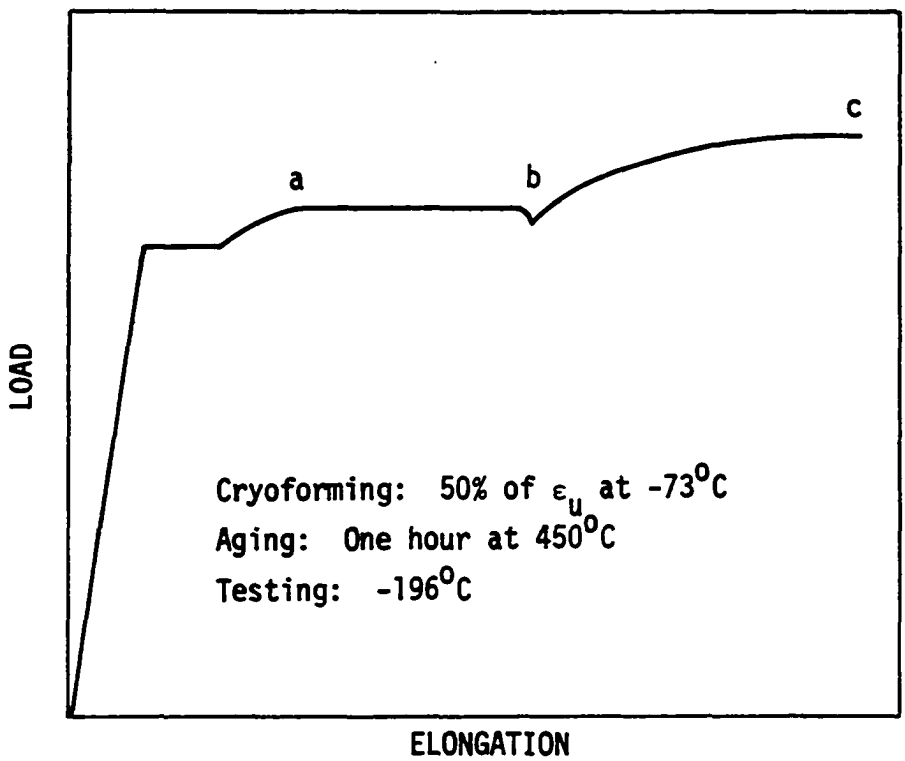

Figure 27. Schematic load-elongation curve showing levels of interrupted testing.

Table 5. Effects of interrupted testing on volume fractions of martensite in specimens deformed 50% of ϵ_u at -73°C

	Condition	$V_{\alpha'}$
i.	Naturally aged	55%
ii.	Aged at 450°C for 1 hour	40%
iii.	As in ii, deformed to a point equivalent to "a" on Figure 2	50%
iv.	As in ii, deformed to a point equivalent to "b" on Figure 27	70%
v.	As in ii, deformed to fracture	100%

of increased strain rate on the nature of the load-elongation curves. It was observed that a tenfold increase in strain rate did not significantly affect the mechanical properties of the specimens (Figure 28).

c. Specimens deformed at room temperature (25°C) and tested at -196°C Specimens deformed to both 50% of ϵ_u and 90% of ϵ_u at room temperature remained fully austenitic. Aging between 250°C and 450°C had no significant effect on thermomechanical properties. This indicated that no precipitation occurred during aging. The aging temperatures employed were also too low to cause recrystallization in the cold worked specimens. The load-elongation curve for both levels of deformation showed an upper yield point followed by rapid martensitic transformation and strain hardening of the martensite and retained austenite (Figure 29). The heavily cold worked

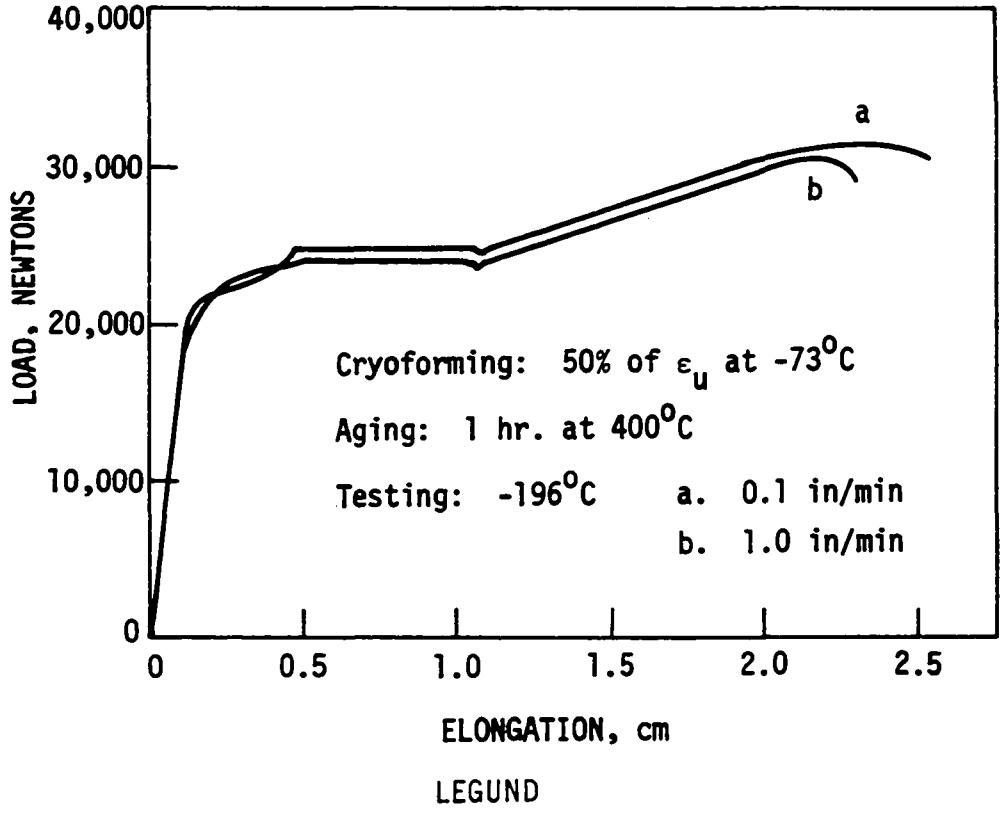

a. Ao = 0.178 cm^2, Sy = 1246 MPa, Su = 1764MPa, Ar = 25%

b. Ao = 0.180cm^2, Sy = 1250MPa, Su = 1700Mpa, Ar = 24%

Figure 28. Load-elongation curves showing the effect of testing rate on mechanical properties.

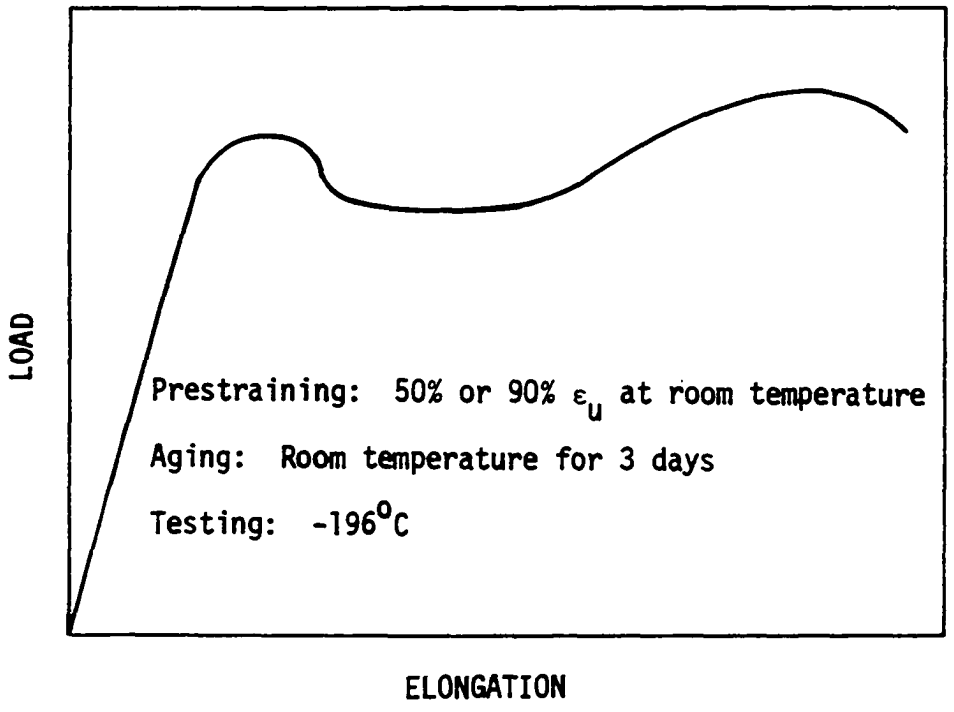

Figure 29. Schematic load-elongation curve for cold worked specimens showing upper yield point phenomenon followed by martensitic transformation and strain hardening.

specimens had higher yield and tensile strengths, as well as better ductility than the less deformed ones. The higher ductility of the heavily cold worked specimens was due to a beneficial effect of martensitic transformation during testing.

C. Effects of Processing Parameters on Martensite Stability

The specimens deformed 90% of ϵ_u at -196°C remained fully martensitic after aging at temperatures as high as 450°C. Those deformed only 50% of ϵ_u at the same temperature underwent some austenite reversion after aging at temperatures above 300°C. All the specimens cryoformed at -73°C underwent austenite reversion after prolonged natural and artificial aging (Figure 30). It was concluded from these observations that increased deformation, and lower deformation temperature, improved the stability of martensite. The free energy change accompanying the $\gamma \rightarrow \alpha'$ transformation increases with decreasing temperature (81, 82). The results indicated that the higher the free energy change accompanying the original transformation of austenite to martensite, the higher the aging temperature required to cause austenite reversion.

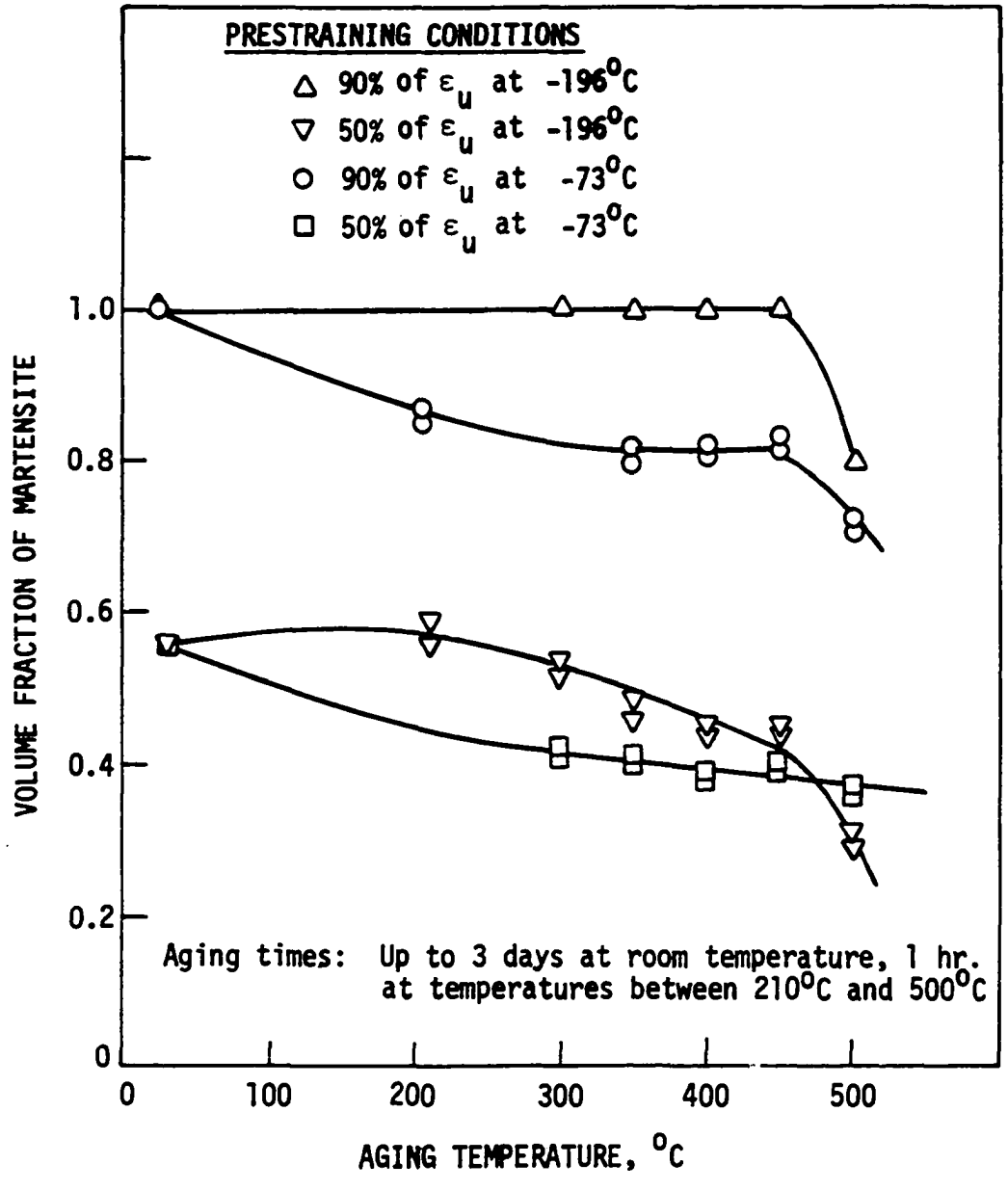

Figure 30. Effects of thermomechanical processing parameters on the stability of strain induced martensite.

D. Morphology of the Transformation Products

X-ray diffraction patterns of some thermomechanically processed specimens are shown in Figure 31. For all levels and temperatures of deformation, the specimens were either partially martensitic and partially austenitic, or fully martensitic with no trace of the hcp ϵ phase present.

Low stacking fault energy materials such as austenitic stainless steel deform initially by localized faulting (83). When faulting occurs on all $(111)_\gamma$ planes, the faulted area diffracts as a hexagonal phase (55, 59). This explains the existence of a maximum volume fraction of ϵ observed at low strains (~5% elongation) by Mangonon and Thomas (20, 21). In the absence of the faulting periodicity, randomly faulted austenite is observed instead of the hcp ϵ (50). To investigate the effects of low strains, diffraction patterns were obtained from specimens deformed at -196°C to approximately 6% and 10% elongation, respectively (Figures 31c, 31d). No ϵ peak was observed in either of the two samples. This indicated that the transformation is of the form $\gamma \rightarrow \alpha'$.

A mechanism has been proposed for the $\gamma \rightarrow \alpha'$ transformation in austenitic stainless steels (52, 57, 60, 61, 84). The transformation is said to occur by a "two-shear" process (52). The first and critical step is a half stacking fault shear along the $(111)_\gamma$ planes in the $[112]_\gamma$ directions. The next step occurs along the $(110)_{\alpha'}$ planes in the $[112]_{\alpha'}$ directions

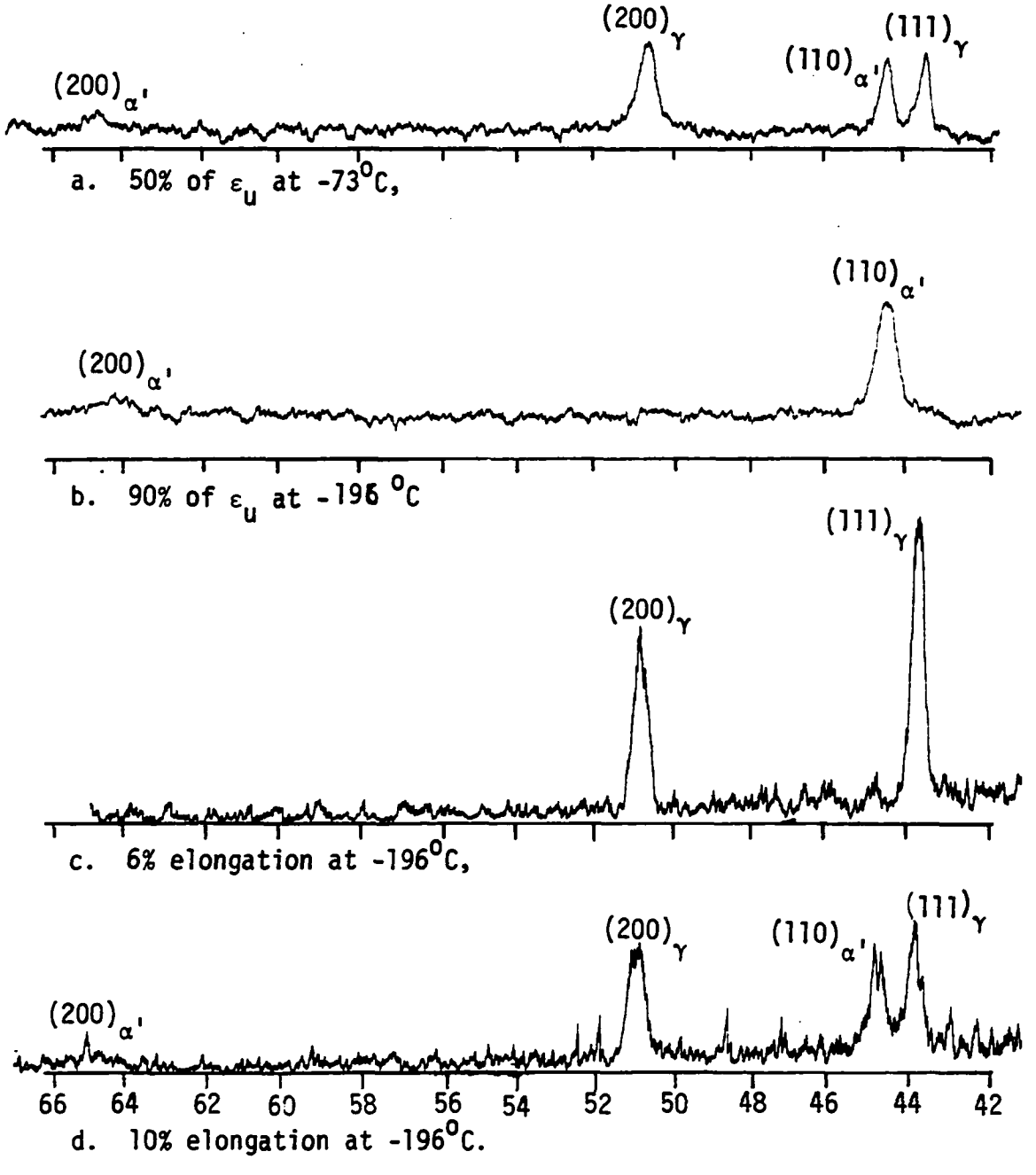

Figure 31. X-ray diffraction patterns of some thermomechanically treated specimens. All the specimens were naturally aged.

accompanied by a small expansion perpendicular to $[112]_{\alpha'}$ (52).

The nature of the first step indicates that stacking fault formation is an intermediate stage in the $\gamma \rightarrow \alpha'$ transformation. Observations made by Kelly and Nutting (52) and Olson and Cohen (85) corroborate this proposition. The mechanism embraces the observations made by Mangonon and Thomas (20) and several other investigators that the ϵ phase may be an intermediate stage in the martensitic transformation. However, the formation of ϵ is not required before the transformation to α' can proceed as postulated by these authors (20, 47, 48, 49, 54-56, 59). The ϵ phase consists of overlapping stacking faults. Hence, it is concluded that faulted austenite either in the form of hcp ϵ or randomly oriented, is the intermediate stage in the $\gamma \rightarrow \alpha'$ transformation in austenitic stainless steels.

Transmission electron micrographs of partially transformed specimens are shown in Figures 32-35. Selected area diffraction and dark field microscopy have been used to identify the phases (Figure 32). The martensite laths contain dense arrays of randomly distributed dislocations. This is because the martensitic transformation is accompanied by the generation of large amounts of dislocations and is often considered as a mode of plastic deformation. Figure 33 indicates the presence of martensite laths in two adjacent grains of different orientation. Within each grain, the martensite laths are parallel to each other. However, the complete suppression of the

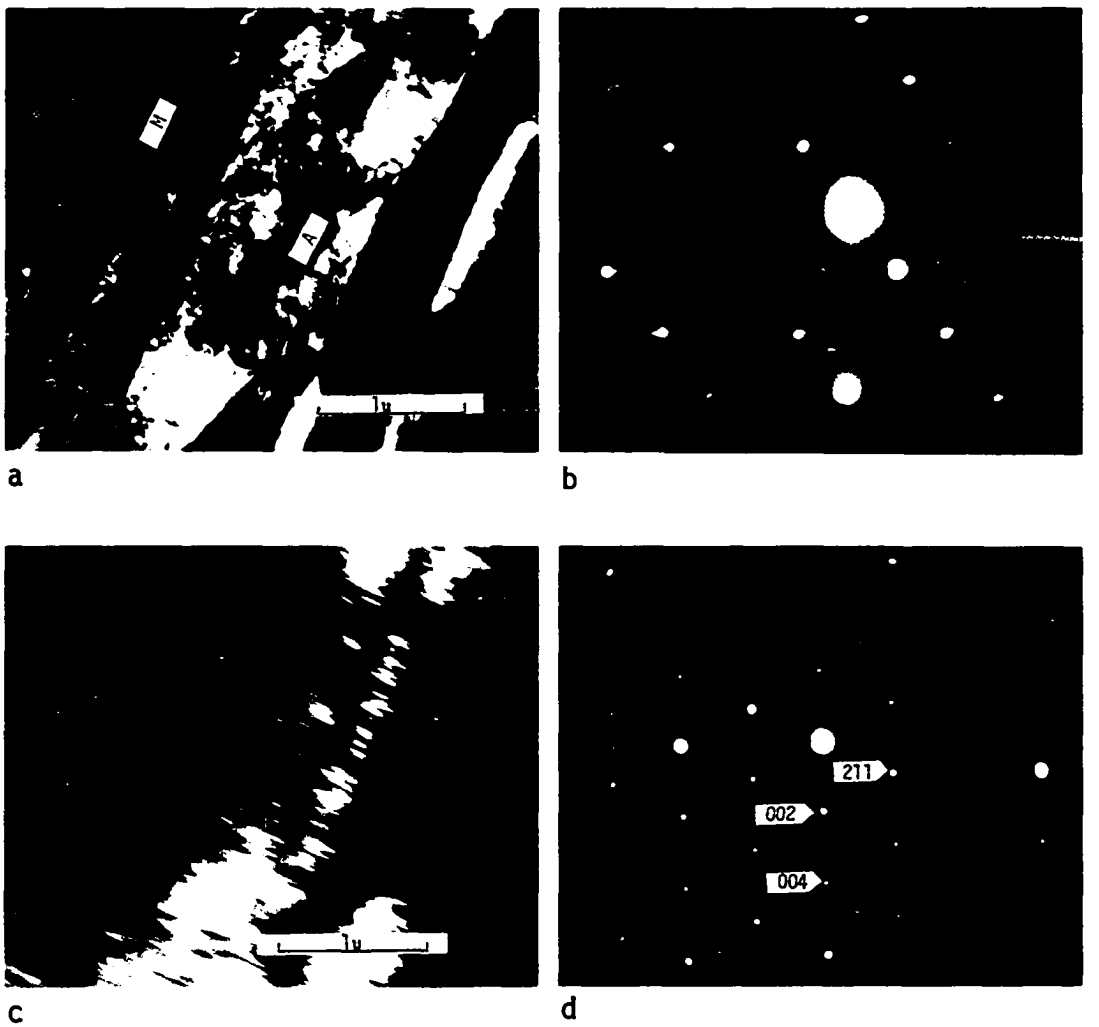

a. Bright field

b. Selected area diffraction pattern of light area

c. Dark field of "a" using $(444)_\gamma$ spot to reveal the austenite matrix identified by letter A.

d. Selected area diffraction from dark band M, indexed to be the 120 reciprocal lattice for a BCC crystal.

Figure 32. Transmission electron micrograph of specimen deformed 50% of ε_u at $-73^{\circ}C$.

a. Bright field showing parallel martensite laths in two adjacent grains of different orientations.

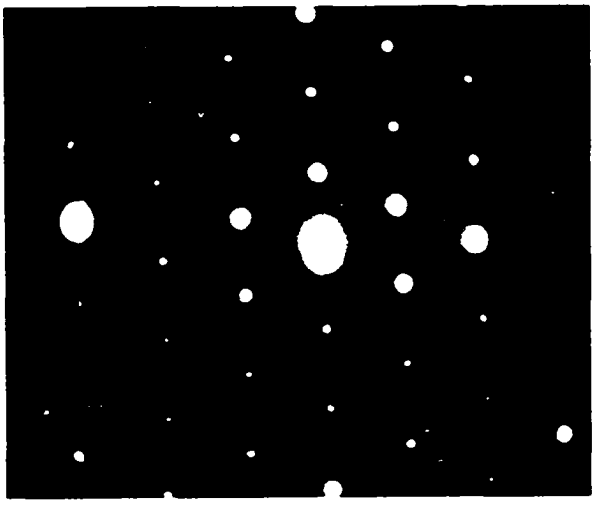

b. Selected area diffraction pattern.

c. Dark field micrograph reversing contrast in one grain and showing complete extinction of contrast in the other.

Figure 33. Transmission electron micrograph of specimen deformed to 50% of ε_u at -196°C.

a. Bright field showing twin contrast T, thickness fringes F.

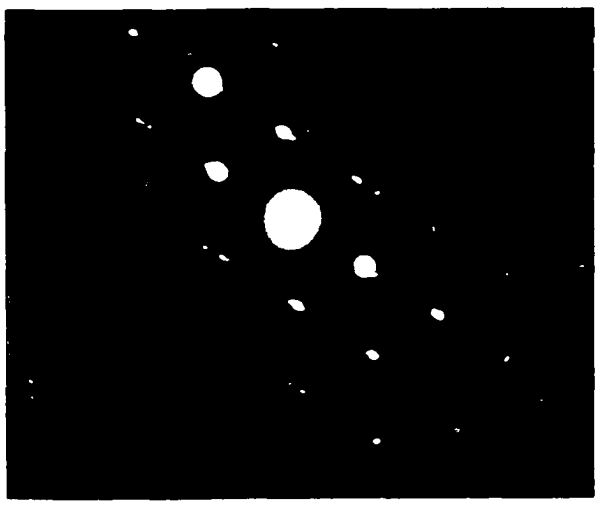

b. Selected area diffraction pattern of "a".

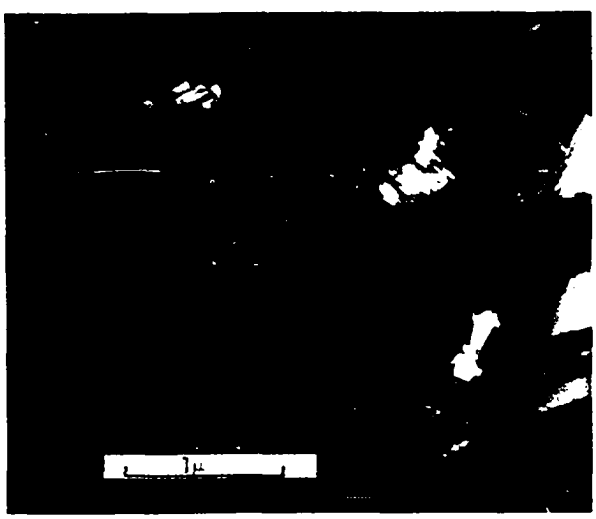

c. Dark field of a showing twin contrast.

Figure 34. Transmission electron micrograph of specimen cryoformed 50% of ε_u at -196°C and naturally aged.

a. Bright field showing twin contrast T

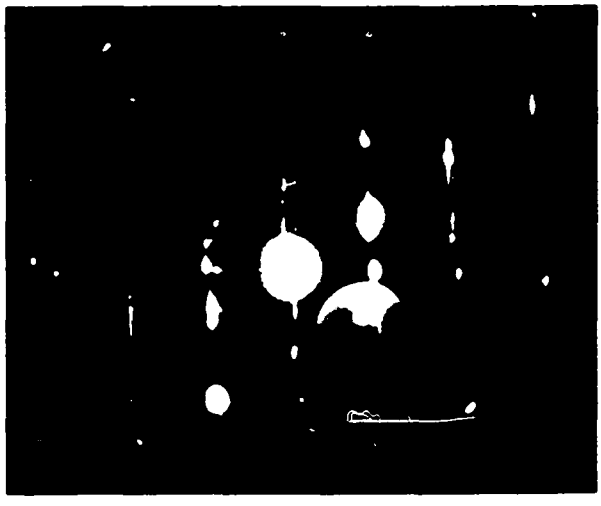

b. Selected area diffraction pattern showing streaks due to stacking faults and extra spots due to twins and carbides

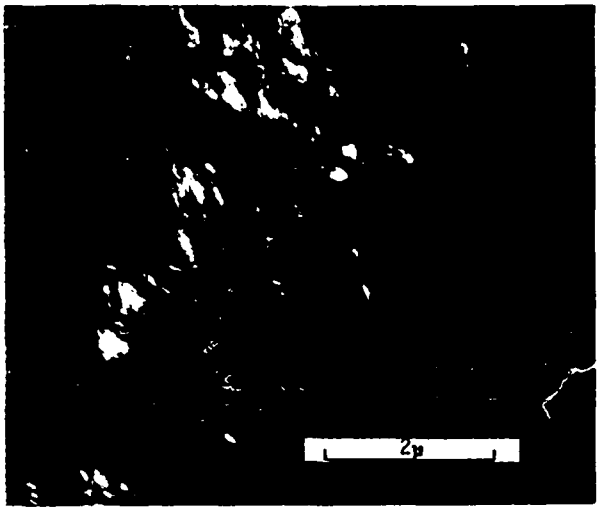

c. Dark field showing twin contrast

Figure 35. Transmission electron micrograph of specimen cryoformed 90% of ε_u at -196°C aged for one hour at 400°C.

contrast in one grain with dark field imaging from the other, indicated that the laths in the two grains were oriented differently (Figure 33c). Figures 34 and 35 are transmission micrographs of partially and fully transformed specimens, respectively. The diffraction patterns and the dark field images show clearly the nature of the substructure of the martensite. The presence of twin spots and streaks in the diffraction patterns confirm the existence of twins and stacking faults, respectively. The bright field image revealed little dislocation substructure in areas where twin bands appear and vice versa. Deformation by slip and by twinning are competing phenomena during martensitic transformation where one predominates, therefore, the other is suppressed.

Optical micrographs of the partially transformed austenitic stainless steel are shown in Figures 36 and 37. During the deformation, the grains transformed heterogeneously due to orientation effects. Thus it was possible within the same specimen to have some grains almost fully transformed, while others remained austenitic. Similar results have been reported by Lagneborg (61) and Goodchild et al. (86). In the presence of an applied stress, the separation of partial dislocations varies with the orientation of the stress axis. Tensile stress can raise the stacking fault energy of a grain to the level where cellular rather than planar dislocations would be produced (86). Also, the applied stress could be oriented with respect to the slip planes in a particular grain

a.

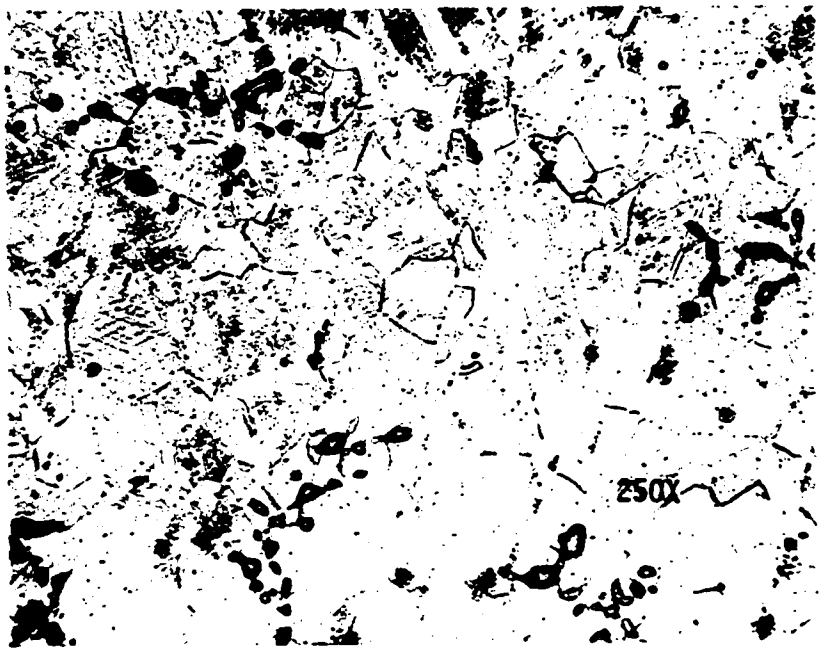

b.

Figure 36. Optical micrograph of specimen deformed 50% of ε_u at -73 °C.

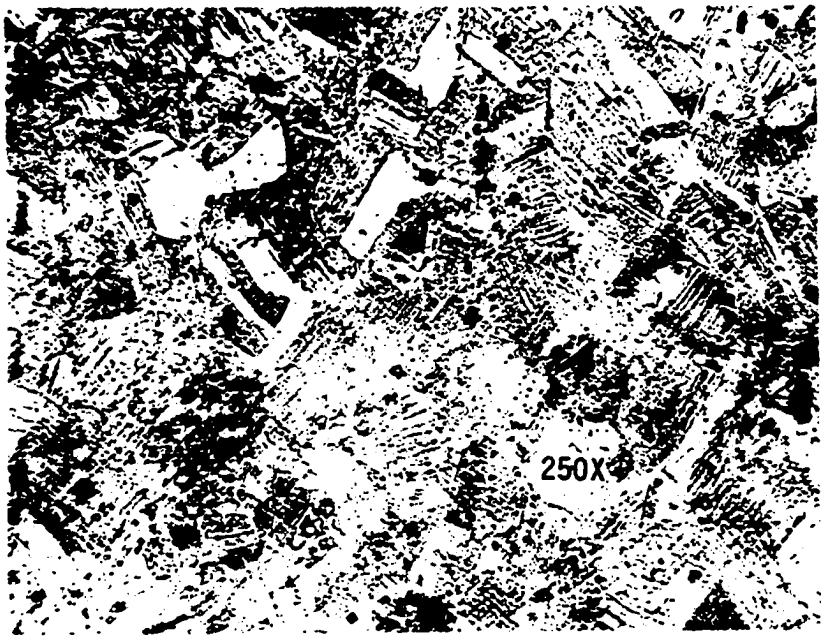

a.

b.

Figure 37. Optical micrograph of specimen deformed 50% of ε_u at -196 °C.

such that dislocations are not extended by the stress. These would suppress the formation of stacking faults and inhibit martensitic transformation.

The indexed Debye-Scherrer diffraction pattern obtained from a fully martensitic specimen is shown in Figure 38. The diffuse nature of the lines is due to the presence of lattice imperfections and orientation effects introduced by plastic deformation. Using the Nelson-Riley correlation and regression analysis, a lattice parameter of 2.8662 Å was determined for the martensitic structure (Appendix B.2). This value is in good agreement with that reported by Reed and Guntner (59).

E. Optimum Effects of Cryoforming and Aging on Cryogenic Mechanical Properties

The optimum cryogenic mechanical properties obtained by thermomechanical treatment are listed in Table 6. For any of the processes, the yield strength was higher when the specimen was tested at -196°C than at -73°C. This indicated that there was no stress-induced martensitic transformation during testing. Had stress-induced transformation occurred, the yield strength would be lower at the lower temperature as a result of the reduced austenite stability. Yield and tensile strengths in excess of 2000 MPa at -196°C have been attained by prestraining at both -196°C and -73°C. The specimens prestrained at -73°C had better ductility at -196°C than those cryoformed at -196°C (Figures 39 and 40).

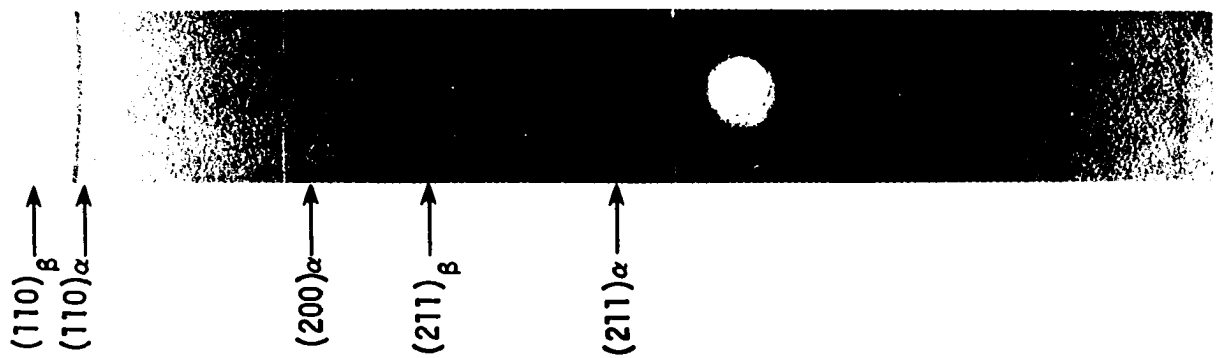

Figure 38. Debye-Scherrer diffraction pattern of 100% martensite structure.

Table 6. Optimum properties of thermomechanically treated austenitic stainless steel at -73°C and -196°C

Predeformation temperature %	Processing conditions	Yield strength MPa		Tensile strength Mpa		Area reduction %	
		Testing temp.		Testing temp.		Testing temp.	
		-73°C	-196°C	-73°C	-196°C	-73°C	-196°C
-196°C	90% ϵ_u, aged at 400°C for 1 hr[a]	1722 1831	2271 2279	2009 1972	2439 2420	3 10	2 5
	75% ϵ_u, aged at 425°C for 1 hr	1865 1728	2113 2061	2044 1975	2236 2150	18 9	13 13
	50% ϵ_u, aged at 400°C for 1 hr	1083 1069	1272 1392	1409 1485	1808 1862	26 25	25 26
-73°C	90% ϵ_u, aged at 400°C for 1 hr	1668 1589	2037 2007	1760 1671	2093 2067	8 13	21 21
	75% ϵ_u, aged at 425°C for 1 hr	1563 1522	1689 1718	1689 1624	1887 1922	20 16	25 24
	50% ϵ_u, aged at 450°C for 1 hr	1081 1041	1252 1314	1313 1319	1721 1783	34 31	28 28
25°C	90% ϵ_u, naturally aged	1096 1042	1319 1293	1180 1266	1802 1762	32 34	26 29
	50% ϵ_u, naturally aged	905 840	1085 1040	1181 1136	1724 1706	33 37	23 21

[a]Specimens had Ar ≤ 10%, not suitable for functional design.

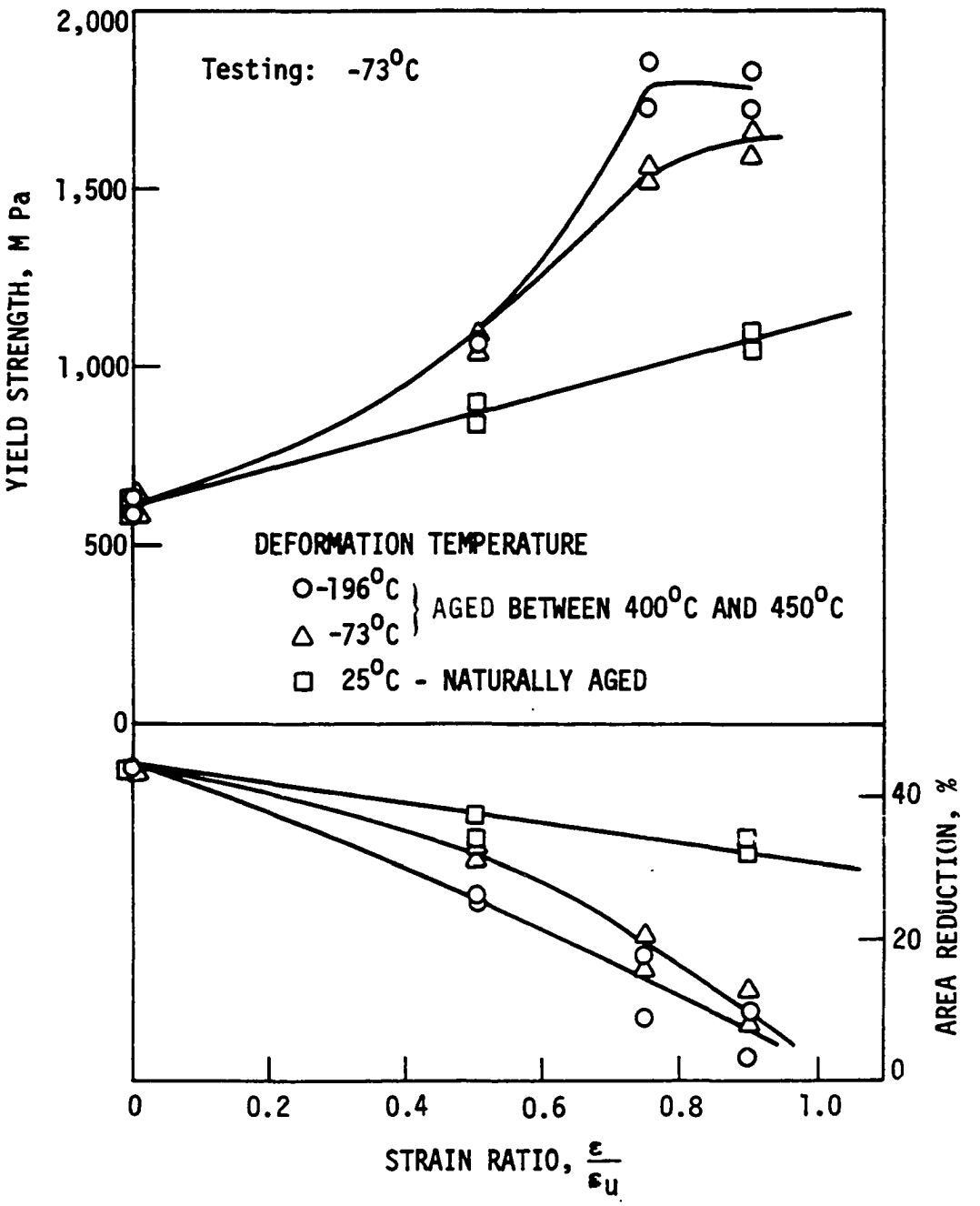

Figure 39. Effects of temperature and level of deformation on optimum mechanical properties.

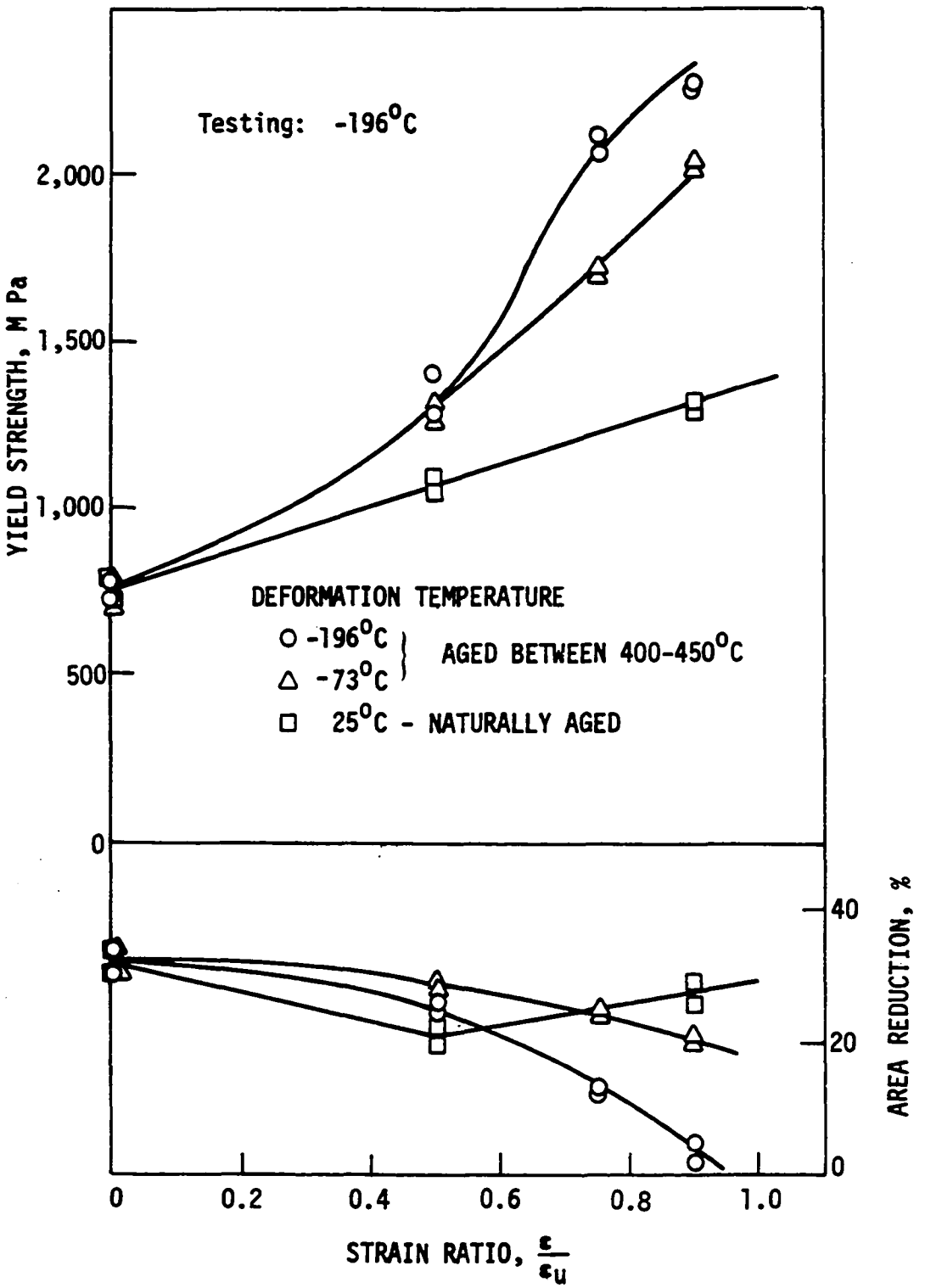

Figure 40. Effects of temperature and level of deformation on optimum mechanical properties.

The ductility enhancement due to martensitic transformation was much greater when the specimens prestrained at -73°C were tested at -196°C. The stability of the available austenite was lower, and the degree of transformation per unit strain more extensive. The results indicated that, for this combination of processing and testing conditions, the martensitic transformation during testing improved the ductility.

The highest yield and tensile strengths at -73°C were observed in specimens deformed to 75% of ϵ_u at -196°C. The slightly lower yield and tensile strengths obtained in the specimens deformed to 90% of ϵ_u at -196°C suggest that the temperature selected for aging was not optimum. In view of their poor ductility, these specimens were considered undesirable for practical applications. No further investigations were conducted to determine the optimum aging temperature. These specimens were fully martensitic even after artificial aging at 400°C; consequently, no further martensitic transformation contributed to improved ductility could occur during testing. Specimens deformed to 75% of ϵ_u and artificially aged were about 10% austenitic. During testing, transformation of the austenite to martensite contributed to their higher ductility.

The load-elongation curves of the specimens deformed at -73°C did not show the load drop due to the "burst transformation" observed when similarly processed specimens were tested at -196°C (Figure 41). The rate of formation of the embryos

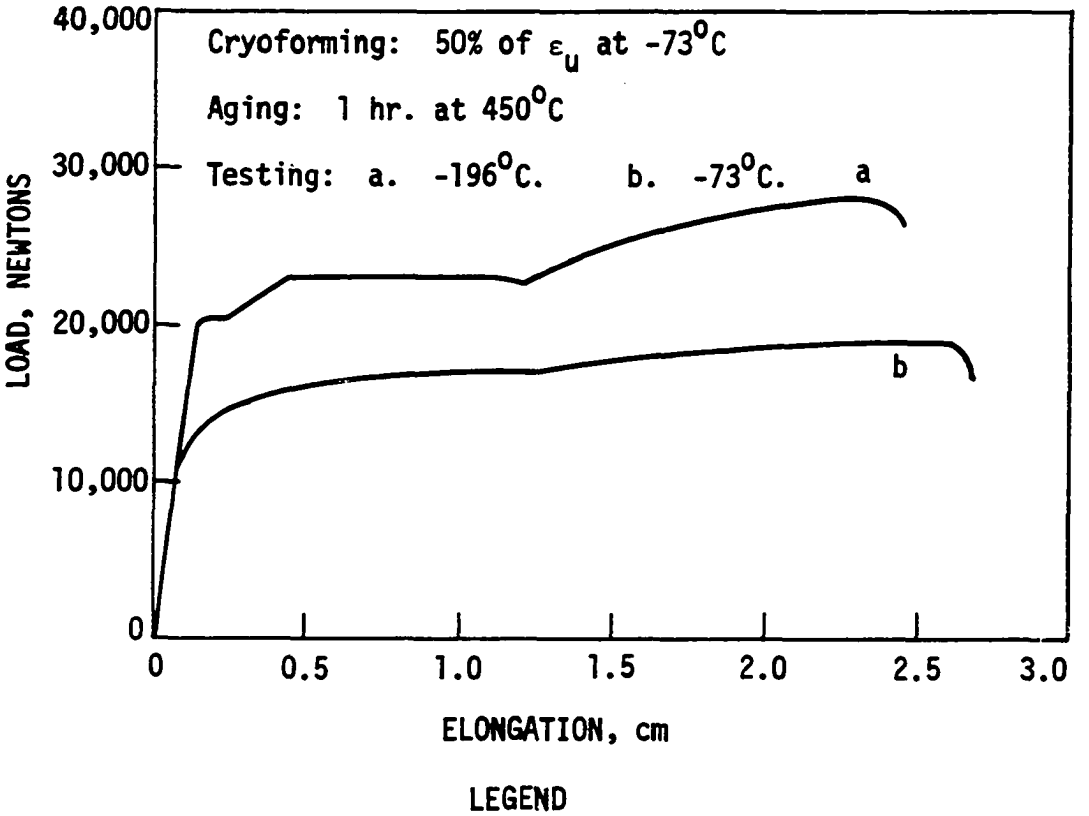

LEGEND

a. $A_o = 0.165\ cm^2$, $S_y = 1252$ MPa, $S_u = 1721$ MPa, $A_r = 28\%$

b. $A_o = 0.144\ cm^2$, $S_y = 1042$ MPa, $S_u = 1319$ MPa, $A_r = 31\%$

Figure 41. Load-elongation curves showing the effects of testing temperature on martensite transformation rate.

responsible for burst transformation increases with increasing driving force. At the higher temperature, the driving force and the rate of faulting decreased, suppressing the phenomenon.

When tested at -196°C, the specimens deformed at -73°C exhibit equal or better ductility than those deformed 50% of ϵ_u at room temperature. The austenite stability level in the latter specimens was much lower than in the former. The amounts of prior strain were the same for specimens prestrained 50% of ϵ_u at both -73°C and 25°C. The larger free energy change between 25°C and -196°C accounted for the lower austenite stability in the cold worked specimens. The results suggest that the faster transformation rate resulted in premature fracture in the less ductile martensite.

F. Correlations Between Structure and Mechanical Properties

Since martensitic transformation occurred during tensile testing, only the yield strength could be directly related to the structure of the thermomechanically treated alloy. The work hardening rate increased with progressive transformation, making it meaningless to relate the tensile strength to the microstructure of the as-processed material. The ductility was dependent on the martensite transformation rate during testing. The ductility is enhanced if, upon the initiation of necking, sufficient martensite is formed to cause localized strengthening in the neck region. Further deformation occurs

in the surrounding austenite grains resulting in increased ductility. In the absence of a stress-induced martensitic transformation, as was the case in this study, the yield strength is directly related to the structure of the thermo-mechanically treated alloy.

Data for complete correlations between the microstructure and the yield strength have been obtained only for specimens tested at -196°C. It was expected that the mechanisms contributing to the yield strength increase were independent of testing temperature. Separate correlations were established between the microstructure and yield strength of naturally and artificially aged specimens.

1. Naturally aged specimens

The improved yield strength of the naturally aged specimen was due to the formation of strain-induced martensite and work hardening of both the freshly formed martensite and retained austenite. At low prestrain levels, strengthening was due predominantly to strain-induced martensite. At higher prestrain levels strain hardening of martensite and austenite contributed significantly to the yield strength. The following relationships were established between the yield strength S_y at -196°C and the volume fration of martensite V_α, (Figure 42):

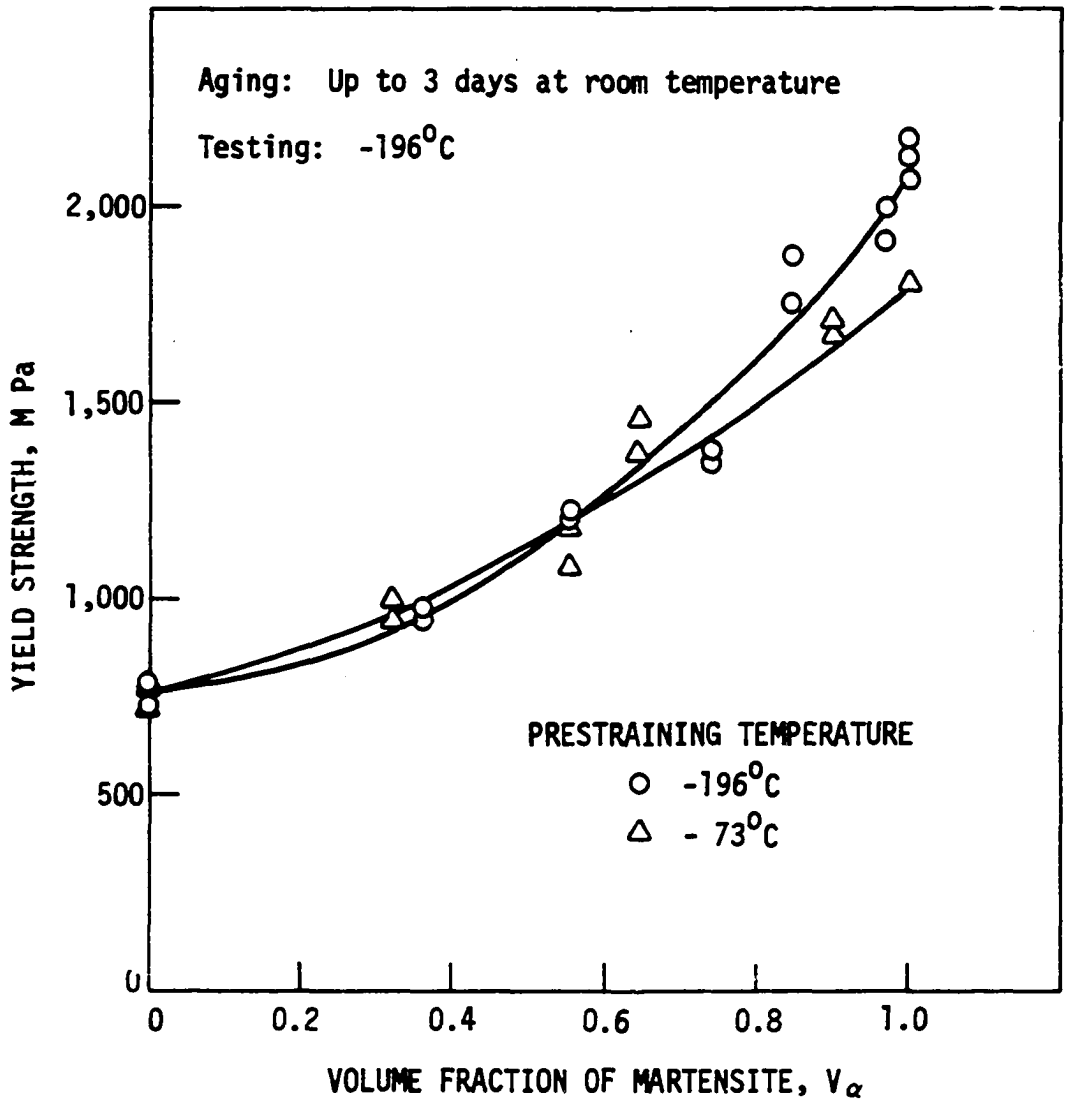

Figure 42. Correlation between yield strength and volume fraction of martensite.

For specimens prestrained at -196°C,

$$S_y = 756 + 1326\ V_{\alpha'}^{1.88} \qquad \text{(III-2)}$$

For specimens prestrained at -73°C,

$$S_y = 756 + 1002\ V_{\alpha'}^{1.32} \qquad \text{(III-3)}$$

The values of S_y for $V_{\alpha'} = 0$ in both equations represents the yield strength of the annealed material at -196°C.

Increased dislocation density was responsible for the strengthening due to strain hardening. The martensite transformation is accompanied by severe deformation of the surrounding austenite (52). At any prestrain level, both the retained austenite and freshly formed martensite were heavily dislocated. The strain hardening contribution to the yield strength increased with increasing prestrain level, and decreasing cryoforming temperature. At higher strains the applied mechanical energy was utilized predominantly in the work hardening of the retained austenite and the strain-induced martensite. The martensite formed at a lower cryoforming temperature had a higher dislocation density than that formed at a higher temperature. This increased the strain hardening contribution to strength.

Strengthening mechanisms proposed to date for cryoformed austenitic stainless steels have neglected the contribution of strain hardening. The load-elongation curve of the annealed material tested below the M_d temperature showed a strong effect of strain hardening at high strains.

It was therefore not surprising that the strength of highly prestrained specimens would be improved further by strain hardening.

2. Artificially aged specimens

The appearance of precipitates in the matrix of the artificially aged specimen contributed to increased yield strength. On the other hand, depletion of carbide forming elements from the matrix, dislocation annihilation, and austenite reversion weakened the matrix. When dislocations cut through precipitates, the contribution to yield strength is directly proportional to the square root of the particle size (74). In order for precipitates to increase both the yield and tensile strengths, they must be stronger than the matrix so as to resist shearing.

For dislocation bowing to be the deformation mechanism, the particle sizes must exceed a critical value. Kelly and Nicholson (74) have shown that the critical size r_c of a particle which would resist shearing is given by:

$$r_c = \frac{2Gb^2}{\pi\beta} \qquad \text{(III-4)}$$

where:

G = the shear modulus of the matrix

b = the Burgers vector of the matrix

β = the interfacial energy per unit area between the particle and matrix.

The average interface energy β_{ave}, is given by:

$$\beta_{ave} = 0.03\ G'b' \qquad \text{(III-5)}$$

where:

G' = the shear modulus of the carbide particle

b' = the Burgers vector of the particle.

By substituting the corresponding equivalent values of G, b and β in equation III-4, it was estimated that r_c was of the order of 6 Å (Appendix D.1). The carbides observed in the thermomechanically treated specimen were larger than the estimated r_c values. Therefore, dislocation bowing rather than particle shearing was the mode of plastic deformation.

For unsheared particles, the contribution to strengthening is predicted by the modified Orowan relationship (73) as:

$$\Delta S_y = \frac{G\ b\ \phi}{2\ (d-2r)} \ln \frac{d-2r}{2b} \qquad \text{(III-6)}$$

where:

G = shear modulus of the matrix

b = Burgers vector of a dislocation

r = mean particle radius

d = mean spacing between particles

$\phi = \frac{1}{2}(1 + 1/1-\nu)$

ν = Poisson's ratio

By substituting the corresponding values of G, b, and ν in the

Orowan relationship, it has been shown that values of d ranging from 200 Å to 800 Å can produce yield strength increases of 225 MPa to 650 MPa (Appendix D.2). The spacings observed in this study range from about 200 Å to 500 Å and satisfy the values of d required for effective strengthening. These results indicate that the carbide distribution in the artificially aged material can account for the secondary hardening observed in the cryoformed austenitic stainless steel. Mangonon and Thomas (21) have completely neglected the contribution of carbides to the secondary strengthening of a thermomechanically treated austenitic stainless steel in spite of the fact that they observed them. Chukleb and Martynov (10) have attributed some strengthening to carbide precipitation but do not provide any quantitative justification for the conclusion.

IV. CONCLUSIONS AND RECOMMENDATIONS

A. Conclusions

1. Relationships of the form $V_{\alpha'} = A\epsilon+B$ have been derived between the volume fraction of martensite and the true strain. The constant A is inversely proportional to austenite stability, and its values are 3.85 at -196°C and 3.48 at -73°c.
2. Martensite transformation can enhance the low temperature ductility of both annealed and thermomechanically treated austenitic stainless steels. An optimum rate of transformation exists for the ductility improvements.
3. The combined effects of cryoforming and aging can produce a cryogenic yield strength in excess of 2000 MPa, with good ductility. Extensive room temperature deformation produces yield strengths of only up to 1300 MPa.
4. The stability of strain-induced martensite increased with an increasing amount of deformation and decreasing deformation temperature.
5. Short-time room temperature exposure produces an upper yield point phenomenon due to dislocation pinning by carbon atoms.
6. Artificial aging of the cryoformed material causes precipitation of $(FeCr)_{23}C_6$ carbides.
7. The factors affecting the strength are:
   a. Strain-induced martensitic transformation

b. Strain hardening of retained austenite and freshly formed martensite

c. Processes occurring during aging:

i. Precipitation of iron-chromium carbides

ii. Growth and coalescence of the precipitates

iii. Depletion of carbide-forming elements from the matrix

iv. Austenite reversion.

8. The major strengthening mechanisms in the naturally aged specimens are strain-induced martensite and work hardening of martensite and retained austenite. The yield strength at -196°C is related to the volume fraction of martensite as follows:

For specimens cryoformed at -196°C:

$$S_y = 756 + 1326\ V_{\alpha'}^{1.88}$$

For specimens cryoformed at -73°C:

$$S_y = 756 + 1002\ V_{\alpha'}^{1.32}$$

9. Precipitates alone can contribute between 225 and 650 MPa to the yield strength of the artificially aged specimens. The net effect of aging on the strength is the sum of the strengthening contribution due to precipitates, and the weakening due to matrix depletion, austenite reversion, and dislocation annihilation.

10. Aging the cryoformed material for 1 hr between 400°C and 450°C is sufficient to produce optimum mechanical properties. Aging for up to 12 hrs has no significant advantage

over aging for 1 hr.

11. The mechanical properties are rate independent within the testing range of 0.05 min^{-1} to 0.5 min^{-1}.
12. The M_d temperature of the alloy is lower than 25°C but higher than -73°C. M_s is lower than -196°C.

B. Recommendations

1. Quantitative correlations between the strength, microstructure and prestrain level should be established for the thermomechanically treated material at temperatures other than -196°C. For specimens tested above the M_d temperature, the correlations should be established between the microstructure and both the yield and tensile strengths. For those tested below M_d, only the yield strength should be related to the microstructure.
2. The effects of an interrupted cryogenic tensile test on the strength of the previously cryoformed and aged alloy should be studied. Since the objective of such a study would be to capitalize on further martensitic transformation during interrupted testing, only specimens known to be partially martensitic after the initial thermomechanical treatment should be studied.
3. The effects of a wider range of strain rates than those employed in this study on the rate of martensitic transformation and ductility of the cryoformed material should be studied.

4. The effects of cryoforming by rolling on the structure and mechanical properties of the austenitic stainless steel should be investigated.
5. The effects of cryoforming on the mechanical properties of an alloy, which does not undergo an allotropic transformation during cryostraining, should be studied. For alloys possessing higher ϵ_u at cryogenic temperatures than at ambient, the effects of uniform prestrain levels attainable only at cryogenic temperatures should be evaluated.
6. The effects of cryoforming by rolling on the structure and mechanical properties of a wide range of engineering materials should be studied.

V. REFERENCES

1. Duckworth, W. E. "Thermomechanical Treatment of Metals." J. Met. 18 (August 1966): 915.

2. Dula, E. B., and Radcliffe, S. V. "Thermomechanical Treatment of Steel." J. of Metals 15 (1963): 755.

3. Justusson, W. M., and Clark, R. "Thermomechanical Treatments, Processing and Properties." Mechanical Working and Processing Conference 4 (1969): 481.

4. Binder, W. O. "Effect of Cold Work at Low Temperature on Austenitic 18-8." Met. Prog. 58 (August 1950): 201.

5. Krivobok, V. N., and Talbot, A. M. "Effect of Temperature on the Mechanical Properties, Characteristics, and Processing of Austenitic Stainless Steels." Proc. ASTM 50 (1950): 895.

6. McDowell, D. W., Jr., and Mihalisin, J. R. "Zerolling Boosts Strength of Stainless Sheet." Mater. Engr. Des. 53 (May 1961): 10.

7. Llewellyn, D. T., and Murray, J. D. "Cold Worked Stainless Steels." Iron and Steel Inst. Spec. Report No. 86 (1964): 197.

8. Fiedler, H. C., Averbach, B. C., and Cohen, M. "The Effect of Deformation on the Martensitic Transformation in Austenitic Stainless Steels." Trans. ASM 47 (1955): 267.

9. Mayne, C. R. "Effect of Zerolling on Properties of Modified Type 346 Stainless Steel." ASTM STP No. 287 (1960): 150.

10. Chukleb, A. N., and Martynov, V. P. "Phase Transformations $\gamma \rightleftarrows \alpha$ During the Aging of 1808 Type Steels Previously Deformed at a Negative Temperature." Phys. Met. Metallogr. 10(2) (1960): 80.

11. Maxwell, P. C., Goldberg, A., and Shyne, J. C. "Stress-Assisted and Strain-Induced Martensites in Fe-Ni-C Alloys." Met. Trans. 5 (June 1974): 1305.

12. Herzog, R. G., Osgood, S. H., and Lighty, D. "Properties of Cryogenically Worked Materials." Final Report, Martin Marietta Corp., Denver, Colorado (August 1971) NASA CR-72798.

13. Grigokin, V. I. "Thermomechanical Treatment of Austenitic Steels." Phys. Met. Metallogr. 14(2) (1962): 45.

14. Masteller, R. D., Brown, H. J., Herzog, R. G., and Osgood, S. H. "Properties of Cryogenically Worked Materials." Interim Report, Martin Marietta Corp., Denver, Colorado. NASA CR-72638, May 1, 1970.

15. Shlyameneva, I. A., Galov, A. G., Vasil'eva, A. G., Prokoshkin, D. A., and Stepanov, G. A. "Aging of Stainless Precipitation Hardening Steels After Low-Temperature Deformation." Met. Sci. Heat Treat. Met. 17(2) (Jan.-Feb. 1975): 157.

16. Rozkhova, S. B., and Osintseva, A. L. "Mechanical Properties of Austenitic Steels After Low Temperature Deformation and Tempering." Met. Sci. Heat Treat. Met. 17(2) (Jan.-Feb. 1975): 160.

17. Novikov, N. V., and Gorodyskii, N. I. "Effects of Low Temperature Elongation on Mechanical Properties of Steel Kh18NIOT." Met. Sci. Heat Treat. Met. 17(2) (Jan.-Feb. 1975): 164.

18. Schwartzberg, F., and Kiefer, J. T. "Properties of Cryogenically Worked Metals." NASA CR-1345757, 1975.

19. Floreen, S., and Mihalisin, J. R. "High-Strength Stainless Steel by Deformation at Low Temperatures." ASTM STP No. 369 (1965): 17.

20. Mangonon, P. L., and Thomas, G. "The Martensite Phases in 304 Stainless Steel." Met. Trans. 1 (June 1970): 1577.

21. Mangonon, P. L., and Thomas, G. "Structure and Properties of Thermal-Mechanically Worked 304 Stainless Steel." Met. Trans. 1 (June 1970): 1587.

22. Ziegler, N. A., and Brace, P. H. "Hardening of Austenitic Stainless Steels by Mechanical Working at Sub-Zero Temperatures." Proc. ASTM 50 (1950): 861.

23. Fujimura, Y., and Ishii, H. "Tensile Behavior of High Cr Low Ni Two-Phase Stainless Steels at Room and Low Temperature." J. Japan Inst. Met. 37(1) (1973): 33.

24. Spiridonov, B. D., Kuz'minskaya, L. N., and Gordeev, Y. P. "Strengthening of Cr-Ni Steels with Unstable Austenite." Met. Sci. Heat Treat. Met. 15(3-4) (March-April 1973): 271.

25. Shteinberg, M. M., Goikhenberg, Y. N., Smirnov, M. A., and Mirzaev, D. A. "Strengthening of Stainless Steels by Deformation, the Martensitic Transformation, and Aging." Met. Sci. Heat Treat. Met. 14(7-8) (July-Aug. 1972): 586.

26. Fahr, Dieter. "Stress- and Strain-Induced Formation of Martensite and Its Effects on Strength and Ductility of Metastable Austenitic Stainless Steels." Met. Trans. 2 (July 1971): 1883.

27. Maxwell, P. C., Goldberg, A., and Shyne, J. C. "Influence of Martensite Formed During Deformation on the Mechanical Behavior of Fe-Ni-C Alloys." Met. Trans. 5 (June 1974): 1319.

28. Alper, R. W. "Cryogenically Stretch-Formed Type 301 Stainless Steel for Cryogenic Service." Mater. Res. Stand. 4 (1964): 525.

29. Kunsagi, L., Svend, M., and Apblett, W. R., Jr. "Method for the Explosive Section Forming of Pressure Vessels." Foster Wheeler Corp., New York. U.S. Patent No. 3,344,509, October 1967.

30. Cozewith, A. "Cryogenic Stretch Forming Improves Strength of Vessels." Met. Prog. 96 (July 1969): 64.

31. Lyulicheva, N. N., and Pisareva, N. V. "Effect of Rolling at Sub-Zero Temperatures on Mechanical Properties of Austenitic Steels." Met. Sci. Heat Treat. Met. 4 (April 1959): 23.

32. Post, C. B., and Eberly, W. S. "Stability of Austenite in Stainless Steels." Trans. ASM 39 (1947): 868.

33. Bain, E. C., and Paxton, H. W. Alloying Elements in Steel. ASM (1961): 57-68.

34. Eichelman, G. H., Jr., and Hull, F. C. "The Effect of Composition on the Temperature of Spontaneous Transformation of Austenite to Martensite in 18-8 Type Stainless Steel." Trans. ASM 34 (1953): 77.

35. Angel, T. "Formation of Martensite in Austenitic Stainless Steels." J. of Iron and Steel Inst. 177 (May 1954): 165.

36. Gerberich, W. W., Thomas, G., Parker, E. R., and Zackay, V. F. "Metastable Austenites: Decomposition and Strength." Proc. Second Inst. Conf. on the Strength of Metals and Alloys, Asilomar, Calif., 2 (August 1970): 894.

37. Cohen, M. "On the Development of High Strength in Steel." J. Iron and Steel Inst. 201 (1963: 833.

38. Duckworth, W. E., Taylor, P. R., and Leak, D. A. "Ausforming Behavior of En24, En30B and Experimental 3% Cr-Ni-Si Steel." J. Iron and Steel Inst. 202 (1964): 135.

39. Grange, R. A. "Strengthening Steel by Austenite Grain Refinement." Trans. ASM 59 (1966): 26.

40. Marder, A. R., and Krauss, G. "The Effect of Morphology on the Strength of Lath Martensite." Proc. Second International Conf. on the Strength of Metals and Alloys, Asilomar, Calif., 2 (August 1970): 894.

41. Breedis, J. F., and Kaufman, L. "Formation of HCP and BCC Phases in Austenitic Alloys." Met. Trans. 2 (1971): 2359.

42. Patel, J. R., and Cohen, M. "Criterion for the Action of Applied Stress in the Martensitic Transformation." Acta Met. 1 (1953): 531.

43. Bressanelli, J. P., and Moskowitz, A. "Effects of Strain Rate, Temperature and Composition on Tensile Properties of Metastable Austenitic Steels." Trans. ASM 59 (1966): 223.

44. Kurdjumov, G. V. "Martensite Crystal Lattice, Mechanism of Austenite-Martensite Transformation and Behavior of Carbon Atoms in Martensite." Met. Trans. 7A (1976): 913.

45. Zackay, V. F., Parker, E. R., Farr, D., and Busch, R. "The Enhancement of Ductility in High-Strength Steels." Trans. ASM 60 (1967): 252.

46. Rosen, A., Jago, R., and Kjer, T. "Tensile Properties of Metastable Stainless Steels." J. Mat. Sci. 7 (1972): 870.

47. Cina, B. "Effect of Cold Work on the $\gamma \rightarrow \alpha$ Transformation in Some Fe-Ni-Cr Alloys." J. Iron Steel Inst. 177 (August 1954): 406.

48. Cina, B. "A Transition of HCP Phase in the $\gamma \rightarrow \alpha$ Transformation in Certain Fe-Base Alloys." Acta Met. 6 (1958): 748.

49. Breedis, J. F., and Robertson, W. "The Martensitic Transformation in Single Crystals of Iron-Chromium-Nickel Alloys." Acta Met. 10 (November 1962): 1077.

50. Kelly, P. M. "The Martensite Transformation in Steels With Low Stacking Fault Energy." Acta Met. 13 (June 1965): 635.

51. Bhandarkar, D., Zackay, V. F., and Parker, E. R. "Stability and Mechanical Properties of Some Metastable Austenitic Steels." Met. Trans. 3 (1972): 2619.

52. Kelly, P. M., and Nutting, J. "The Morphology of Martensite." J. Iron Steel Inst. 197 (1961): 199.

53. Henessy, D., Steckel, G., and Altstetter, C. "Phase Transformation of Stainless Steel During Fatigue." Met. Trans. 7A (1976): 415.

54. Reed, R. P. "The Spontaneous Martensitic Transformation in 18% Cr-8Ni Steels." Acta Met. 10 (September 1962): 865.

55. Otte, H. M. "The Formation of Stacking Faults in Austenite and Its Relation to Martensite." Acta Met. 5 (1967): 614.

56. Breedis, F. J. "Martensitic Transformations in Iron-Chromium-Nickel Alloys." Trans. Met. Soc. AIME 230 (December 1964): 1583.

57. Lecroisey, F., and Pineau, A. "Martensitic Transformation Induced by Plastic Deformation in the Fe-Ni-Cr-C System." Met. Trans. 3 (February 1972): 387.

58. Kurdjumov, G., and Sachs, G. "Über den Mechanismus der Stahlhärtung." Z. Physik. 64 (1930): 325.

59. Reed, R. P., and Guntner, G. J. "Stress-Induced Martensitic Transformation in 18Cr-8Ni Steel." Trans. Met. Soc. AIME 230 (1964): 1713.

60. Venables, J. A. "The Martensite Transformation in Stainless Steel." Phil. Mag. 7 (1962): 35.

61. Lagneborg, R. "The Martensite Transformation in 18% Cr-8% Ni Steels." Acta Met. 12 (July 1964): 823.

62. Maki. T., Shimooka, S., Umemoto, M., and Tamura, I. "The Morphology of Strain-Induced and Thermally Transformed Martensite in Fe-Ni-C Alloys." Trans. Japan Inst. Met. 14 (1973): 62.

63. Maki, T., Shimooka, S., Arimoto, T., and Tamura, I. "The Morphology of Thin Plate-Like Martensite in Fe-Ni-C Alloys." Trans. Japan Inst. Met. 14 (1973): 62.

64. "The Ardeform Process." Rep. P-30715C, Arde-Portland, Inc., Paramus, N.J. U.S. Patent No. 3,197,851, Jan. 25, 1964.

65. Powder Diffraction File. ASTM, Philadelpha, Pa., 1967.

66. Cullity, B. C. "Elements of X-ray Diffraction." Addison Wesley, Cambridge, Mass., 1967.

67. Smakula, A. "High-Precision Density Determination of Solids." In Methods of Experimental Physics, 6A, p. 283. K. L. Horowitz, Editor. Academic Press, New York, 1959.

68. Kayser, F. X., Litwinchuk, A., and Stowe, G. L. "The Densities of High Purity Iron Carbon Alloys in the Spheroidized Condition." Met. Trans. 6A (1975): 55.

69. Rogers, H. C., and Coffin, L. F., Jr. "Investigation of the Nature of Structural Damage in Metal Forming Processes." NOW66 0546 General Electric Research Co., Schenectady, New York, 1967.

70. Hozelitz, K. Ferromagnetic Properties of Metals and Alloys. Oxford Clarendon Press, Oxford, 1952.

71. Parr, J. G. "X-ray Investigation of the Epsilon Phase in an Fe-Mn Alloy." J. Iron and Steel Inst. 171 (1952): 137.

72. Andrews, K. W., Dyson, D. J., Keown, S. R. In Interpretation of Electron Diffraction Patterns. Hilger and Watts, London, 1967.

73. Cahn, J. W. "Nucleation on Dislocations." Acta Met. 5 (March 1957): 196.

74. Kelly, A., and Nicholson, R. B. "Precipitation Hardening." Prog. Mater. Sci. 16(3) (1963): 151-391.

75. Glover, S. G., and Smith, T. B. "The stabilization of Austenite." In Mechanism of Phase Transformation in Metals, p. 265. Inst. of Metals, London, 1959.

76. Fletcher, S. G., Averbach, B. L., and Cohen, M. "The Dimensional Stability of Steel - Part II - Further Experiments on Subatmospheric Transformations." Trans ASM 40 (1948): 703.

77. Hornbogen, E. "Physical Metallurgy of Steels." In Physical Metallurgy, p. 619. R. W. Cahn, Editor. North Holland Publishing Co., Amsterdam-London, 1970.

78. Speich, G. R., and Leslie, W. C. "Tempering of Steel." Met. Trans. 3 (1972): 1043.

79. Tekin, E., and Kelly, P. M. "Precipitation from Iron Base Alloys." Inst. Met. Society Conferences 28 (1963): 173.

80. Wilson, G. F. "Tempering of Carbon and Low Alloy Steels." in Martensite, Fundamentals and Technology, p. 143. E. R. Petty, Editor. Longmans, New York, 1970.

81. Fisher, J. C. "The Free Energy Change Accompanying the Martensite Transformation in Steels." Metals Trans. 185 (1949): 688.

82. Christian, J. W. "Phase Transformations." In Physical Metallurgy, p. 552. J. W. Cahn, Editor, North Holland Publishing Co., Amsterdam-London, 1970.

83. Swann, P. R. "Dislocation Arrangements in Face-Centered Cubic Metals and Alloys." In Electron Microscopy and Strength of Crystals, p. 131. G. Thomas, and J. Washburn, Editors. Interscience, New York, 1963.

84. Jaswon, M. A. "The Nucleation Problem in Martensite." In The Mechanism of Phase Transformations in Metals, p. 173. Inst. of Metals Monograph Report Series No. 18, Inst. Met., London, 1956.

85. Olson, G. B., and Cohen, M. "Kinetics of Strain-Induced Martensitic Nucleation." Met. Trans. 3 (1972): 2619.

86. Goodchild, D., Roberts, W. T., and Wilson, D. V. "Plastic Deformation in Textured Austenitic Stainless Steel." Acta Met. 18 (1970): 1137.

87. Zener, C. "Theory of Growth of Spherical Precipitates from Solid Solution." J. Appl. Phys. 20 (1949): 950.

88. Scott, T. E. "Calculations Concerning Precipitate Growth During Impact Extrusion." US-ERDA Report, Ames, Iowa 1975. Contract No. W-7405-eng-82.

89. Huntz, A. M., Guiraldenq, P., Aucouturier, M., and Lacombe, P. "Relation entre les phenomenes de diffusion du fer et du chrome radioactifs dans les alliages fer-chrome de 0a 15% de chrome et leur transformations $\alpha \rightleftarrows (\alpha + \gamma)$." Memoires Scientifiques Rev. Metallurg. 66(2) (1969): 85.

90. Metals Handbook, 1 (1961): 644. ASM, Metals Park, Ohio.

ACKNOWLEDGMENTS

The author is grateful to Prof. Alexander Henkin for his supervision of this work.

Special thanks are due Dr. Vernon F. Mayer for supervising the study while Dr. Henkin was on faculty improvement leave.

The author would like to thank Prof. Tom E. Scott for useful suggestions offered during the course of the study.

The author wishes to express gratitude to Profs. S. Bahadur, H. M. Black and J. D. Verhoeven for serving on the doctoral committee.

The author is grateful to Messrs. Lester K. Reed, Harlan H. Baker, Jerry Amenson, George Steininger, Robert Steed, and Larry Couture for their assistance.

He wishes to express profound gratitude to Mrs. Ina Couture for doing an excellent typing job and to Mr. Andrew Manu for his encouragement during the preparation of this report.

He is grateful to Mr. Malay Kar for seeing the report through the final stages of publication.

VII. APPENDIX A. MARTENSITE VOLUME FRACTION DETERMINATION

1. Error analysis on density measurements:

The density, ρ, of the partially transformed material is given by

$$\rho = \rho_\gamma V_\gamma + \rho_\alpha, V_\alpha, \qquad \text{(A.1-1)}$$

where:

ρ_γ, ρ_α, = densities of pure austenite and martensite, respectively

V_γ, V_α, = volume fractions of pure martensite and austenite, respectively

but

$$V_\gamma + V_\alpha, = 1 \qquad \text{(A.1-2)}$$

$\therefore$ equation A.1 becomes

$$V_\alpha, = \frac{\rho_\gamma - \rho}{\rho_\gamma - \rho_\alpha,}$$

Since ρ_γ, ρ_α, are constants, the only variable in this relationship is ρ, i.e., $V_\alpha, = f(\rho)$

$$\Delta V_\alpha, = \frac{-\Delta\rho}{\rho_\gamma - \rho_\alpha,} \qquad \text{(A.1-3)}$$

where:

ΔV_α, = error in V_α,

$\Delta\rho$ = error in ρ

but

$$\rho = \frac{W_a}{W_a - W_w} \cdot \rho_w$$

where:

W_a = weight of specimen in air

W_w = weight of specimen in water

ρ_w = density of distilled water

= 1.0000 g/cm^3

$$(\Delta\rho)^2 = \left(\frac{\partial\rho}{\partial W_a}\right)^2 \cdot \Delta W_a^2 + \left(\frac{\partial\rho}{\partial W_w}\right)^2 \cdot \Delta W_w^2$$

$$= \left[\frac{W_a - (W_a - W_w)}{(W_a - W_w)^2}\right]^2 \Delta W_a^2 + \left[\frac{-W_a}{(W_a - W_w)^2}\right]^2 \Delta W_w^2$$

$$= \left[\frac{W_w}{(W_a - W_w)^2}\right]^2 \cdot (\Delta W_a)^2 + \left[\frac{W_a}{(W_a - W_w)^2}\right]^2 (\Delta W_w)^2$$

For the balance used $\Delta W_a \approx \Delta W_w = 0.0002$ g

Sample calculations: For smallest specimen used in this study leading to largest $\Delta V_{\alpha'}$:

$W_a = 2.8332$ g

$W_w = 2.4772$ g

$$(\Delta\rho)^2 = \left[\frac{2.4772}{(0.356)^2}\right]^2 \cdot (0.0002)^2 + \left[\frac{2.8332}{(0.356)^2}\right]^2 (0.0002)^2$$

$$= 1528 \times 10^{-8} + 1999 \times 10^{-8}$$

$$\Delta\rho = 0.00594 \text{ g/cm}^3$$

From equation A.3

$$\Delta V_{\alpha'} = \frac{0.00594}{0.1451} = 0.041$$

For the specimen sizes used in this study, the largest variation in the volume fraction of martensite obtained by density measurement was of the order of $\pm$ 5%, corresponding

to a variation in density of 0.006 g/cm^3.

2. Density measurements:

$$V_{\alpha'} = \frac{\rho_\gamma - \rho}{\rho_\gamma - \rho_{\alpha'}} \qquad \text{(A.2-1)}$$

where:

$V_{\alpha'}$ = volume fraction of martensite

ρ_γ = density of pure austenite

$\rho_{\alpha'}$ = density of pure martensite

ρ = density of thermomechanically treated specimen

but

$$\rho_{\alpha'} = \frac{a_\gamma^3}{2a_{\alpha'}^3}\,\rho_\gamma \qquad \text{(A.2-2)}$$

where

a_γ = lattice parameter of austenite

$a_{\alpha'}$ = lattice parameter of martensite

Measured values:

$\rho_\gamma = 7.9584\ g/cm^3$

$a_\gamma = 3.5891$ Å

$a_{\alpha'} = 2.8662$ Å

$$\rho_{\alpha'} = \frac{(3.5891)^3}{2(2.8662)^3}\,(7.9584)$$

$$= 7.8133\ g/cm^3$$

From equation A.2-1:

$$V_{\alpha'} = \frac{7.9584 - \rho}{7.9584 - 7.8133} = \frac{7.9584 - \rho}{0.1451} \qquad (A.2\text{-}3)$$

Sample results:

Specimens deformed 50% of ϵ_u at -196°C

Post deformation treatment	Weight in air W_a g	Weight in water W_w g	Density ρ g/cm^3	Martensite content $V_{\alpha'}$ %
Room temperature for 3 days	5.4806	4.7850	7.8790	55
	5.4806	4.7850	7.8770	55
210°C for 2 hrs	7.5486	6.5903	7.8770	56
	7.5488	5.5899	7.8724	59
210°C for 12 hrs	7.1976	6.2831	7.8705	61
	7.1976	6.2831	7.8705	61
300°C for 1 hr	7.2373	6.3190	7.8812	53
	7.2374	6.3193	7.8830	52
350°C for 1 hr	7.5554	6.5976	7.8883	48
	7.5554	6.5978	7.8900	47
400°C for 1 hr	5.5504	4.8472	7.8930	45
	5.5503	4.8473	7.8952	44
450°C for 1 hr	6.6733	5.8279	7.8937	45
	6.6732	5.8278	7.8935	45
500°C for 1 hr	4.2312	3.6965	7.9132	31
	4.2310	3.6965	7.9158	29

3. Magnetic measurements:

$$V_{\alpha'} = \frac{\sigma}{\sigma_s} \qquad \text{(A.3-1)}$$

where:

σ_s = saturation magnetic moment per unit mass for 100% martensite

σ = saturation magnetic moment per unit mass for thermomechanically treated specimen

The value of σ_s was determined using the specimens deformed 90% of ϵ_u at -196°C and aged at temperatures up to 450°C.

Post deformation treatment	Specific saturation moment σ kilogauss/g	Square of standard error of mean $(\sigma - \sigma_s)^2$
Naturally aged	128.02	5.41
	127.82	4.51
300°C for 1 hr	123.37	5.41
	121.60	16.77
350°C for 1 hr	127.42	2.98
	125.56	0.02
400°C for 1 hr	127.43	3.01
	129.42	13.88
450°C for 1 hr	121.18	20.39
	125.13	0.32
Summation	1256.95	72.70

$$\sigma_s = \frac{\Sigma\sigma}{n} = \frac{1256.95}{10} - 125.695 \pm 4.532$$

to 99.9% confidence limit.

$$\sigma_s = 125.70 \pm 4.53 \text{ kilogauss/g}$$

Sample results:

Specimens deformed 50% of ϵ_u at -196°C

Post deformation treatment	Moment μ kilogauss	Mass m g	Specific moment σ kilogauss/g	Martensite content V_α, %
Room temperature	10.60	0.158	67.16	53
3-4 days	10.63	0.158	67.28	54
210°C for 1 hr	11.24	0.165	70.25	52
	11.26	0.160	70.38	56
210°C for 12 hrs	18.12	0.242	74.88	60
	17.95	0.242	74.17	59
300°C for 1 hr	13.57	0.212	64.09	51
	13.50	0.212	63.68	51
350°C for 1 hr	13.55	0.244	52.76	45
	14.10	0.244	57.78	46
400°C for 1 hr	6.33	0.110	57.52	46
	6.30	0.110	57.27	46
450°C for 1 hr	16.33	0.307	53.20	42
	16.35	0.307	53.20	42
500°C for 1 hr	10.59	0.269	39.37	31
	10.61	0.269	39.44	31

VIII. APPENDIX B. LATTICE PARAMETERS OF AUSTENITE AND MARTENSITE

Equations used:

The interplanar angle θ is given by:

$$\theta^{0} = \frac{180^{0}\ (Sx10)}{2} \qquad \text{(B-1)}$$

where S is the distance in cm from a diffraction line to the point where the incident beam struck the film.

The Nelson-Riley function, NR, is given by

$$NR = \tfrac{1}{2}\left(\frac{\cos^2\theta}{\sin^2\theta} + \frac{\cos^2\theta}{\theta}\right) \qquad \text{(B-2)}$$

The lattice parameter a, of a cubic crystal, is given by:

$$a = \frac{\lambda}{\sin\theta}\,(h^2 + k^2 + l^2)^{\frac{1}{2}} \qquad \text{(B-3)}$$

where

λ = wavelength of radiation used

hkl = indices of the diffracting plane

for Crk_{α} radiation: $\lambda_{\beta} = 2.0848$ Å

$\lambda_{\alpha} = 2.2909$ Å

1. Lattice parameter of austenite:

Table B1. Values of crystal properties from Debye-Scherrer pattern

Indices hkl	S cm	Interplanar angle θ degrees	Lattice parameter a Å	Nelson-Riley coefficient NR
111_{α}	12.0655	29.673	3.6471	1.4913
111_{α}	11.3630	33.185	3.6247	1.2445
200_{β}	10.9630	35.185	3.6182	1.1235
200_{α}	10.1640	39.180	3.6261	0.9148
220_{β}	7.0632	54.684	3.6133	0.3799
220_{α_1}	5.1540	64.230	3.5955	0.1892
$\alpha\alpha 0_{\alpha_2}$	5.0499	64.7500	3.5861	0.1811
311_{α}	3.1505	74.2475	3.5922	0.0667

Regression Analysis

Table B2. Values used in regression analysis

x	y	xy	x^2	y^2
1.4913	3.6471	5.4387	2.2240	13.3013
1.2445	3.6247	4.5109	1.2488	13.1384
1.1235	3.6182	4.0650	1.2623	13.0914
0.9148	3.6261	3.3172	0.8369	13.1486
0.3799	3.6133	1.3727	0.1443	13.0559
0.1892	3.5955	0.6803	0.0358	12.9276
0.1811	3.5861	0.6494	0.0328	12.8601
0.0667	3.5922	0.2396	0.0045	12.9039
Summation 5.5910	28.9032	20.2740	6.0894	104.4272

$$a = \frac{\Sigma x^2 \Sigma y - \Sigma x \Sigma xy}{N\Sigma x^2 - (\Sigma x)^2}$$

where

N = number of data points

$$a_\gamma = \frac{176.0031 - 113.3519}{48.7152 - 31.2572} = \frac{62.6512}{17.4500} = 3.5891 \text{ Å}$$

2. Lattice parameter of martensite

Table B3. Values of crystal properties from Debye-Scherrer pattern

Indices hkl	S cm	Interplanar angle θ degrees	Lattice parameter a Å	Nelson-Riley coefficient NR
110_β	11.745	31.275	2.8392	1.3728
110_α	11.052	34.740	2.8415	1.1493
200_α	7.355	53.225	2.8600	0.4166
211_β	5.358	63.210	2.8602	0.2059
211_α	2.355	78.225	2.8661	0.0365

Regression Analysis

Table B4. Values used in regression analysis

x	y	x^2	xy	y^2
1.3727	2.8396	1.8943	3.8979	8,0633
1.1494	2.8415	1.3210	3.2660	8.0743
0.4166	2.8601	0.1736	1.1915	8.1802
0.2059	2.8604	0.0424	0.5890	8.1819
0.0365	2.8661	0.0013	0.1046	9.1245
Summation 3.1810	14.2677	3.4326	9.0450	40.7208

$$a_{\alpha'} = \frac{48.9753 - 28.7849}{17.1630 - 10.1188} = \frac{20.1904}{7.0442} = 2.8662 \text{ Å}$$

IX. APPENDIX C. CARBIDE PARTICLE SIZE ATTAINABLE BY DIFFUSION CONTROLLED GROWTH DURING AGING

Cahn (73) has shown that heterogeneous nucleation of precipitates in the presence of dislocations is several orders of magnitude faster than homogeneous nucleation. Thus, in the presence of a highly dislocated structure such as is produced during cryoforming, diffusion-controlled growth would be the limiting process for precipitation.

Zener (87) has proposed that particle size at any time t is given by:

$$S = \alpha_\lambda (Dt)^{\frac{1}{2}} \qquad \text{(C-1)}$$

where S is the growth coordinate, or half width for plate growth, and the radius for cylindrical and spherical growth; D is the diffusivity of the solute, α_λ is a parameter called the growth coefficient which is dependent on the pertinent solute concentrations. α_λ is determined from the solution of a partial differential equation which satisfied the following equation:

$$_\lambda(\alpha_\lambda) = \frac{2\zeta}{(\alpha_\lambda)^\lambda \exp(\frac{\alpha_\lambda^2}{4})} \qquad \text{(C-2)}$$

where

$$\zeta = \frac{C_\infty - C_\alpha}{C_\beta - C_\alpha}$$

C_∞ = concentration of solute at a distance far from the precipitate (atomic fraction)

C_β = concentration of solute in precipitate

C_α = concentration of solute in the matrix in equilibrium with the precipitate

Zener (87) has provided graphical representations of α_1 and α_3 for plate and spherical growth, respectively. Scott (88) has provided the equivalent plot for cylindrical growth. He has suggested that to be consistent with the assumption that precipitation occurred on dislocations, the growth should be considered cylindrical.

For the austenitic stainless steel, considering chromium diffusion:

$C_\infty = 0.201$

$C_\alpha = 0.00$ in the limiting case

$C_\beta = 0.79$

$$\xi = \frac{0.201}{0.79} = 0.254$$

From Figure 2 of Zener (87), $\alpha_2 = 0.75$

For cylindrical growth:

$$S = 0.75\ (Dt)^{\frac{1}{2}}$$

For diffusion of Cr in α (89)

$$D = 1.25 \times 10^{-1} \exp\left(\frac{-52,000}{RT}\right)$$

T = aging temperature ^oK

R = 1.987 cal/g atom ^oK

Temperature T °C (°K)	Diffusivity D cm/s	Particle radius S (Å)
500°C (773°K)	2.476×10^{-16}	70.7
400°C (673°K)	1.618×10^{-18}	5.7
300°C (573°K)	1.827×10^{-20}	< 1

The size of the carbide particles formed by aging at 500°C for 1 hr is within the resolution range of the transmission microscope.

X. APPENDIX D. ESTIMATE OF PARTICLE SIZE AND MEAN INTERPARTICLE SPACING FOR EFFECTIVE STRENGTHENING OF PRECIPITATES

1. Critical particle size for deformation by dislocation bowing:

Critical size for particle not to shear

$$r_c = \frac{2Gb^2}{\pi\beta} \qquad \text{(D-1)}$$

where:

G = shear modulus of matrix

b = Burger's vector of matrix

β = interfacial energy per unit area between the particle and the matrix

The average interfacial energy β_{ave} is given by

$$\beta_{ave} = 0.03\ G'b'$$

where:

G' = the shear modulus of the carbide particle

b' = Burger's vector of the particle

Although no precise data are available for G', and b' for the $(FeCr)_{23}C_6$ carbides, the following approximate values have been used to estimate the critical size.

For intermetallic compound or ceramic oxide (90):

$$524 \times 10^3 \leq E' \leq 723 \times 10^3 \text{ MPa} \qquad \text{(D-2)}$$

where:

E' = elastic modulus of the particle

and

$$0.21 \leq \nu' \leq 0.28$$

where:

ν' = Poisson's ratio of the particle

$$G' = \frac{E'}{2(1+\nu')}$$

$$\therefore\ 205 \times 10^3 \leq G' \leq 282 \times 10^3 \text{ MPa}$$

But $G = 74 \times 10^3$ MPa $\qquad\qquad \therefore\ G' \approx 3G$

The lattice parameter for $Cr_{23}C_6 \approx 10.6214$

$$\therefore\ b' = \frac{10.6214}{\sqrt{2}} = 7.510 \text{ Å}$$

$$b = 2.482 \text{ Å} \qquad\qquad b \approx 3b$$

From equation D-1

$$r_c = \frac{2Gb^2}{\pi(0.03)3G \cdot 3b}$$

$$= \frac{2b}{0.848}$$

$$b = 2.482$$

$$r_o = 5.85 \text{ Å}$$

The resolution of the transmission electron microscope used in this study was of the order of 25 Å. Since the carbides were observed after aging at both 400°C (Fig. 14) and 500°C (Fig. 22), it is concluded that the precipitates formed at these temperatures had radii larger than the critical value. Therefore, dislocation bowing was the mechanism of plastic deformation.

2. Use of Orowan Equation to estimate mean spacing for effective strengthening:

From the modified Orowan Equation:

$$\Delta S_y = \frac{Gb\phi}{2\pi(d-2r)} \cdot \ln \frac{d-2r}{2b} \qquad \text{(D-3)}$$

where:

G = shear modulus of the matrix

b = Burger's vector of a dislocation

r = mean particle radius

d = mean spacing between particles

$\phi = 1/2\ (1 + 1/1-\nu)$

ν = Poisson's ratio

ΔS_y = increase in yield strength due to precipitation

$$G = \frac{E}{2(1+\nu)} = \frac{28 \times 6.89 \times 10^3}{2(1+0.28)} = 75.36 \times 10^3 \text{ MPa}$$

$\phi = 1/2\ (1 + 1/0.72) = 1.194$

(1) If precipitates are in martensite matrix, the smallest possible Burger's vector, predicting the lowest increase in yield strength, is:

$$\underline{b} = \frac{a}{2}(111)$$

$a = 2.8662$ Å

$= 2.482$ Å

$$\Delta S_y = \frac{35.544}{(d-2r)} \cdot 10^4 \cdot \ln \frac{d-2r}{4.9640}$$

Since X-ray diffraction did not detect any carbides the volume fraction of carbides $V_{carbide} < 0.05$

but $V_{carbide} = \frac{2r}{d}$

$\therefore d \geq 40r$

Therefore the interparticle spacing was the factor controlling the strength of the aged materials.

$$\therefore \Delta S_y \approx \frac{35.544}{d} \cdot 10^4 \cdot \ln \frac{d}{4.9640}$$

d Å	ΔS_y MPa
200	655
300	486
400	390
600	284
800	226

(2) If precipitates were in γ

$$\underline{b} = \frac{a}{2}(110)$$

$$a = 3.5891$$

$$b = 2.5382 \text{ Å}$$

$$\Delta S_y = \frac{36.348}{d} \cdot 10^4 \cdot \ln \left(\frac{d}{5.0764}\right)$$

d Å	ΔS_y MPa
200	668
400	430
600	289
800	250

Interparticle spacings ranging from 200 Å to 800 Å can contribute yield strength increases of between 225 MPa and 650 MPa.